Probabilistic Design

Of Gravity Based Foundations

Master's Thesis

Anders S. Poulsen Mads B. Randers Torben Sørensen

AALBORG UNIVERSITY
STUDENTS REPORT

Aalborg University
Department of Civil Engineering
Sohngårdsholmsvej 57
Phone: 96 35 97 31
Fax: 98 13 63 93
http://www.bsn.aau.dk

Title: Probabilistic Design of Gravity Based Foundations
Theme: Analysis and Solution of an Advanced Civil and/or Structural Engineering Problem
Project period: B10K, Spring Semester 2012
Project group: B123b

Group members:

Anders S. Poulsen

Mads B. Randers

Torben Sørensen

Supervisor: John D. Sørensen
Lars Bo Ibsen

Print runs: 7
Numbers of pages: 126
Appendix: 43 pages + CD
Completed: 1st of June 2012

Synopsis:

The purpose of the thesis is to investigate, which potential gains that can be obtained from designing gravitational foundations by a probabilistic approach compared to the well known deterministic approaches used for design. Further, investigations treat the effect of including information about the correlation length in the design.

For this purpose two test sites are chosen for collecting soil characteristics for the analyses. One test site containing sand, and the other provides characteristics for a clay. A spatial analysis of the test sites reveals small correlation lengths in the range of 0.1 - 0.5 m and 1.5 - 2.5 m in vertical and horizontal direction respectively.

Deterministic designs of a gravity based surface footing for a wind turbine are performed for both the frictional and the cohesive soil. The reliability index is found for the designs. It is found that the reliability indices are respecting present demands. This leads to an investigation of the reduction potential of the partial safety factors. It is found that the partial safety factors are strongly dependent on the given design situation and the available information of the soil characteristics. Nonetheless, a great reduction potential of the partial safety factors is outlined.

Preface

This thesis is a product of group B123b's project work at the 4th semester of the master degree study in Structural and Civil Engineering at Aalborg University. The project is completed within the period 13th of February to 1st of June 2012 under the supervision of John D. Sørensen and Lars Bo Ibsen. The thesis is prepared and made in compliance with the current curriculum of the 4th semester in M.Sc. Structural and Civil Engineering.
The thesis is specified in compliance with the supervisors and aims to contribute to the discussion of advantages of probabilistic design compared to traditional deterministic design. Based on a simple gravitational foundation for an onshore wind turbine analyses are performed on a foundation installed on sand and clay respectively. Further the probabilistic analysis will be used for calibration of partial safety factors.

Reading Guide

The thesis consists of three parts: a main report, an appendix, which are found in the back of the report, and an electronic appendix on an attached CD. The main report refers to the appendix and CD, where the appertaining calculations and extensional documents are to be found. The files used in the different software, e.g. MATLAB and Fortran, are attached to the electronic appendix CD. All references to the appendix starts with an Arabic letter. E.g. the first section in appendix A is thus to be referred to as Appendix A.1.

Figures and tables are numbered in accordance with the chapter they appear within. E.g. the first figure in the third chapter has been given the number 3.1, the second 3.2 etc. Captions will appear under each figure and above each table. If no source of reference has been submitted in the caption, the picture or table is created by the group.

This thesis uses the Harvard method of bibliography with the name of the author and year of publication inserted into brackets after the text, e.g. [Ayyub and McCuen, 2002]. If the source reference is positioned before a full stop it only refers to the very sentence whereas if it is placed behind the full stop it refers back to the whole text section. A source reference in the beginning of a section is valid for the whole following section unless other is stated. A list of all the source references is given in the bibliography list at the end of the main report.

Different programmes are used for calculations and simulations throughout the thesis. These are mentioned as MATLAB, Fortran, LimitState:Geo and PLAXIS 3D. The used version of MATLAB is version 7.11.0.584 (R2010b). The Fortran version is Compaq Visual Fortran Standard Edition 6.6.0. The reference for LimitState:Geo is made for version 2.0.f.11094. Finally the used version of PLAXIS 3D is 2011.1.7847.8250.

Table of Contents

Part I

Introduction

Chapter 1

Introduction

Focus on the renewable energy sector has increased during the last decades and the most dominant player in this sector is the wind energy. Much energy and resources have been spend in order to optimize the design of wind turbines. The aerodynamic design, size of blade span and optimisation of the foundation are all areas to which much attention has been focused in order to maximize the power output from the turbines, while the total costs are minimized. The foundation is known to amount up to 35% of the total costs of an offshore wind turbine in certain cases [Ibsen, 2012]. Therefore this area include a huge potential, when it comes to costs reduction, which is why this thesis will treat this very specific area.
Many different mathematical models for the design of the wind turbine foundations are used worldwide. Ongoing discussions constantly keep these formulations under the loop as an economical optimisation of design dimensions is a number one priority among most developers. In Denmark design of wind turbines has been performed in accordance with guidelines from Det Norske Veritas (DNV) and Eurocodes since 2009, where Eurocodes became the required national design codes. The mentioned codes use the Terzaghi's bearing formulas as design criterion for gravity based foundations. Therefore this thesis will be centered on the use of Terzaghi's bearing capacity formulas. The focus however will be regarding the beneficial gaining that are associated with probabilistic modelling of a gravity based foundation compared to a regular deterministic approach using partial safety factors and characteristic values. The deterministic design approach requires great knowledge and a precise description of the soil parameters, which is often a difficult task to determine. Therefore uncertainties are taken into account by using partial safety factors and characteristic values for the loads and the strength parameters. However this approach could lead to a conservative design. Using the probabilistic design approach uncertainties for the soil parameters are taken into account in the entire design phase by modelling the parameters associated with uncertainties as stochastic variables. The calculations will result in a reliability analysis and the foundation will be designed to comply with an annual target reliability, β_T, of 3.72 which is the value recommended in the Eurocodes. For illustration a foundation for a wind turbine foundation will be designed using both approaches and a comparison of the results will be presented. In connection with the comparison of the results it has been found interesting to investigate the reduction potential of the currently used partial safety factors for the strength parameters.

1.1 Thesis Statement

The topics presented in the introduction have been found very interesting and will be treated throughout the thesis. The following statements will form the basis of the thesis.

- What are the potential gains from designing gravitational foundation by a probabilistic approach compared to design by accepted codes for both sand and clay?
- What are the possible gains from a spatial analysis of the soil prior to the design?

1.2 Delimitations of Thesis

The scenarios and load cases presented in the thesis are chosen to be similar to well-known situations for onshore wind turbines. The choice of foundation will in this thesis purely be based on simple surface footings, which is a great simplification, when actual design situations are considered. Nevertheless the choice seems reasonable, as the main focus of the thesis is on the influence of the spatial variation of the soil strength parameters on the bearing capacity of the foundations. By simplifying the foundations much time is saved from designing the actual foundations and transferred into analysis of the main area of interest of this thesis.

In this thesis the soil is the area of focus, which is why only failure of the soil will be considered. Construction elements above the ground and foundations will be considered as rigid elements. Service limit state analysis are not considered, wherefore only ultimate limit state analysis are performed.

Different distributions will be assigned to strength parameters throughout the thesis. In order to do this, the used data needs to be statistically independent and from the same population. The statistically independence will be assured by only including data points that are separated with the found correlation lengths. The CPTu tests performed at the same location will be considered as being from the same population.

In the thesis the considered soils will be considered as perfect cohesive or perfect frictional soils. I.e. the strength parameters for the soil will be only an undrained shear strength or an effective friction angle. In nature a combination of the strength parameters will typically be present in the soils, which is not considered in the thesis.

When the characteristic bearing capacities are found in the thesis, they will be found using 5% quantiles of the strength parameters instead of 5% quantiles of the calculated bearing capacities, which is prescribed in the Eurocodes.

The above described delimitations are of general concern throughout the thesis. Additional and more specific delimitations will be presented in the appropriate chapters and sections.

1.3 Chronology of the Thesis

In the following section a presentation of the thesis will be described. The thesis is build up in a chronological order with the statements presented in Section 1.1 as a final goal. The subjects treated to answer the thesis statement are presented in bullet points in the chronological order they appear:

- Description of the uncertainties related to the analyses and formulations used in the thesis.
- Presentation of the test site.
- Analysis of CPTu tests performed on sand and clay in order to find strength characteristics.
- Spatial analyses of test results.
- Deterministic design of gravity based foundations.
- Numerical simulations to estimate the uncertainties associated with applying known analytical formulations.
- Probabilistic design of gravity based foundations.

- Review and discussion of the current applied partial safety factors based on the probabilistic design.

In addition to this, two separate studies follows and include:

- Case study on the influence of the correlation lengths on the bearing capacity.
- Probabilistic calculation using an advanced limit state function.

Chapter 2

Uncertainties

Throughout the work done in this project, there will be some uncertainties connected with the different models and used approaches. Uncertainties can in general be divided into two main types, which are the aleatory and epistemic uncertainties.
The aleatory uncertainties are due to natural randomness of a physical quantity and can therefore not be reduced, whereas the epistemic uncertainties is due to the lack of knowledge connected to a mathematical model or due to a poor statistical basis. The uncertainties dealt with in this project are listed as follows:

- Physical uncertainty
- Measurement uncertainty
- Statistical uncertainty
- Model uncertainty

2.1 Physical Uncertainty

Physical uncertainty, which is an aleatory uncertainty, could e.g. be the natural randomness of the strength parameters in a soil from point to point. This kind of uncertainty will be included in the ongoing analysis, as the undrained shear strength and the effective friction angle will be modelled as a stochastic variables in the probabilistic design.

2.2 Measurement Uncertainty

Imperfections of the equipment or other uncertainties related to the measurements for the field tests are present for most cases. This will also provide a contribution to the total model uncertainty, which should have been accounted for. This kind of imperfection falls into the epistemic category.

2.3 Statistical Uncertainty

In order to carry out a proper statistical analysis sufficient data needs to be available. This means that before modelling a stochastic variable a minimum of 25 - 30 observations needs to be at disposal. Furthermore the data needs to be independent and from the same population. Statistical uncertainties are regarded as epistemic uncertainties, as the uncertainties can be reduced by a greater statistical basis.

2.4 Model Uncertainty

The model uncertainty can be due to simplifications and idealisations made regarding a mathematical model. Therefore model uncertainties are regarded as an epistemic uncertainty, as they are due to lack of knowledge. The model uncertainty regarding the mathematical models used throughout this project, is found as the difference between the

analytical expression and the numerical simulated values. So the numerical values is regarded as the exact result. A comparison of these can be modelled as shown in Figure 2.1.

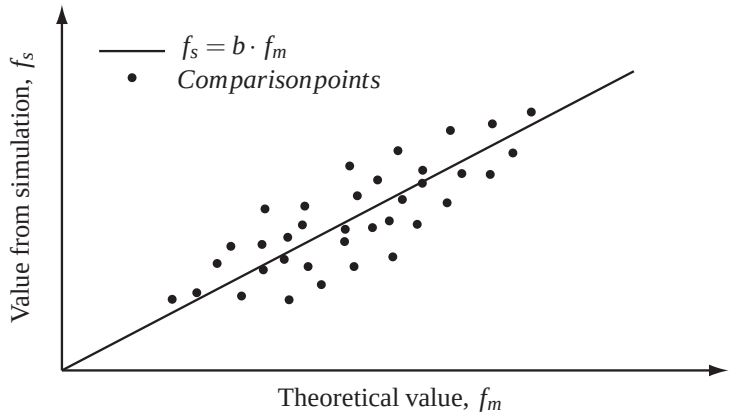

Figure 2.1: *Illustration of the better fit for modelling the model uncertainties.*

The best fit of the line shown in Figure 2.1 would provide the bias, b, for the comparison from which the standard deviation can be determined as the deviation from the fitted line. In order to take the physical uncertainties into account a similar comparison between experimental test results and a numerical model could be done.

2.5 Uncertainties Related to CPTu Interpretations

Throughout the thesis CPTu measurements will be used for further analysis. Such are always associated with measurement uncertainties, that can occur in various forms. Problems might be observed with the mechanism and components, which might induce inaccurate results. Therefore a calibration of the equipment is needed on regular basis. A model uncertainty should also be appointed to the mathematical expressions used to interpret the measured results, e.g. the expression in Equation (5.1). The mentioned uncertainties have not been taking into account, as additional measurements and calibrations tests are out of the scope of this thesis.

The different uncertainties presented in this chapter will be commented upon and referred to throughout the work done is this thesis.

Chapter 3

Design Scenario

In the following chapter the loads and partial safety factors used for design are presented. The design situation for the foundation installed on frictional soils and the foundation installed on cohesive soils, only differs in the soil conditions.
The wind turbine will be designed after design situation DLC 1.1 in accordance to [IEC, 2005]. This is an ultimate limit state analysis for a wind turbine during operation under normal wind conditions.

In Figure 3.1 the design scenario can be seen.

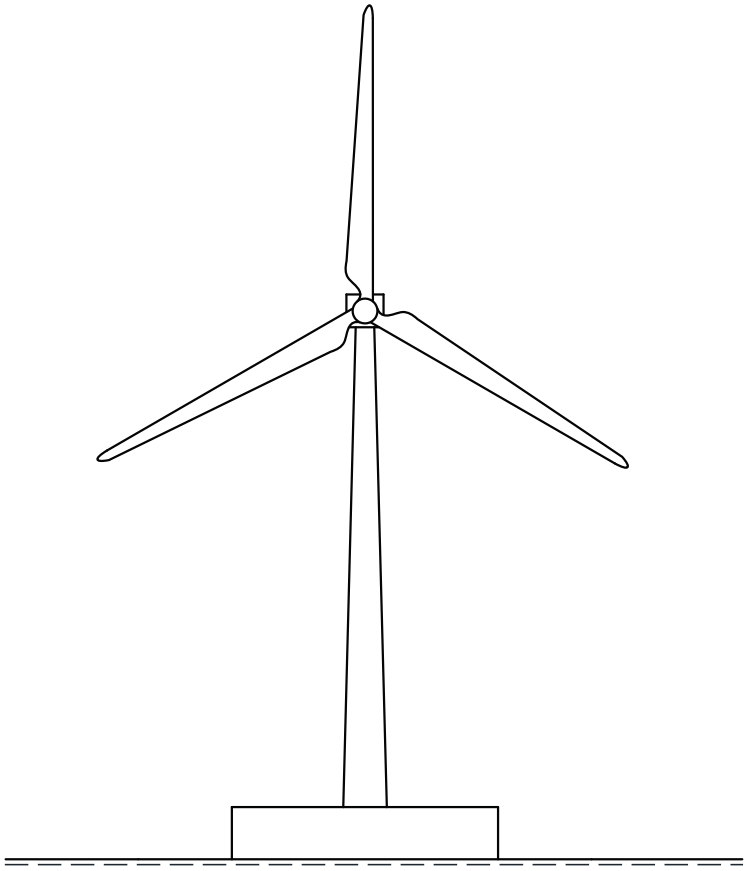

Figure 3.1: *The design scenario is shown in the figure.*

Figure 3.1 shows a gravity based foundation placed on the surface of a soil. It shall be mentioned that the structural elements will be regarded as rigid elements as it is the failure of the soil that is of interest in this thesis. From Figure 3.1 it is seen that the phreatic surface and surface of the soil are coinciding.

3.1 Partial Safety Factors

The partial safety factors used in the deterministic approach can be seen in Table 3.1.

Table 3.1: *Partial safety factors used in the project.*

Parameter	Symbol	Value
Partial safety factor for aerodynamic loads	γ_Q	1.35
Partial safety factor for self-weight	γ_G	1.0
Partial safety factor for undrained shear strength	γ_{c_u}	1.4
Partial safety factor for effective friction angle	$\gamma_{\varphi'}$	1.25

The partial safety factor for aerodynamic loads, γ_Q, is chosen in accordance to [IEC, 2005], whereas γ_{c_u} and $\gamma_{\varphi'}$ is from [Eurocode 7-1, 2007]. I should be noticed that the values of γ_{c_u} and $\gamma_{\varphi'}$ is 1.8 and 1.2, respectively, in the Danish addendum to Eurocode 7 [Eurocode 7-1 DK NA, 2008], but the general values will be used for further evaluation.

3.2 Design Loads

In the following section the loads will be presented. For the deterministic approach the 98% quantile of the aerodynamic loads will be used for design.
In order to determine the aerodynamic loads on a wind turbine precisely a numerical computer programme should be used together with site measurements. Since it is out of the scope of this project to determine the exact loads on the wind turbine, estimates of the wind loads from [Andersen, 2012] are chosen as design basis. The characteristic 98% quantile loads at the top of the foundation can be seen in Table 3.2.

Table 3.2: *Characteristic loads.* Self-weight of the wind turbine without foundation.*

Parameter	Symbol	Value	Unit
Horizontal load	H_c	740	kN
Moment	M_c	74,000	kNm
Self-weight*	G_c	5,000	kN

The design loads used for the deterministic approach are given in Table 3.3.

Table 3.3: *Design loads.*

Parameter	Symbol	Value	Unit
Horizontal load	H_d	1,000	kN
Moment	M_d	100,000	kNm
Self-weight	G_d	5,000	kN

The entire self-weight of the structure, wind turbine and foundation, can be determined when the height and diameter of the foundation is known.
The presented loads will all be used for the further work presented in the following chapters.

Chapter 4

Presentation of Test Site

When analysing in situ test from the test sites an important supplemental tool is to get an overview of the geological history from the area. Knowledge about this can help interpreting and explain unusual observations. In this chapter the test sites treated in this thesis are presented and the most important geological history at the sites are described. In this project CPTu tests will be used to gain knowledge about strength parameters of the soil. As the thesis will concern modelling of foundations in both clay and sand, two locations will be presented in the following.

4.1 Sand Site

The location for extracting the sand CPTu's are at the eastern part of Aalborg located at Vulkanvej. The position of the test site is shown in Figure 4.1.

Figure 4.1: *Specification of location for soil tests. [Google, 2012] - edited*

4.1.1 Geological Expectations and Soil Properties

In the following a brief description of the most important geological historic events of the area will be described. The geological description is kept in mind when characterising the soil.

The geologic layers of interest are the more recent layers due to the fact that only ultimate limit state analyses are performed and the CPTu tests are limited to a depth of approximately eight meters. Therefore the limits of the Yoldia

Sea and the Stone Age Sea will be shortly described in the following, as these are known to have great influence of the deposits at the top layers. In Figure 4.2 and 4.3 the sea levels are described for the Yoldia and Stone Age Sea.

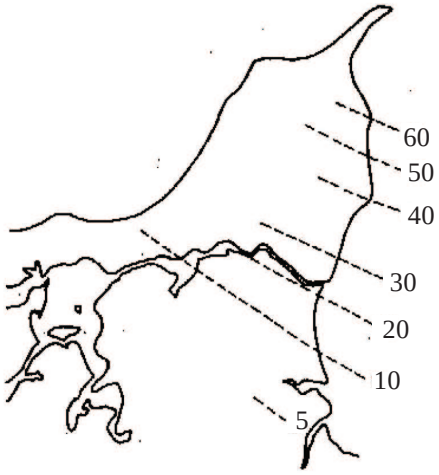

Figure 4.2: *The levels of coverage for the Yoldia Sea. Approx. 7,000 B.C. Units are in meters. [Pedersen et al., 2011] - edited*

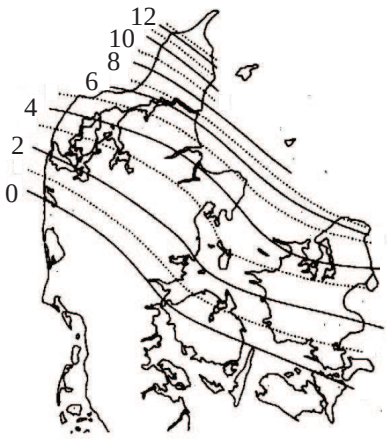

Figure 4.3: *The levels of coverage for the Stone Age Sea. Approx. 5,500 B.C. Units are in meters. [Pedersen et al., 2011] - edited*

From the figures it is clear that both the Yoldia and the Stone Age Sea cover the test location. As the surface and the test location is in the range of 2.5 - 3 m above sea level deposits from both historical events from the late glacial time can be expected. In spite of Aalborgs position near sea water, the deposits in the Aalborg area is known not to be deposits directly from the sea because of freshwater flow. Instead the deposits are more likely to be from fresh- or brackish waters. The typical stratigraphy of the area is Yoldia Clay (known as Aalborg Clay when no organic material is present), with sandy deposits above and underneath. The sand deposits are denoted Saxicava-sands (also known as Aalborg Sand when no organic material is present). [Berthelsen, 1987]

For the tests performed at the location only the layers containing primary sand will be analysed. A few classification tests have been performed for the sands at Vulkanvej in connection with a concurrent thesis. The results obtained from the classification tests are presented in Table 4.1. The results can be reviewed in [Geron and Iliescu, 2012].

Table 4.1: *Available classification results for the used sand. The saturated unit weight has been estimated from [Chr. Jensen, 2009].*

d_s	γ_{sat}	w
[-]	[kN/m^3]	[%]
2.66	19	16.65 - 26.51

In connection to the classification tests a sieving analysis has been performed for the sand as well. The results are presented in Figure 4.4.

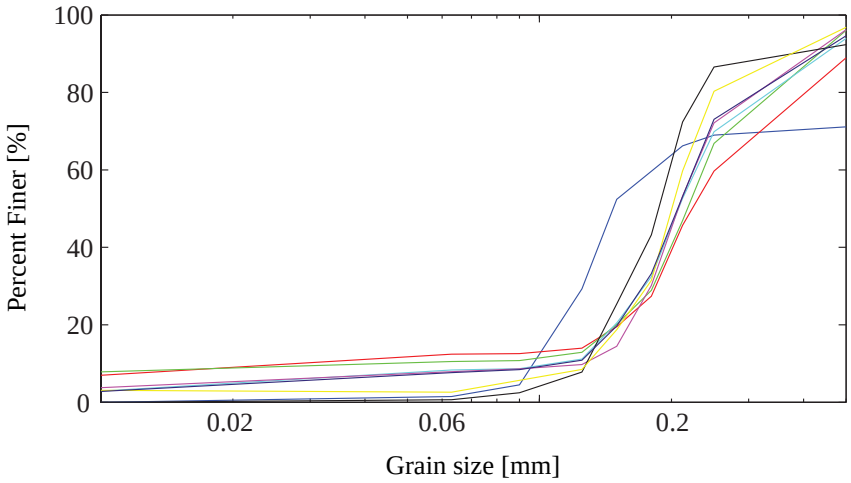

Figure 4.4: *Sieving analysis for the sand from different locations at the test site. [Geron and Iliescu, 2012]*

According to [Krebs Ovesen et al., 2007] the grain size of silt is in the interval of 0.02-0.06 mm. If the definition is applied to the results obtained in Figure 4.4, it is observed, that the average silt content is just below 5%, which will be used in the calculations to come.

4.1.2 Tests at Vulkanvej

A total of nine CPTu's have been performed in the area. The local positioning of the tests are shown in Figure 4.5. The CPTu's performed at the location are all within the range of seven to eight meters in depth and have layers of cohesive and organic materials in the first well over three meters of depth after which frictional soils follow. The soil containing non-frictional soil is removed in order to analyse homogeneous soil in the further work even though inhomogeneous soil are present. A representative stratigraphy from the location is shown in Figure 4.6.

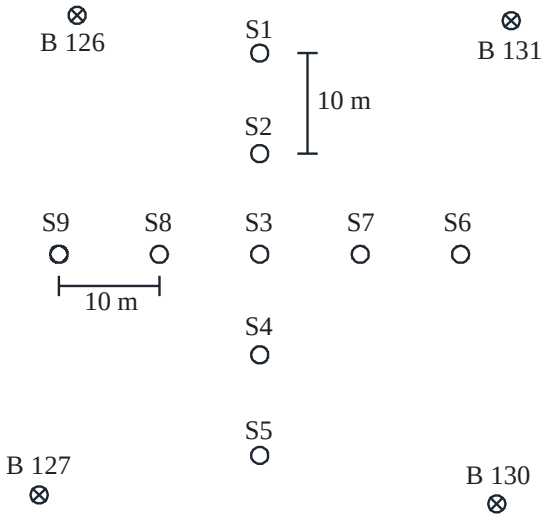

Figure 4.5: *The local positioning of the CPTu tests at the test site at Vulkanvej. B symbolises bore holes and S indicates a sounding.*

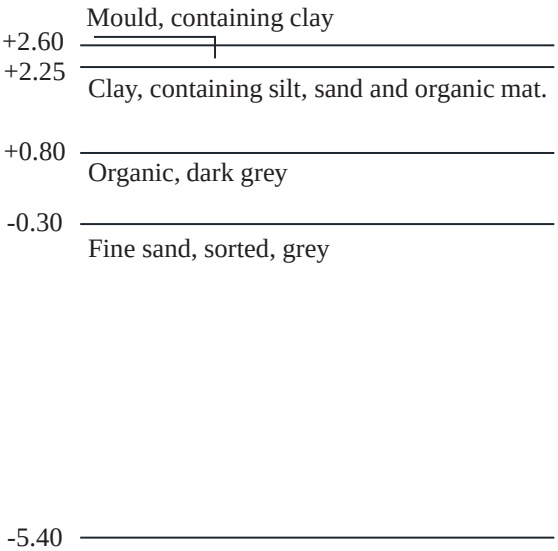

Figure 4.6: *Stratigraphy from bore hole 130. The layers containing non frictional materials are removed from the measurements.*

The pattern seen in Figure 4.5 has been found appropriate for this thesis as spatial dependencies will be determined in Chapter 8. A suitable number of distance pairs should be present in both vertical and horizontal directions, which is the case of the placing of the tests in Figure 4.5.

The stratigraphy in Figure 4.6 is seen to be in some compliance with the expectations, as the fine sand might be associated with Aalborg sand. This is also concluded from the absence of organic material in the sand. Although it should be noted that further classification of the soil is needed in order to make a final judgement call. As a remark for the location at Vulkanvej the very area of the soundings was not geologically mapped at the time of the publication of the used literature [Berthelsen, 1987]. Therefore a description of the entire Aalborg area as a whole has been used.

Sounding S1 and S9, see Figure 4.5, have been removed from further investigations, as these contained primarily cohesive materials. All the results from the soundings and the stratigraphies from the bore holes are presented in CD Appendix A.

4.2 Clay Site

In the following the site containing primarily clay will be briefly introduced. The location is in Frederikshavn, where a site between the local school, Håndbækskolen, and the road Suderbovej has been used for analysis. The location is shown in Figure 4.7.

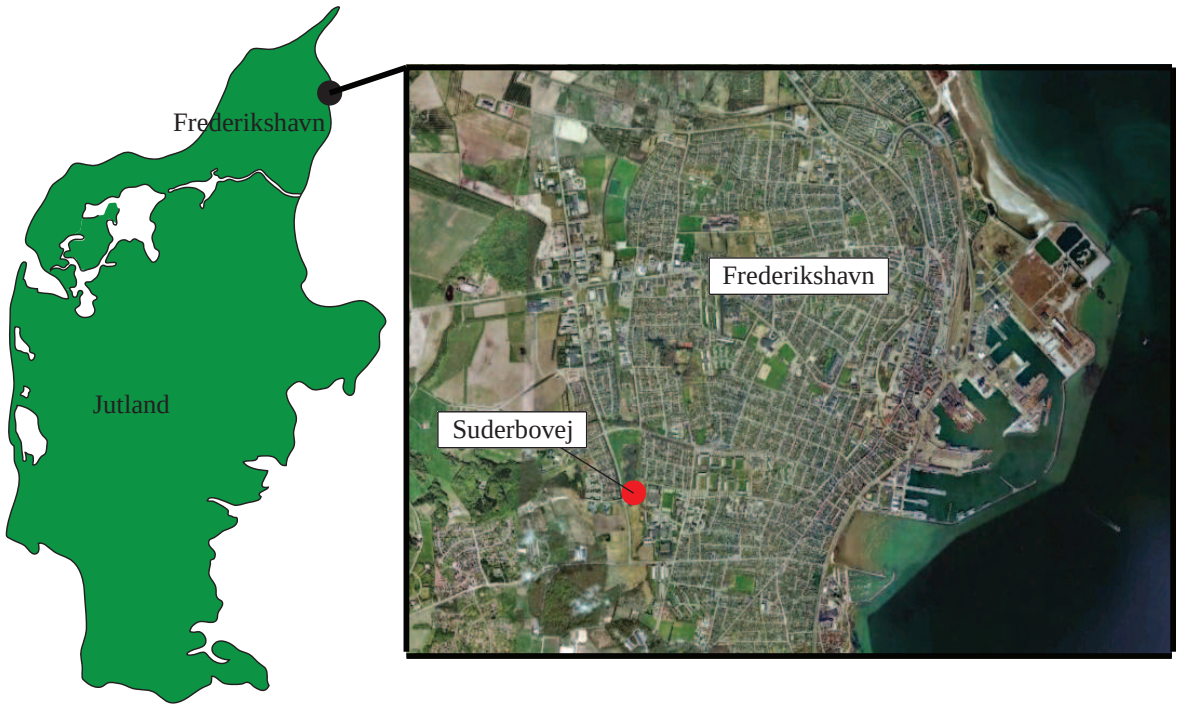

Figure 4.7: *Specification of location for soil tests. [Google, 2012] - edited*

4.2.1 Geological Expectations and Soil Properties

Different observations are made, when considering Figure 4.2 and 4.3 for the Frederikshavn area. The borings and the CPTu's are performed in the range of 25 - 30 m above sea level. As the Stone Age Sea only is expected up till approximately 12 m above sea level, no deposits are expected from the Stone Age Sea. Therefore the clay deposits found at the location is expected to be Yoldia Clay.

In general the Frederikshavn area is typically dominated by moraine hills with deposits of Older Yoldia Clay. Sand deposits from melted glacial water are rather common as well. Deposits from the Yoldia Sea can be found in up to 60 meters above sea level due to the rising of the land from when the Weichsel Ice withdrew from the area. [Andersen and Sjørring, 1992] The covering of the glacial ice, Weichsel, is shown in Figure 4.8.

Figure 4.8: *The covered areas of the Weichsel ice in the latest ice age. The covered area is northeast of the drawn line. The melting of the last ice are expected to have taken place 11,000 B.C. [Pedersen et al., 2011] - edited*

The landscape in the Frederikshavn area is rather rolling. This is a result from the repeated unsteady movement of the ice just east of Frederikshavn, which have caused the deposits to be pushed together forming the hills. [NearshoreLAB Frederikshavn A/S, 2007]

The main purpose of the tests at the location in Frederikshavn is to subtract clay characteristics that can be used for later analysis. Therefore the layers that are not dominated by clay will be excluded from further analysis. At the time of the writing of this thesis, no classification tests have been performed on the clay. Therefore it is assumed that the clay at the test site is Yoldia Clay and it should be noted, that Yoldia Clay is known to have a preconsolidation stress level in the range of 200-250 kPa, wherefore high horizontal stresses could be expected. [Luke, 1994]

4.2.2 Tests at Suderbovej

At the site located as specified in Figure 4.7 a total of 12 CPTu's have been carried out. The position of the CPTu's is seen in Figure 4.9, and the stratigraphy of the location is presented in Figure 4.10. The stratigraphy is produced on background of two borings performed on the line covering CPTu number 1 - 7 as indicated in Figure 4.9. The profiles from the two bore hole tests are presented in Appendix B.

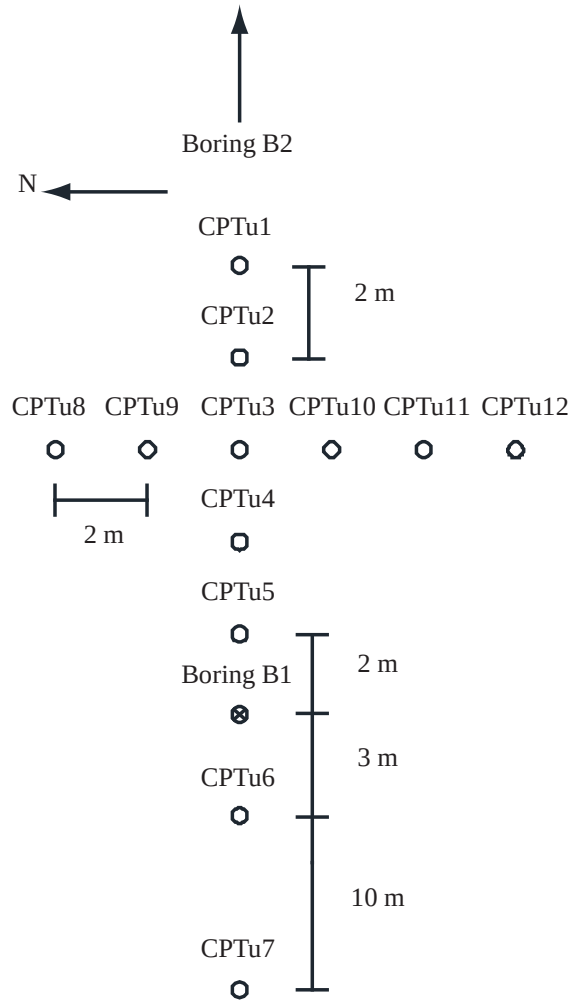

Figure 4.9: *The local positioning of the CPTu tests at the test site at Suderbovej. B symbolises bore holes and S indicates a sounding.*

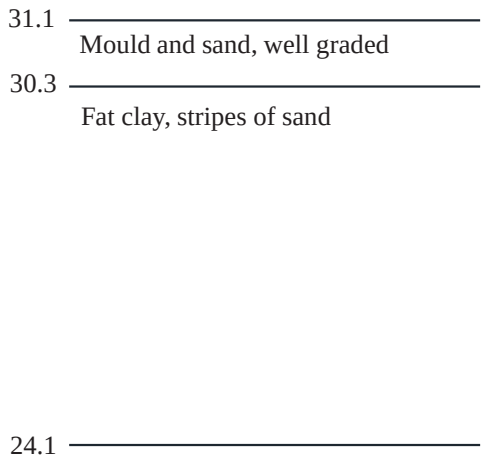

Figure 4.10: *Stratigraphy of the test site at Suderbovej. Stratigraphy is from bore hole test 1.*

The mutual placing of the tests in Figure 4.9 are motivated by the same considerations as those for the sand site.

In Figure 4.10 it is observed, that the soil layers are in rather good agreement with the expected from the geological history of the area. The dominating fat clay could indicate a Yoldia Clay, which has been covered by a layer of sand and mould in the years to follow.

Part II

Stochastic Modelling of the Soil

The present part will concern the treatment of the CPTu data measured at the given test locations. First a description of the choices made regarding the modelling of the frictional soil will be presented and the results are commented upon. Afterwards similar presentation of the cohesive material is performed. The strength parameters are described as stochastic variables. Finally a spatial analysis will be performed for both soils, as the correlation length will be included in the probabilistic design in the following parts.

Chapter 5

Modelling of Frictional Soil

In the following chapter the characteristics of the frictional soil used for the later deterministic and probabilistic analysis will be determined and presented. Results and theoretical approaches for treatment of the CPTu tests will be described.

5.1 Determination of Sand Characteristics

A noticeable number of analysis methods are available for treating CPTu results in frictional soils. For this thesis it has been chosen to use two different interpretation methods introduced by Bolton in 1986 and Mayne in 2007 respectively. The two methods use rather different approaches. The method proposed by Mayne is semi-empirical and easy to implement in a calculation programme like MATLAB and is only dependent on the measured cone resistance and the vertical overburden pressure. The method is one of the newest accepted analysis methods for clean sands [Ibsen, 2012].
The method presented by Bolton is also semi-empirical. The main difference is that Bolton's method takes the grain distribution and the relative density of the sand into consideration. Additionally the dilation angle, Ψ, can be estimated. When both the dilation angle and the friction angle are calculated, it is possible to calculate the reduced friction angle, φ_d, which will be described in the following.

Recent research has shown that the reduced friction angle is an important parameter, when the found friction angle is to be used in known theoretical bearing capacity formulas. The reasons for this is found in the derivation of many of these formulas. The assumption of associated plasticity is an important part of many well known theories. Although, when the friction angle is determined this aspect has not been taken into account and needs to be corrected for in order for the input parameters to be consistent with the assumptions of the formulas. Associated plasticity can be obtained by reducing the friction angle until the plastic yield development is orthogonal to the failure envelope. The situation is illustrated in Figure 5.1 and 5.2.

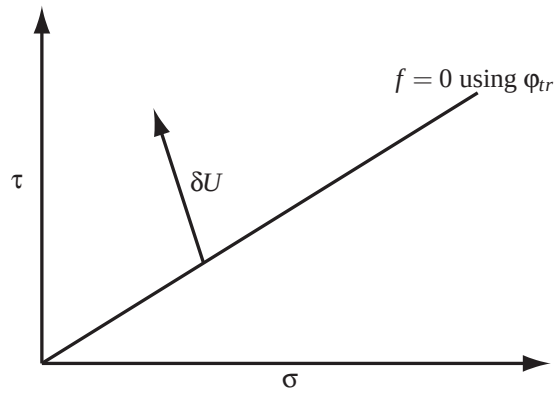

Figure 5.1: *Non-associated plasticity, which is in disagreement with some bearing capacity formulas.*

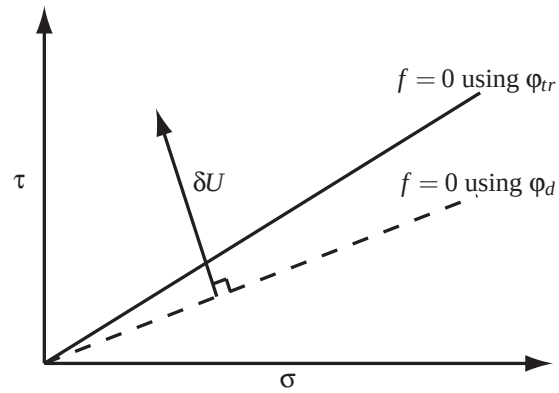

Figure 5.2: *Associated plasticity is obtained by reducing the angle of internal friction.*

Therefore both the mentioned methods will be used and compared in the following analysis. For an overall idea of the soil strength, the friction angle is plotted along the depth for all CPTu's in the right figures in Appendix G. Here the friction angle is calculated using Bolton's method.

5.1.1 Method and Assumptions (Mayne)

From the CPTu results obtained from Vulkanvej the triaxial effective angle of internal friction (in the following referred to as the effective friction angle), φ', is determined in accordance with Mayne's empirical expression for clean sands, cf. Equation (5.1) [Mayne, 2006].

$$\varphi'_{tr} = 17.6 + 11 \cdot \log_{10}\left(\frac{(q_c/P_a)}{(\sigma'_{V0}/P_a)^{0.5}}\right) \tag{5.1}$$

where

φ'_{tr}	Triaxial effective friction angle [°]
q_c	Cone tip resistance [kPa]
P_a	Atmospheric pressure, 100 [kPa]
σ'_{V0}	Effective overburden pressure [kPa]

In Equation (5.1) it is observed that the pressures are normalised with respect to the atmospheric pressure. Furthermore, the normalised cone tip resistance is normalised with respect to the square root of the normalised effective overburden pressure. This incorporates sands compressibility and and grain crushing effects to some extend [Mayne, 2006].

The calculated effective friction angles will be assumed LogNormal distributed. This is done, as strength parameters are known to typically follow a Normal or a LogNormal distribution, from which the LogNormal distribution cannot produce negative values. Furthermore, strength parameters were assigned a LogNormal distribution when partial safety factors were calibrated in the Eurocodes [Sørensen, 2012]. In order to be able to perform a proper comparison the same assumptions are provided for the two different approaches. Before being able to assign a distribution to the strength parameters, it is needed to ensure that the calculated values are statistically independent. This is ensured by only including values with a minimum distance of separation corresponding to an average correlation length. The used correlation lengths are described in Chapter 8.

For illustration the data will be plotted along with the assigned distributions. This is done using the Weibull plotting formula, which is presented in Equation (5.2).

$$F = \frac{i}{1+N} \tag{5.2}$$

where

F	Weibull distribution [-]
i	i'th realisation of the data [-]
N	Total number of realisations [-]

Finally the 5% quantile will be calculated for the effective friction angle. As the effective friction angle is assumed to be LogNormal distributed this can be done using Equation (5.3) for small COV's [Sørensen, 2011].

$$\varphi'_{0.05} = \mu_{\varphi'} \exp\left(-1.645\, \mathrm{COV}_{\varphi'}\right) \tag{5.3}$$

where

$\varphi'_{0.05}$	5% quantile of the effective friction angle [°]
$\mu_{\varphi'}$	Mean value of the effective friction angle [°]
$\mathrm{COV}_{\varphi'}$	Coefficient of variation of the effective friction angle [-]

As the characteristics of the sand will be used for both numerical simulations and a deterministic calculation, a tail fit for the 30% lowest values of the effective friction angle will be provided along with a LogNormal fit. The two different characteristics are presented, as a LogNormal fit is needed for the numerical simulations, where the soil will be given one single mean value. The characteristics for the tail fit will be used for the deterministic calculations, where a 5% quantile commonly is used for design. A tail fit will provide a better fit around the lower strength values and is therefore preferable for the 5% quantile. To obtain the characteristics for the tail fit various values of the mean value and the standard variation are used. The optimal fit will be decided using least square method (LSM), cf. Equation (5.4). [Sørensen, 2011]

$$\min_{\underline{\theta}} \sum_{i}^{n} \left(F_i - F_X\left(x_{i,\underline{\theta}}\right)\right)^2 \tag{5.4}$$

where

n	Number of data [-]
F_i	Accumulated distribution for the i'th value of the dataset [-]
$\underline{\theta}$	Vector containing the characteristics to be optimised [-]
$F_X(x_{i,\underline{\theta}})$	Calculated accumulated distribution for the i'th value for the fitted distribution [-]

When the distribution is found the standard deviation is estimated without taking depth dependency into consideration. This is done, as the sand soil will be described with only one single value in the ongoing calculations.

The loading and the size of foundation influence on the failure domain under the foundation. Because of relatively short CPTu test compared to the size of the failure for the treated loading scenarios, the results presented in this chapter are assumed to describe the whole failure domain under the foundation.

5.1.2 Results (Mayne)

The MATLAB programme containing the calculations can be found in CD Appendix A.
By applying the above described method and assumptions the effective friction angle for the sand located at the test site at Vulkanvej has been calculated and fitted to the LogNormal distribution, as indicated in Figure 5.3.

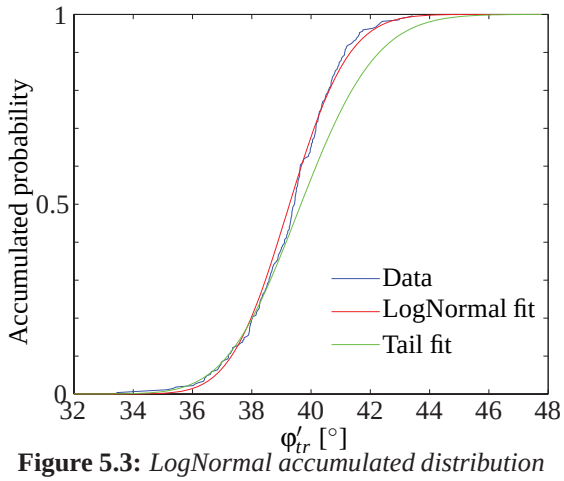

Figure 5.3: *LogNormal accumulated distribution and tail fit of the effective friction angle.*

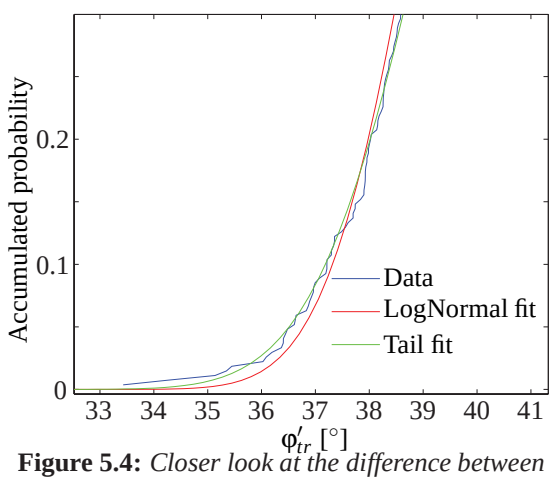

Figure 5.4: *Closer look at the difference between the fits at the lower values.*

As expected the tail fit provides a very good fit around the lower values, cf. Figure 5.4, while the tail fit deviates much at the higher values, cf. Figure 5.3. The different fit will be used for the different purposes presented earlier. The mentioned characteristics of the sand have been determined and are presented in Table 5.1.

Table 5.1: *Characteristics of the effective friction angle. F = 0.05 is the 5% quantile found from the data set. *Values will not be used in the further analysis, but are presented to give an overall description of the characteristics leading to the 5% quantile for the tail fit.*

	$\mu_{\varphi'}$ [°]	$\sigma_{\varphi'}$ [°]	$\varphi'_{5\%}$ [°]	COV [-]	$F = 0.05$ [°]
LogNormal fit	39.31	1.57	36.78	0.04	36.54
Tail fit	39.71*	2.00*	36.51	0.05*	36.54
			$\tan(\varphi')$		
LogNormal fit	0.8196	0.0454	0.7471	0.06	0.7411
Tail fit	0.8281*	0.0540*	0.7423	0.07*	0.7411

Typically values of the effective friction angle of friction is known to lie within the range of 36-42° according to [Chr. Jensen, 2009] for a sand that has been deposited by glacial melt water. This indicates that the sand could be the expected Aalborg sand as described in Section 4.1. The values in Table 5.1 will be compared to those obtained using the method presented by Bolton.

5.1.3 Method and Assumptions (Bolton)

After having viewed the results obtained for the effective friction angle using the method presented by Mayne, Bolton's method will be presented in the following. Basically the calculation of the effective friction angle, φ_{tr}, is calculated from four contributions as expressed in Equation (5.5).

$$\varphi'_{tr} = \varphi'_{crit} + 3^\circ\, I_R - 3^\circ\, D_r - \Delta\varphi_1 \tag{5.5}$$

where

φ'_{tr}	Triaxial effective friction angle [°]
φ'_{crit}	Critical effective friction angle [°]
I_R	Relative dilatancy index [-]
D_r	Relative density [-]
$\Delta\varphi_1$	Correction factor due to content of silt [°]

The critical effective friction angle (referred to as critical friction angle) has been analysed and found for various types of sand in the literature. It has been found that the critical friction angle only varies within 1 to 2° with a mean of 33° [Bolton, 1986]. Therefore 33° has been chosen as the critical friction angle for this thesis.

The relative dilatancy index, I_R, is calculated as stated in Equation (5.6). The values obtained for the relative dilatancy index should be kept within the interval 0 - 4. The values below 0 will not give any physical sense, and the method is limited to a upper ceiling of 4.

$$I_R = D_r \left(Q_{min} - \ln \frac{p'_{mean}}{1\,\text{kPa}} \right) - 1 \tag{5.6}$$

where

Q_{min}	Particle strength parameter, 10 for quartz [-] [Bolton, 1986]
p'_{mean}	Mean effective stresses [kPa]

Equation (5.6) is an empirical expression taking into account the relative density, mean effective stresses and the sand type in terms of grain distribution, mineralogy and grain shape, also suggested by Bolton.

The relative density, D_r, is calculated using Jamiolkowski's expression presented in Equation (5.7).

$$D_r = \frac{1}{2.96} \ln \left(\frac{q_c / P_a}{24.94 \left(p'_{mean} / P_a \right)^{0.46}} \right) \tag{5.7}$$

The sand considered from Vulkanvej is considered to be normally consolidated. Therefore the effective mean pressure, p'_{mean}, and the coefficient of earth pressure at rest, K_0, can be calculated from Equation (5.8).

$$K_0 = 1 - \sin\left(\varphi'\right) \qquad p'_{mean} = \frac{\sigma'_{V0} \left(1 + 2\,K_0\right)}{3} \tag{5.8}$$

The last part that needs to be taken into consideration when using Equation (5.5) is the reduction factor due to the content of silt, $\Delta\varphi_1$. The needed reduction can be found from Table 5.2.

Table 5.2: *Reduction due to the fraction of silt.*

$\Delta\varphi_1$ [°]	Silt content [%]
2	5 - 10
5	10 - 20

As the silt fraction was found to be just below 5% as an average in Section 4.1 it has been chosen to use a reduction factor, $\Delta\varphi_1$, of 1° for the calculations.

Hereby the theory for calculating the effective friction angle has been presented. In order to take the issue concerning associated plasticity into consideration the reduced effective friction angle, φ'_d, is calculated. This is done by the expression in Equation (5.9) [Ibsen et al., 2012].

$$\tan\left(\varphi'_d\right) = \frac{\sin\left(\varphi'\right)\,\cos\left(\psi\right)}{1-\sin\left(\varphi'\right)\,\sin\left(\psi\right)} \tag{5.9}$$

where

φ'_d	Reduced effective friction angle [°]
ψ	Angle of dilation [°]

In accordance with Bolton's theory the angle of dilation, ψ, can be calculated from the relative dilatancy index, I_R, by the use of Equation (5.10).

$$\psi = \varphi'_{tr} - \varphi'_{crit} = 3^\circ\, I_R \tag{5.10}$$

For the Bolton approach the reduced effective friction angle, φ'_d, will be used for further analysis. As for the case of the calculations using the expression by Mayne, the strength parameter will be assumed to be LogNormal distributed. The distributions will be presented in the following section.

5.1.4 Results (Bolton)

The MATLAB programme containing the calculations can be found in CD Appendix A.
In the following the results obtained from the seven CPTu's are presented for the effective friction angle, φ'_{tr}, will be presented at first. The calculation and fitting of a LogNormal distribution has resulted in the graph shown in Figure 5.5.

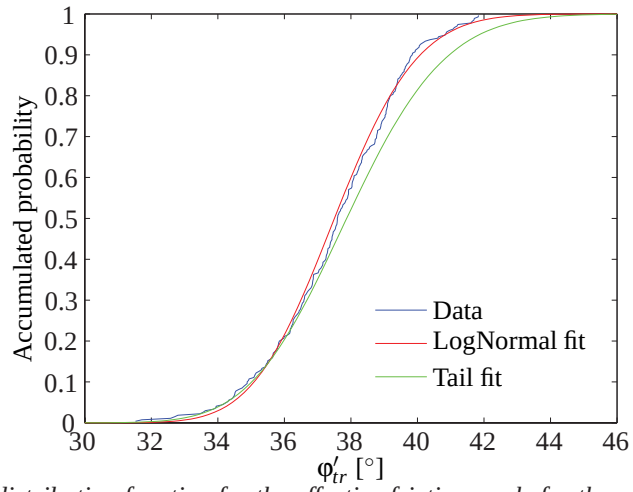

Figure 5.5: *Accumulated distribution function for the effective friction angle for the sand at the test site at Vulkanvej.*

Figure 5.5 shows that φ'_{tr} provides a rather good fit to the LogNormal distribution. From the fitted distributions the characteristics of the sand has been calculated and are presented in Table 5.3.

Table 5.3: *Characteristics of the effective friction angle using Bolton's theory. F = 0.05 is the 5% quantile found from the data set. *Values will not be used in the further analysis, but are presented to give an overall describtion of the characteristics leading to the 5% quantile for the tail fit.*

	$\mu_{\varphi'}$ [°]	$\sigma_{\varphi'}$ [°]	$\varphi'_{5\%}$ [°]	COV [-]	$F = 0.05$ [°]
LogNormal fit	37.56	1.95	34.44	0.05	34.26
Tail fit	37.95*	2.32*	34.25	0.06*	34.26
			$\tan(\varphi')$		
LogNormal fit	0.7703	0.0540	0.6848	0.07	0.6812
Tail fit	0.7783*	0.0642*	0.6773	0.08*	0.6812

The values in Table 5.3 are generally lower than those calculated using Mayne's method. This is expected primarily to be due to the fraction of silt that is taken into considerations by using Bolton's method. Though it should be mentioned, that caution should be used when comparing the two methods, as they both build on assumptions regarding different parameters. For instance the critical friction angle is set to be 33° for the Bolton approach. The calculations will be very sensitive for this assumption, since it is a constant term, that is added to the other contributions. Therefore triaxial tests should be performed prior to the calculations in order to specify this factor and to link a model uncertainty to the expression. Such have been omitted for this thesis.

The reduced effective friction angle, φ'_d, has also been evaluated using Equation (5.9). The resulting distributions are shown in Figure 5.6.

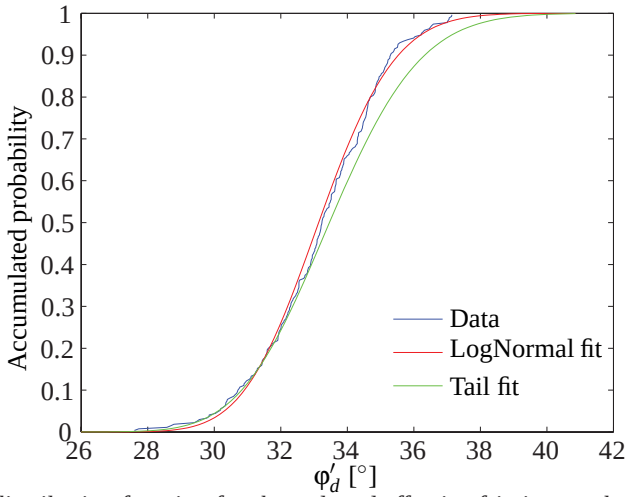

Figure 5.6: *Accumulated distribution function for the reduced effective friction angle for the sand at the test site at Vulkanvej.*

Again the characteristics of φ_d have been calculated, cf. Table 5.4.

Table 5.4: *Characteristics of the reduced effective friction angle using Bolton's theory. F = 0.05 is the 5% quantile found from the data set. *Values will not be used in the further analysis, but are presented to give an overall description of the characteristics leading to the the 5% quantile for the tail fit.*

	$\mu_{\varphi'}$ [°]	$\sigma_{\varphi'}$ [°]	$\varphi'_{5\%}$ [°]	COV [-]	$F = 0.05$ [°]
LogNormal fit	33.19	1.81	30.30	0.05	30.14
Tail fit	33.53*	2.15*	30.12	0.06*	30.14
			$\tan(\varphi')$		
LogNormal fit	0.6551	0.0449	0.5839	0.07	0.5807
Tail fit	0.6618*	0.0534*	0.5778	0.08*	0.5807

As expected from the visualisation of the reduced effective friction angle in Figure 5.2, the characteristics of this has been found to be lower in order to gain associated plasticity. As the results obtained for the reduced effective friction angle are in best compliance with the theory described in Section 5.1, the values from Table 5.4 will be used in the remaining of the thesis.

5.1.5 Comments and Discussion

In the above description of the sand characteristics the methods are used on the CPTu data without further concern. A few comments should be added, as the resulting characteristics have some physical difficulties.

From studies of sand characteristics, it is known that the effective friction angle has a minimum limit of 30°. This is the loosest deposit that can be observed [Ibsen, 2012]. When this is compared to the values found in Table 5.4 it is observed that the distribution of the reduced effective friction angle will include strength values, that are below this lower threshold. Therefore not all of the calculated reduced effective friction angles in the distribution will possess any physical meaning. In order to perform a proper description of the sand, these values should be excluded from the determination of the final characteristics.

Furthermore it should be noted that the calculation of the angle of dilation also has been performed without considering the physical aspects hereof. Again studies have shown, that sands, with an effective friction angle of 30° or less, do not dilate [Ibsen, 2012]. This is due to the very loose state the sands are in, when the effective friction angle becomes this low. Therefore it should be incorporated to ignore the angle of dilation calculated for the points with effective friction angles below 30°, in order to keep the physics of the nature intact.

The two aspects discussed above might rise question of the applicability of the used method. The mean calculated from the Bolton theory of 37.56° is in great agreement with expected values of a late glacial sands, which are in the range of 36-42° according to [Chr. Jensen, 2009]. Therefore it is more the combination of Bolton's theory and the calculation of the reduced effective friction angle, given by [Ibsen et al., 2012], that is questioned. Also the found angles of dilation was in between 0 - 12° with an average mean of 6.5°. Also this might seem rather high, when it is compared with the calculated mean of 37.56°. According to Equation (5.10) this will provide a critical friction angle of 31.06°, which is lower than the angle of 33° assumed from the beginning. With all this in mind it is important

to note, that the discussion presented here is only based on data from a single test site, and many more is needed in order to make any conclusive statements. One thing is for certain, which is that the theories should not be used in combination without great caution.

Although the above discussed matters are important for the description of the sand, the methods described in this chapter has been used without including these aspects. This will cause the characteristics to be lower of what could be expected of the real deposits. Nonetheless, it will not have any significant influence of the later treated issues, as they require a description of a sand, where a set of strength parameters is needed combined with a real measure of the spatial variation of the same soil. Therefore it has been found sufficient to continue with the presented characteristics in Table 5.4.

Chapter 6

Modelling of Cohesive Soil

In the following chapter the undrained shear strength, c_u, for the cohesive soil used for the probabilistic and deterministic design will be determined. For the deterministic design a 5% quantile will be determined, whereas for the probabilistic design a distribution of the strength parameter is sought. Furthermore, for the probabilistic design the correlation length will be determined for c_u in both horizontal and vertical direction, which is the topic of Chapter 8. The undrained shear strength is determined based on CPTu measurements, which will be described in the following.

6.1 Determination of Clay Characteristics

The clay modelled in the following has been described in Section 4.2. Before the characteristics of the clay will be calculated and presented a description of the observations and analysis of the results will be discussed.

6.1.1 Observations, Method and Assumptions

During the performance of the CPTu tests the project group visited the test site on March 26th 2012. This was done in order to inspect the test site and furthermore to see if there were any problems during the tests. An observation that is not detectable from the sets of CPTu data is the location of a layer of drop stones in the depth of 2.5 m from the top of the CPTu's, which is deposits from the melting ice. Additionally it was observed that the phreatic surface was located approximately 0.5 m below the surface, for which reason the clay is considered as saturated. Pictures from this field trip can be seen in CD Appendix A.

It was observed that the sleeve friction became too large, when the cone reached a depth of approximately 4 meters. This meant that CPTu measurements were stopped and a drilling was performed in order to continue CPTu measurements. This could indicate, that the clay possesses very high horizontal stresses, since the sleeve friction on the rods was this massive. The observation is in agreement with the expectations for the soil properties commented upon in Section 4.2, as Yoldia Clay is known to possess high horizontal stresses due to preconsolidation. From Figure 6.1 the soil profile from one of these necessary drills can be seen.

Figure 6.1: *The figure shows that there is sand in the top layer of the soil profile.*

It is observed that approximately the first meter consist of a sand layer, which also is confirmed by the bore hole profiles, see Appendix B. From observations of the test results it is clear that the soil is inhomogeneous. In the left part of Figure 6.2 the untreated data obtained from CPTu 10, see Figure 4.9 for placing, are shown. Here sudden peaks of the cone resistance are observed at approximately 0.3 and 4.5 m of depth. This in an indication of, that sand stripes are present in between the clay layers. In the ongoing analysis these peaks have been removed from the data set, as a description of a cohesive material is sought. After having discarded the peaks from the test results the data used for analysis are as presented in the right part of Figure 6.2.

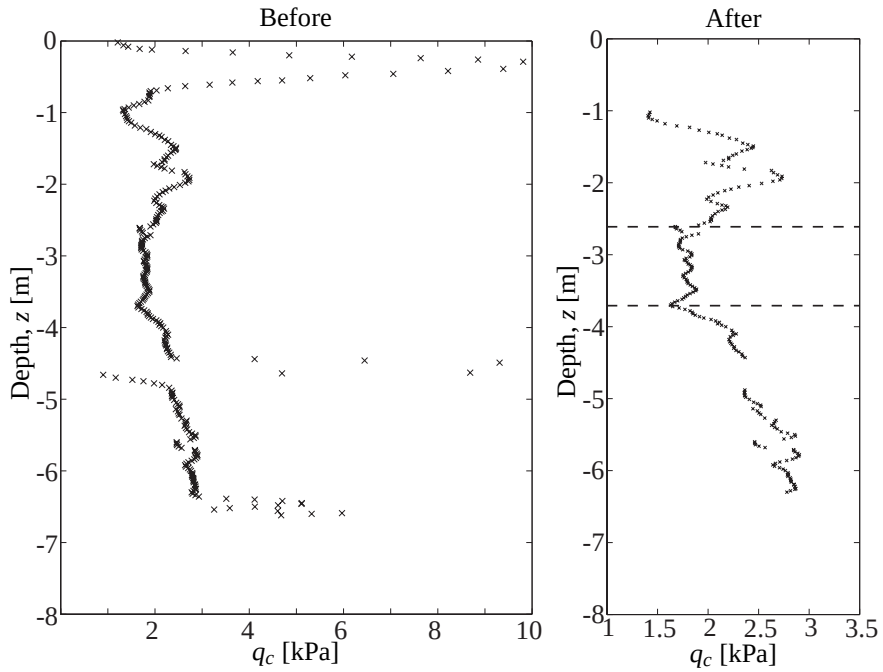

Figure 6.2: *Difference in unsorted and sorted data set. The example is from CPTu 10.*

To the right in Figure 6.2 two dashed lines have been drawn in order to indicate changes in the observed results, which might be caused by different layers. At the time of the writing of this thesis no laboratory tests have been performed

on the clay from Suderbovej, which is why the following explanation will be based on qualified judgement. The two top layers in Figure 6.2 does not have a regular increase of the cone resistance with depth as would be expected from normally consolidated clays. Therefore these layers are expected to be overconsolidated to some degree, which is in good accordance with the described Yoldia Clay, cf. Section 4.2. In the third layer the depth dependency of the cone resistance is quite obvious, which is why this layer is expected to be normally consolidated. The physical meaning of this is rather unclear, as normally consolidated layers are expected to be located above overconsolidated layers in general practice. One explanation to this could be that the area around Frederikshavn is known to have great geological activity, why different layers of soil could have been pushed on top of one another [Nordahl, 2012]. It is important to note, that the exact description of the happenings are not known, and will remain unknown until further analysis of the local soil has been carried out.

In Appendix C it is seen, that five out of the twelve CPTu's have a large change in the measured cone resistance at the depth of 4 m. An example of this is shown in Figure 6.3.

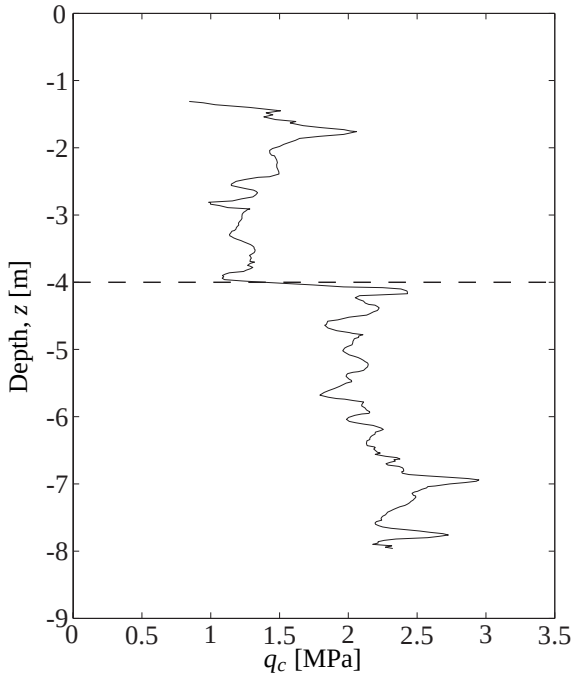

Figure 6.3: *Example of how the measurements change at 4 m of depth. Here CPTu 6 is shown with sand layers discarded.*

The change in the measurements are suspected to be due to one of the two following reasons: One opportunity might be that the a change of the soil properties is present around this level. If this is the actual situation similar results are expected for the CPTu's located next to the ones showing the change. If the locations of the CPTu's, cf. Figure 4.9, is compared to the CPTu's experiencing the significant change of cone resistance, cf. Appendix C, it is found that they are not located right next to one another. In fact CPTu's without the change at 4 m of depth are located in between CPTu's which experience the change. Therefore this opportunity seems unlikely. Although it should be mentioned that local soil deposits may be present at various location, which could cause the great changes. The second opportunity is that when the execution of the tests was interrupted at 4 m of depth, when drilling of the first 4 m was necessary in order to continue the test, some technical disturbance of the equipment might have resulted in differences of the measured results. Once again more classification tests are needed in order to describe the soil properly.

Finally some peculiar observations are made for the pore pressure data. In Figure 6.4 an example of this is shown and will be commented upon in the following.

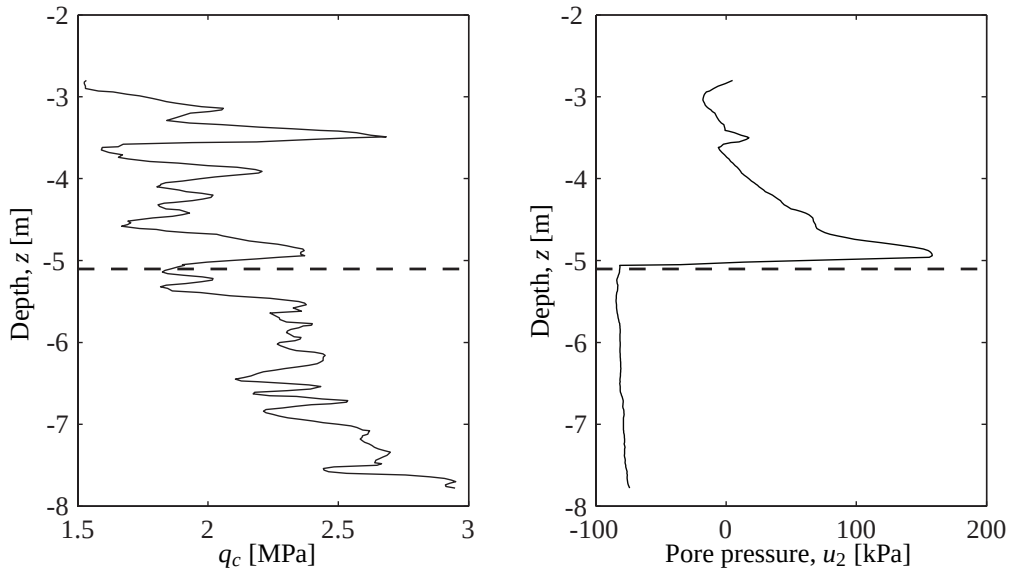

Figure 6.4: *Illustration of the peculiar measurements of the pore pressure. The data is from CPTu test number 12.*

The dashed line in Figure 6.4 marks the dramatic changes in pore pressure that was observed. The line therefore could be an indication of a change in the soil structure. Although from the right part of Figure 6.4 an increase in pore pressure is observed until it drops down below zero. This could be an indication of the soil changing from a cohesive material to a friction material although the pore pressure should only be reduced to zero, unless capillary stresses are present. This is not consistent with the observation from the bore profiles nor the left part of Figure 6.4, where, what could be, normally consolidated clay is observed below the dashed line. Furthermore, Per Brøndrum from Grontmij, who was in charge of the execution of the tests, expressed his concern of the measured pore pressure, as the values were unpredictable and unusual. He indicated that the equipment for measuring the pore pressure might have suffered defects. This is considered as the most likely reason for this behaviour.

Treatment of Data for Further Analysis

Based on the above explained observation choices have been made for the further analysis. In the following analysis only the description of a clay is of interest. It is important to note, that it is not a design situation that will be considered in the remaining of the thesis, but an investigation of the gains and advantages that can be seen in attachment to a probabilistic approach rather than a deterministic approach. This have influenced the decisions to some extent.

As the subdivision of the different layers are not fully investigated, all the data expected to contain clay has been used in the following. This means that what might be normally consolidated and overconsolidated clay are mixed in the following. This will add a larger standard deviation for the characteristics of the clay, as their mean strength parameter are approximately the same. Furthermore the change in cone tip resistance found at 4 m of depth has been treated in the following way. The mean value of all the CPTu's performed has been found to be around 2 MPa. Therefore it has been chosen to exclude the upper or the lower part of the datasets, that experience the dramatic

change at 4 m of depth, that deviates the most from the calculated mean of 2 MPa.

Furthermore the top 1-3 m has been removed from all the CPTu's as they contained frictional and organic materials.

As only limited data was collected from CPTu number 11, cf. Appendix C, and the results are questionable, CPTu number 11 has been discarded from further work.

All the sorted data that is a part of the further analysis can be reviewed in Appendix D.

Regarding the measured pore pressures, it has been chosen to use the uncorrected cone resistance for the further analysis of the data and calculation of the undrained shear strength, c_u. The undrained shear strength, c_u, will be determined from Equation (6.1).

$$c_u = \frac{q_c - \sigma_{v0}}{N_c} \tag{6.1}$$

where

c_u	Undrained shear strengh [kPa]
q_c	Cone resistance [kPa]
σ_{v0}	In-situ vertical stress [kPa]
N_c	Theoretical cone factor [-]

The raw data from the CPTu measurements can be found in CD Appendix A.

In order to obtain an appropriate cone factor, N_c, for the given location a calibration will be performed. The cone factor will be calibrated in accordance with a shear vane test performed right next to bore hole 1 at the location specified in Section 4.2. The values have been delivered by Grontmij, who performed the CPTu tests at Suderbovej. The provided strength values and corresponding depths are presented in Table 6.1. [Grontmij, 2012]

Table 6.1: *Undrained shear strength provided by Grontmij.*

Depth [m]	Shear strength, c_v [kPa]
2.8	140
3.8	112
4.8	126
5.8	266
6.8	224
7.8	168

In Table 6.1 a large change in values of the undrained shear strength are detected between 4.8 and 5.8 m of depth. This could indicate a change of layers in the stratigraphy. Due to the concerns explained previously when describing the measurements of the cone resistance, the possibility of a new layer has been neglected in what to come. The

values in Table 6.1 are considered as the exact values in the calibration of the cone factor. For the calibration of the cone factor the five measurements nearest the depth of the value obtained from the shear vane test will be averaged and compared to the values in Table 6.1. When determining the cone factor uncertainties are present as well. This includes uncertainties in connection with the measurements, model uncertainty and statistical uncertainty as the number of calibration points is sparse, cf. Chapter 2. A minimum number of samples needed in order to determine the cone factor within a given confidence interval could have been calculated as well. This has been omitted, as no further shear vane tests will be performed.

In order to verify the shear strengths obtained from the shear vane tests additional vertical load tests or similar should be performed, from which precise values of the cohesive strength can be calculated. The last aspect is out of the scope of this thesis as well.

In the results presented below the failure domain for the design case is considered. In Chapter 3 and 12 the loading and foundation is specified, which is considered when determining the characteristics of the soil in this chapter. It is assumed that the failure reach a depth of half the foundation diameter, which is determined to 13.82 m in Chapter 12. Therefore only soil measurement for the depth of interest is analysed to avoid too strong strength characteristics as a result of strength increase with depth.

Two different characteristics are needed for the clay. One should be very similar to the one describing the sand, where a single mean value and standard deviation describes the entire soil volume. This approach is needed for the deterministic calculation with characteristic values. An additional description of the characteristics are needed for the modelling of the stochastic field. Here the depth dependency should be taken into account, and the standard deviation will be found, when the trend is subtracted from the calculated strength parameters. [DNV, 2010] describes a method for handling soil parameters that are subject to depth dependency, which is described in Appendix E.

6.1.2 Results

The MATLAB programme containing the calculations can be found in CD Appendix A. At first the found value of the cone factor, N_c, will be presented in Table 6.2.

Table 6.2: *Characteristic values of the undrained shear strength observed from the CPTu-tests.*

N_c
[-]
10.35

Great uncertainty is connected to this calibration, as only one shear vane test is performed and compared to one CPTu test. In spite of this, the value found in Table 6.2 is around the expected value for a Danish clay, which has an expected value of 10. Therefore the value will be used without further considerations.

Characteristics Without Subtracting Depth Dependency

The described method for determining the undrained shear strength has been implemented in a MATLAB code, in which the measurements from the CPTu's have been analysed. The gathering of the calculated values has resulted in the LogNormal distribution and according tail fit as presented in Figure 6.5.

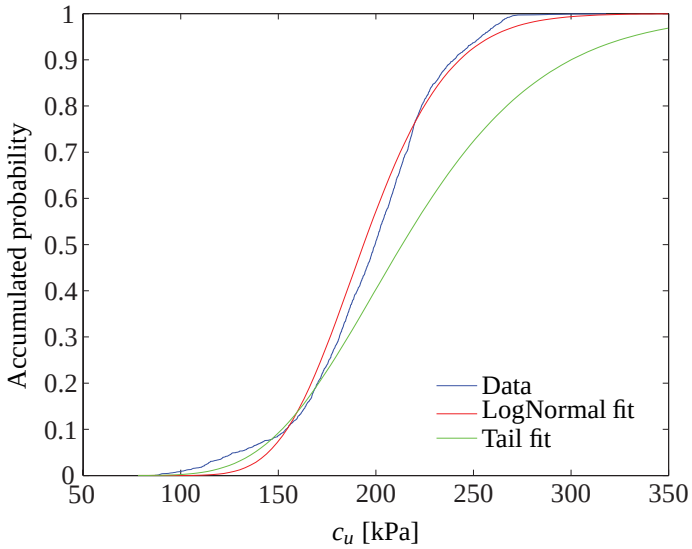

Figure 6.5: *Accumulated distribution function for the undrained shear strength at the test site at Suderbovej.*

The lower tail - i.e. lowest 10% - of the data set differs from the LogNormal fit. The irregularity is seen in the light of the used definition of the population used for determining the distribution. The population includes all the measured values found for the different CPTu tests performed at the location, after having performed the sorting of the data as described in the previous section. The lower values observed in Figure 6.6 are primarily originating from CPTu 4, where the measured cone resistance is found to be approximately 20% lower than the average trend. By excluding the measurements from CPTu 4 the distribution becomes more regular as depicted in Figure 6.6.

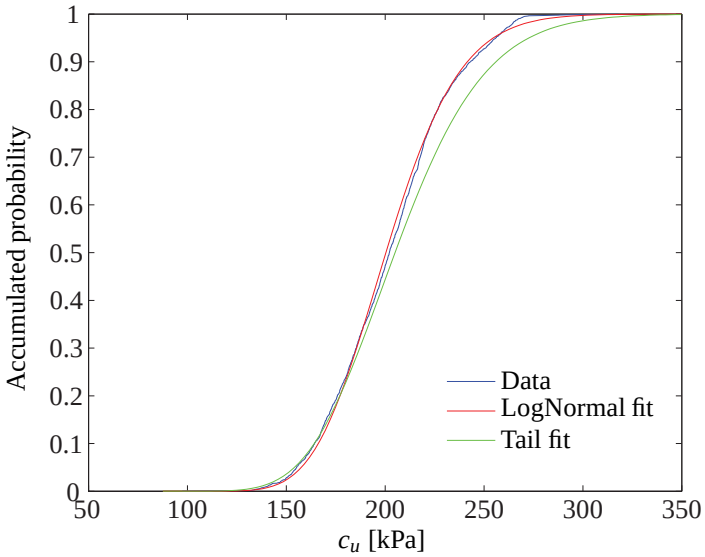

Figure 6.6: *Accumulated distribution function for the undrained shear strength at the test site at Suderbovej. CPTu number 4 has been excluded.*

Despite of the more regular distribution observed by excluding the measurements from CPTu 4, it has been chosen to use the characteristics observed from Figure 6.5, as this will provide a better description of the soil strength as a whole for the location. The distributions presented have resulted in the following characteristics of the clay presented in Table 6.3.

Table 6.3: *Characteristics of the undrained shear strength observed from the CPTu-tests. F = 0.05 is the 5% quantile found from the data set. *Values will not be used in the further analysis, but are presented to give an overall description of the characteristics leading to the 5% quantile for the tail fit.*

	μ_{c_u}	σ_{c_u}	$c_{u,5\%}$	COV	$F = 0.05$
	[kPa]	[kPa]	[kPa]	[-]	[kPa]
LogNormal fit	195.2	34.8	143.6	0.18	128.2
Tail fit	219.4*	59.5*	136.7	0.27*	128.2

In Table 6.3 it is observed that 5% quantile found from the data set is considerable lower than the one calculated from the LogNormal fit, $c_{u,5\%}$. This is due to the low values from CPT number 4, which influences the low values of the plotted data in Figure 6.5. Nonetheless, it has been chosen to use the value for $c_{u,5\%}$ in the following work.

Characteristics Corrected for Depth Dependency

For the stochastic field modelling the depth dependency is modelled. Therefore the method described in Appendix E is applied in order to gain the characteristics presented in Table 6.4.

Table 6.4: *Characteristic values of the undrained shear strength for stochastic field modelling.*

a_0	a_1	σ_{c_u}
[kPa]	[kPa/m]	[kPa]
164.0	8.9	30.9

Here a_1 describes the increase in undrained shear strength along the depth, a_0 is the intercept with the soil surface and σ is the constant standard deviation along the depth. These results are further used in Chapter 13.

Chapter 7

Design Strength Parameters

In the following chapter the design strength parameters used in the deterministic design will be presented. In [Eurocode 0, 2007] it is stated that the characteristic value of the strength or the bearing capacity should correspond to the 5% quantile. In Appendix F it has been investigated, what influence the choice will have on the characteristic bearing capacity. In this project it is chosen to use the 5% quantile of the strength in the design of the foundation, as this is what is done in common engineering practice [Sørensen, 2012].
The characteristic effective friction angle is determined as the 5% quantile of the distribution determined in Chapter 5, which is presented again to set the record straight.

Table 7.1: *Characteristic effective friction angle.*

Parameter	Symbol	Value	Unit
Characteristic effective friction angle	φ'_c	30.30	°

The design value of the effective friction angle is determined on behalf of the partial safety factor of 1.25 as presented in Table 3.1. The design value can be determined from Equation (7.1).

$$\varphi'_d = \tan^{-1}\left(\frac{\tan(\varphi'_c)}{\gamma_{\varphi'}}\right) \tag{7.1}$$

where

φ'_c | Characteristic effective friction angle °

This leads to the design effective friction angle shown in Table 7.2.

Table 7.2: *Design effective friction angle.*

Parameter	Symbol	Value	Unit
Design effective friction angle	φ'_d	25.05	°

The characteristic undrained shear strength, $c_{u,c}$, is presented in Table 7.3.

Table 7.3: *Characteristic undrained shear strength.*

Parameter	Symbol	Value	Unit
Characteristic undrained shear strength	$c_{u,c}$	136.7	kPa

The design value of the undrained shear strength is determined from Equation (7.2).

$$c_{u,d} = \frac{c_{u,c}}{\gamma_{c_u}} \tag{7.2}$$

This leads to the design value shown in Table 7.4.

Table 7.4: *Design undrained shear strength.*

Parameter	Symbol	Value	Unit
Design undrained shear strength	$c_{u,d}$	98.5	kPa

Chapter **8**

Estimation of Correlation Lengths

The main topic of this chapter is spatial analysis of the measurements from the CPTu tests performed on both sand and clay. The purpose is to gain knowledge about the correlation lengths. The correlation length is a measure of the distance beyond which soil parameters are largely uncorrelated. Knowledge about the correlation length can help determining which strength quantile to use in design. For estimation of the correlation length of the strength parameters two methods described in [Baker, J. and Calle, E, 2006] are applied. Two methods for estimating the correlation length are presented in the following. The first method uses trend coefficients and is used to estimate the correlation length in both horizontal and vertical direction, whereas the second method, based on semivariograms, is used for estimation of the vertical correlation length and serve as a verification for the first method.

8.1 Estimation using Trend Coefficients

This method uses field observations and the mutual geometry as a basis for determining the mean value trend and statistics for the soil field. It is assumed that the field tests have mean values that changes with depth and further, the correlation length is assumed to be the same in any horizontal direction. The method is applicable for both frictional and cohesive soils. In the following the method is presented for frictional soil.

8.1.1 Method and Assumptions

The expected mean value trend in any geometric point of the considered soil volume, can be described by applying Equation (8.1).

$$m_p(\underline{x}) = \underline{\hat{a}}^T \, \underline{\underline{F}}(z) \tag{8.1}$$

where

$m_p(\underline{x})$	Expected mean value trend in any geometric point [°]
$\underline{\hat{a}}$	Estimator of trend coefficient vector, $\underline{a}$ [°]
$\underline{\underline{F}}(z)$	Shape function values at the depth, z [-]

The trend coefficients can be estimated using Equation (8.2).

$$\underline{\hat{a}} = \left(\underline{\underline{F}}^T \, \underline{\underline{R}}^{-1} \, \underline{\underline{F}}\right)^{-1} \underline{\underline{F}}^T \, \underline{\underline{R}}^{-1} \, \underline{P} \tag{8.2}$$

where

$\underline{\underline{R}}$	Correlation matrix [-]
$\underline{P}$	Sample values [°]

The correlation coefficients are calculated from Equation (8.3) keeping in mind that the horizontal correlation length is unaffected by the direction.

$$\underline{\underline{R}}(i,j) = \exp\left(-\frac{\sqrt{\Delta x_{i,j}^2 + \Delta y_{i,j}^2}}{D_h} - \frac{|\Delta z_{i,j}|}{D_z}\right) \tag{8.3}$$

where

D_h	Horizontal correlation length [m]
D_z	Vertical correlation length [m]

Shape functions are needed in order to estimate both the expected mean value trend and the trend coefficients. These are assumed linear because of the assumed linear trend of the strength value along the depth.

$$\begin{aligned} \underline{\underline{F}}(i) &= [\underline{F}_1(z_i) \quad \underline{F}_2(z_i)] \\ \underline{F}_1(z_i) &= \frac{z_i}{z_{max}} \\ \underline{F}_2(z_i) &= 1 - \frac{z_i}{z_{max}} \end{aligned} \tag{8.4}$$

where

i	Sample number [-]
z_i	Depth coordinate of sample i [m]
z_{max}	Depth coordinate of deepest sample [m]

Further the variance is determined from Equation (8.5) and it is assumed constant with depth.

$$\hat{\sigma}^2 = \frac{1}{n-m}\left(\underline{P} - \underline{\underline{F}}\,\underline{\hat{a}}\right)^T \underline{\underline{R}}^{-1}\left(\underline{P} - \underline{\underline{F}}\,\underline{\hat{a}}\right) \tag{8.5}$$

where

$\hat{\sigma}^2$	Estimator of field variance, σ^2 [°]
n	Number of sample points [-]
m	Number of shape functions [-]

The correlation coefficients can be obtained from the likelihood expression given in Equation (8.6) as the fluctuating field is considered normally distributed.

$$L_{f_p}(\underline{P};\underline{D}) = \frac{\exp(-\frac{1}{2}(N-M))^{\frac{N}{2}}}{(2\pi)^{\frac{N}{2}}\sqrt{det(\underline{\underline{R}})}\left(\underline{P}^T\left(\underline{\underline{R}}^{-1} - \underline{\underline{R}}^{-1}\underline{\underline{F}}\left(\underline{\underline{F}}^T\underline{\underline{R}}^{-1}\underline{\underline{F}}\right)^{-1}\underline{\underline{F}}^T\underline{\underline{R}}^{-1}\right)\underline{P}\right)^{\frac{N}{2}}} \tag{8.6}$$

Handling a large number of data from the CPTu tests makes the likelihood expression unstable when using numerical computation in e.g. MATLAB. By raising to the power of N/2, where N is in the order of 1,500 - 2,600, MATLAB

assumes infinite numbers. But as the numerator and the first term in the denominator are constants for any combination of the correlation lengths and therefore not a part of the optimisation process, these terms can be replaced by a constant. Another problem arises when handling a great amount of data. The correlation matrix, $\underline{\underline{R}}$, becomes very large and with low values in most entries. Therefore MATLAB returns the value 0, when calculating the determinant of $\underline{\underline{R}}$. Excluding the term $\sqrt{\det(\underline{\underline{R}})}$ leaves an expression that can be handled by taking the natural logarithm, although the degree of accuracy by excluding this term is unknown. Equation (8.6) is then expressed as Equation (8.7).

$$L_{f_p}(\underline{P};\underline{D}) = \frac{1}{\ln\left(\underline{P}^T\left(\underline{\underline{R}}^{-1} - \underline{\underline{R}}^{-1}\underline{\underline{F}}\left(\underline{F}^T\underline{\underline{R}}^{-1}\underline{\underline{F}}\right)^{-1}\underline{F}^T\underline{\underline{R}}^{-1}\right)\underline{P}\right)\ln\left(\frac{N}{2}\right)} \tag{8.7}$$

8.1.2 Results for the Sand at Vulkanvej

The MATLAB programme containing the calculations for the correlation lengths using trend coefficients can be found in CD Appendix A. For analysis of the sand at Vulkanvej, the seven sorted CPTu tests are used. The resulting correlation lengths are presented in Table 8.1, where it is clear that short correlation lengths are present in both vertical and horizontal direction (optimum in bold). The analysis is initially made with a much greater difference in correlation length and the presented results are limited to the results just around the optimum.

Table 8.1: *Correlation lengths for the sand at Vulkanvej.*

D_z [m]	D_h [m]	a_1 [°]	a_2 [°]	$\hat{\sigma}$ [°]	MLM [-]
2.0	0.06	38.10	41.91	0.6709	0.022781
2.0	0.09	38.12	41.87	0.6456	0.023050
2.0	0.12	38.14	41.83	0.6578	0.022917
2.5	0.06	38.10	41.90	0.6707	0.022792
2.5	**0.09**	**38.13**	**41.86**	**0.6455**	**0.023051**
2.5	0.12	38.15	41.82	0.6578	0.022918
3.0	0.06	38.11	41.88	0.6708	0.022781
3.0	0.09	38.13	41.84	0.6457	0.023049
3.0	0.12	38.15	41.80	0.6580	0.022915
3.5	0.06	38.12	41.86	0.6713	0.022776
3.5	0.09	38.14	41.81	0.6463	0.023041
3.5	0.12	38.16	41.77	0.6588	0.022907

Here a_1 and a_2 denotes the expected value in the top and the bottom of the layer respectively. For this analysis the maximum likelihood estimation coincides with the lowest field standard deviation even though the term with $\sqrt{\det(R)}$ is excluded. When observing the expected values great divergence is noted compared to what was calculated in Chapter 5. This might be due to the fact, that the assumption of linear trend along the depth is not well fulfilled.

Further comments on the results include that the method is very sensitive to the input. Calculating, inverting and taking the determinant of matrices in the size of 2,600 x 2,600 with values close to zero in the majority of the entries

gives rise to problems with the likelihood expression. Reducing the number of data for analysis gives more stable calculations, but averaging the soil parameters to use fewer data has an influence on the result as well. The obtained correlation lengths gets larger with greater averaging.

Nonetheless, very low correlation lengths are calculated and to support these calculations an empirical semivariogram will be used to verify the vertical correlation lengths, cf. Section 8.2.

8.1.3 Results for the Clay at Suderbovej

For the analysis on clay the corrected CPTu tests from Chapter 6 are used. In Table 8.2 the results are highlighted. The vertical correlation length is 0.15 m and the horizontal is between 0.12 and 0.16 m dependent of whether $\hat{\sigma}$ or MLM is used as optimisation criterion.

Table 8.2: *Correlation lengths for the clay at Suderbovej.*

D_z [m]	D_h [m]	a_1 [kPa]	a_2 [kPa]	$\hat{\sigma}$ [kPa]	MLM [-]
0.8	0.09	223.9	157.4	25.99	0.021429
0.8	0.12	223.6	157.6	25.17	0.036687
0.8	0.15	223.3	158.0	24.99	0.13733
0.8	0.18	223.0	158.3	25.18	-0.082474
1.2	0.09	224.2	156.7	25.78	0.022228
1.2	0.12	223.9	156.9	25.01	0.039277
1.2	**0.15**	**223.6**	**157.2**	**24.86**	**0.18435**
1.2	0.18	223.3	157.4	25.08	-0.071354
1.6	0.09	224.2	156.5	25.79	0.023748
1.6	0.12	224.0	156.7	25.05	0.044711
1.6	**0.15**	**223.7**	**156.9**	**24.93**	**0.4516**
1.6	0.18	223.5	157.2	25.19	-0.057826
2.0	0.09	224.2	156.7	25.97	0.026018
2.0	0.12	224.0	156.8	25.28	0.054307
2.0	0.15	223.7	157.0	25.18	-0.529
2.0	0.18	223.5	157.3	25.45	-0.046532

An example of the rather unstable likelihood expression is present from the analysis on clay, where the value goes from a maximum to a negative value and if the correlation lengths are increased the expression equals zero whereas the $\hat{\sigma}$ term remains stable.

8.2 Estimation using Empirical Semivariogram

Another way of estimating the correlation length is to use semivariogram. In the following only the vertical correlation is analysed in order to compare with the correlation lengths found in the previous section.

8.2.1 Method and Assumptions

Spatial dependency is calculated through the empirical semivariogram described in [Baker, J. and Calle, E, 2006], where the semivariogram is denoted $\gamma(\tau)$ and follows from Equation (8.8). As the soil deposit has a trend in vertical direction, this trend is subtracted before analysing the CPTu tests. The trend is assumed linear and for each CPTu a linear fit is made for describing the local trend. It is further assumed that the used data is from a statistical homogeneous population. This is sought through sorting the data as described in Chapter 5 and 6.

When describing the method in the following the soil parameter used is the effective friction angle, which is the desired parameter when analysing the sand site at Vulkanvej. For analysis on clay, this parameter is simply replaced with the undrained shear strength in the following equations.

$$\gamma(\tau) = \frac{1}{2} Var\left(\varphi'(d) - \varphi'(d+\tau)\right) \tag{8.8}$$

where

γ	Semivariogram [$^\circ$]
τ	Distance between sample points [m]
φ'	Effective friction angle [$^\circ$]
d	Depth [m]

Equation (8.9) shows a relation between the semivariance and the well-known autocorrelation function, $\rho_{\varphi'}(\tau)$.

$$\gamma(\tau) = (1 - \rho_{\varphi'}(\tau))\,\sigma^2_{\varphi'} \tag{8.9}$$

where

$\rho_{\varphi'}$	Autocorrelation function for the effective friction angle [-]
$\sigma^2_{\varphi'}$	Variance of effective friction angle for the CPTu test [$(^\circ)^2$]

In order to calculate an empirical estimate of the semivariogram Equation (8.10) is used.

$$\gamma^*(\tau) = \frac{1}{2n(\tau)} \sum_{i}^{n(\tau)} (\varphi'(d_i) - \varphi'(d_i+\tau))^2 \tag{8.10}$$

where

γ^*	Empirical semivariogram [$^\circ$]
$n(\tau)$	Number of pairs with distance τ [-]

It is noted that a suitable number of pairs are needed for each τ in order to have a reliable estimate. By combining Equation (8.9) and (8.10) it is possible to plot the semicovariance function and thereby determine the correlation length.

8.2.2 Results for the Sand at Vulkanvej

The MATLAB programme containing the calculations for the correlation lengths using an empirical semivariogram can be found in CD Appendix A. The described method leads to the plots shown in Figure 8.1 and 8.3 where both satisfactory and dissatisfactory results are presented. The appertaining effective friction angles are shown in connection to the semicovariance plots in order to get an impression of the data's influence on the determination of the correlation length. The remaining plots are shown in Appendix G. As the correlation length is an estimate of the distance beyond which the parameter in question is largely uncorrelated, the correlation length is read where the graph reach and flattens around the value of 1.

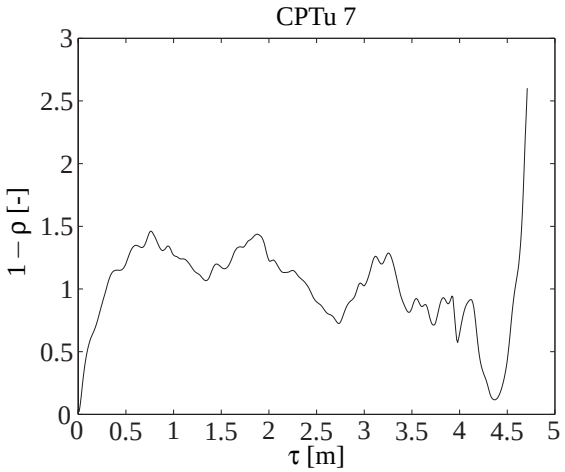

Figure 8.1: *Example of semicovariance function with expected tendency and stable value.*

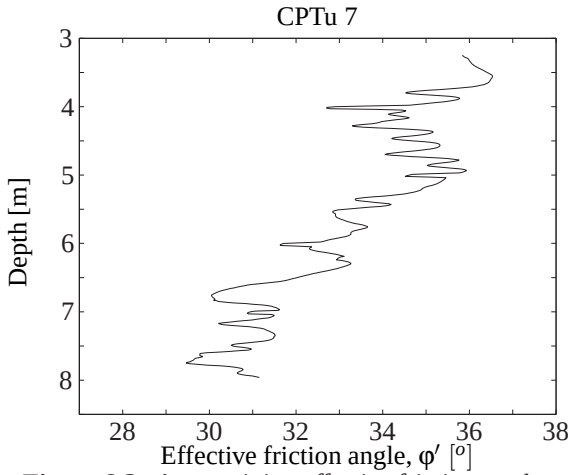

Figure 8.2: *Appertaining effective friction angles from CPTu test.*

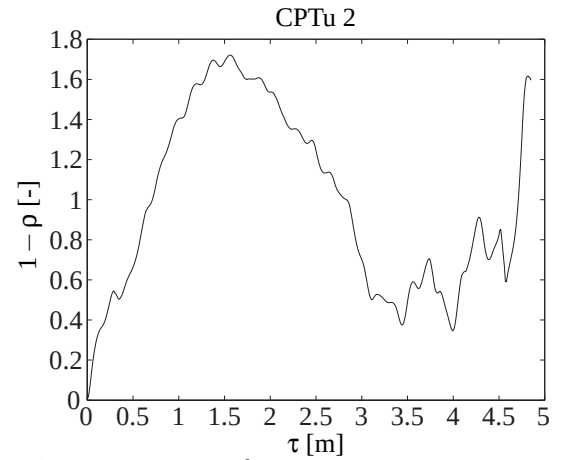

Figure 8.3: *Dissatisfactory semicovariance function for detecting vertical correlation length.*

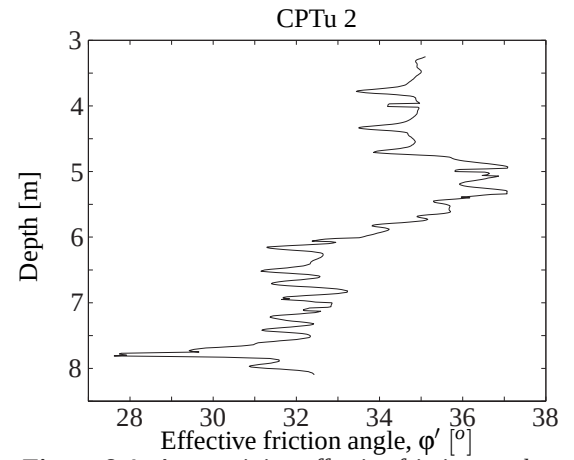

Figure 8.4: *Appertaining effective friction angles from CPTu test.*

As shown in the figures above and in Appendix G some CPTu tests provide fair results, and it is clear that small vertical correlation lengths are present. Other CPTu provide results that are impossible to conclude on. It is observed that there is an agreement between the regular, low fluctuating CPTu tests and good plots for the semivariograms. Opposite a connection between CPTu tests with heavy fluctuation and poor semivariogram plots is observed. This leads back to the assumption concerning linear trend in the depth direction. As can be seen from the plots of the soil strength along the depth divergence from a regular linear trend is observed.

It is concluded that the vertical correlation length is in the order of 0.1 - 0.5 m, which is in good agreement with the observation found by the use of the method using trend coefficients. Therefore the horizontal correlation length estimated to 2.5 m in Section 8.1 is considered reliable as well. The final correlation lengths are presented in Table 8.3.

Table 8.3: *Estimated correlation lengths for the used sand.*

D_z	D_h
[m]	[m]
0.1 - 0.5	2.5

8.2.3 Results for the Clay at Suderbovej

The results for the clay site is poor compared to the sand site. Practically no CPTu test provide fully satisfactory results, where the semicovariance function increase to and oscillate about 1. Some plots show the correct shape as Figure 8.5 and other shows random shapes as Figure 8.7.

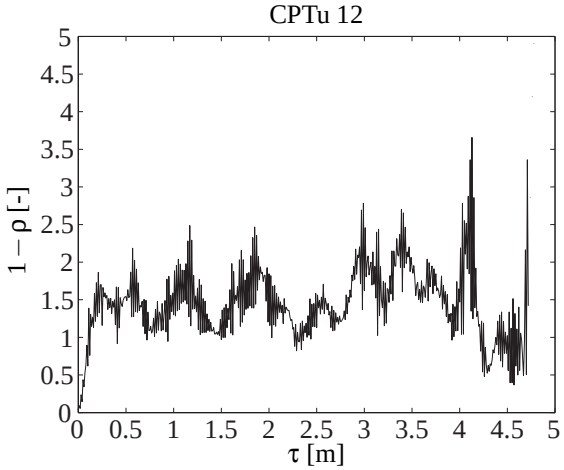

Figure 8.5: *Example of semicovariance function with expected tendency but unexpected stable value.*

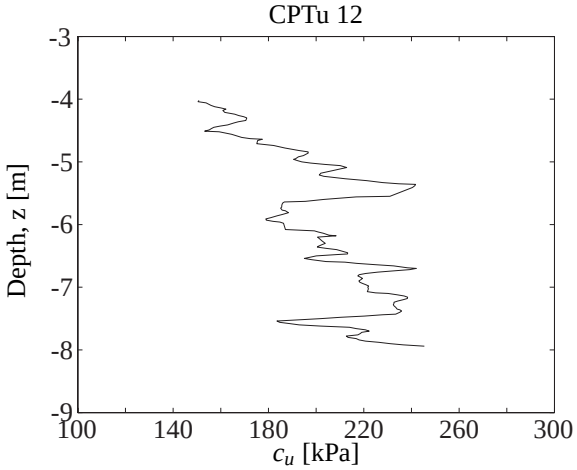

Figure 8.6: *Appertaining effective friction angles from CPTu test.*

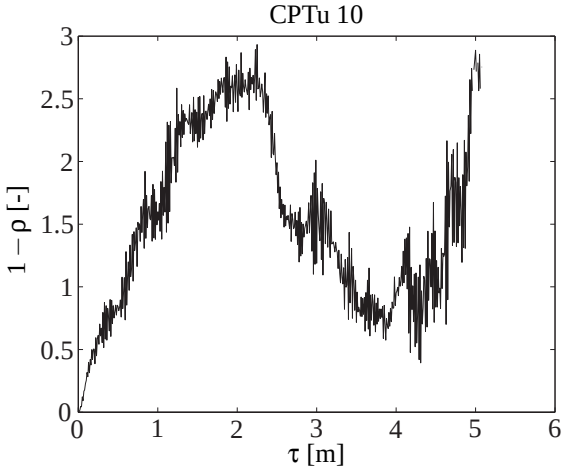

Figure 8.7: *Dissatisfactory semicovariance function for detecting vertical correlation length.*

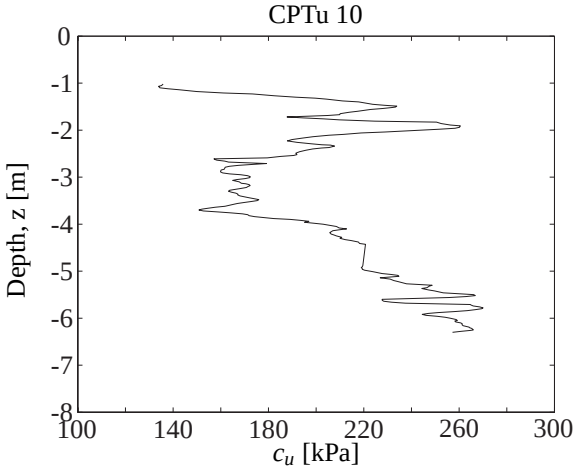

Figure 8.8: *Appertaining effective friction angles from CPTu test.*

It is observed from all plots, see Appendix G, that it is difficult to treat CPTu data from a test site so that reliable correlation lengths can be detected. Same remarks concerning non-fulfilled assumptions as in Section 8.2.2 are noted. Nevertheless, short vertical correlation lengths are indicated in the plots. Few plots show a correlation length in the order of 1 - 1.5 m, whereas the main picture leaves a correlation length below 0.5 m and even as low as 0.1 m. This is coinciding with the method used in Section 8.1 that indicated a vertical and horizontal correlation length on 0.15 m and approximately 1.5 m, respectively. For further use correlation lengths are as follows from Table 8.4.

Table 8.4: *Estimated correlation lengths for the used clay.*

D_z	D_h
[m]	[m]
0.15	1.5

8.3 Concluding Remarks

To summarise, it is clear that methods for estimating the correlation lengths at the test sites used in this thesis are rather difficult to apply. Divergence from earlier calculated trends is present for the estimated trends in this chapter. Further, expressions for finding the optimum of the correlation lengths are manipulated in order to achieve stable values.

Using the semivariogram for estimating the correlation lengths different results are found. Some of the CPTu test provide expected results, but just as many shows unexpected results. It is shown that there is a great connection between acceptable semicovariance plots and CPTu test with a low degree of fluctuation and a clear linear tendency. Therefore the methods used are considered sensitive to input from CPTu tests.

In addition to the above mentioned, it is important to note that analysis in this project are made on only two test sites with rather inhomogeneous deposits, so a generalisation of the problem should be avoided. In spite of the complications in the analyses, all calculations suggest very small correlation length, which is why the presented results in Table 8.3 and 8.4 are accepted and used for further analysis.

Part III

Calculations of two Approaches for Frictional Soil

In the following part the frictional soil described in Chapter 5 will be treated. An analytical model suggested by [DNV/Risø, 2010] will be used to determine the necessary dimensions of the foundation in order to withstand the loads described in Chapter 3. The model uncertainty connected to the analytical model will be determined through a comparison with simulations performed in the 2D numerical programme LimitState:Geo. A reliability index of the foundation will be determined through the First Order Reliability Method (FORM), which is done with the use of standard values of partial safety factors. The partial safety factor for the effective friction angle, $\gamma_{\varphi'}$, will be calibrated in order to ensure that a given target reliability is obtained. Hereby a measure of the potential of probabilistic design is obtained through a tangible parameter.

Chapter 9

Analytical Approach for Frictional Soil

In the following chapter the analytical approach for calculating the necessary dimension of the foundation will be performed in accordance with the expressions given by [DNV/Risø, 2010]. There the bearing capacity formulas proposed by Terzaghi are considered.

9.1 Application of the Terzaghi Bearing Formula

Slightly different formulations of e.g. the bearing capacity factors, N_i, are used in different codes. In the following formulas described by [DNV/Risø, 2010] will be used.

9.1.1 Method and Assumptions

The Terzaghi formulation for homogeneous soil in drained conditions is shown in Equation (9.1). The formula also goes under the name Rupture 1, to which reference will be made later in the thesis.

$$R_d = \left(c'_d \, N_c \, s_c \, i_c + q' \, N_q \, s_q \, i_q + \frac{1}{2} \gamma' \, B' \, N_\gamma \, s_\gamma \, i_\gamma \right) A' \tag{9.1}$$

where

R	Vertical design bearing capacity at the bottom of the foundation [kN]
c'_d	Design value of effective cohesion [kPa]
N_c, N_q, N_γ	Bearing capacity factors, cf (9.6) [-]
s_c, s_q, s_γ	Shape factors [-]
i_c, i_q, i_γ	Factors taking the inclination of the load into account [-]
q'	Effective overburden pressure at the bottom of the foundation [kPa]
γ'	Effective specific weight of the soil, cf. Table 4.1 [kN/m^3]
B'	Effective or equivalent width of the foundation [m]
A'	Effective area of the foundation [m^2]

As the soil will be considered as a pure frictional material, the term including cohesion can be excluded. Also no overburden pressure will be present at the sides of the foundation, as a surface footing is considered. Therefore the term describing the effective overburden pressure is excluded as well. Hereby the bearing capacity can be reduced to Equation (9.2).

$$R_d = \frac{1}{2} \gamma' \, b' \, N_\gamma \, s_\gamma \, i_\gamma \, A' \tag{9.2}$$

The effective width of the foundation, A', which takes the moment induced eccentricity into account, are calculated from Equation (9.3) for circular foundations.

$$A' = 2\left(R^2 \arccos\left(\frac{e}{R}\right) - e\sqrt{R^2 - e^2}\right) \tag{9.3}$$

where

R	Radius of foundation [m]
e	Eccentricity [m]

The eccentricity, e, is calculated from Equation (9.4).

$$e = \frac{M_d}{V_d} \tag{9.4}$$

where

M_d	Design moment load [kNm]
V_d	Design vertical load [kN]

The effective width, B', can be found from Equation (9.5).

$$B' = \frac{L}{L_e} B_e \tag{9.5}$$

where

$$B_e = 2(R - e) \quad , \quad L_e = 2R\sqrt{1 - \left(1 - \frac{B_e}{2R}\right)^2} \quad \text{and} \quad L = \sqrt{A'\frac{L_e}{B_e}}$$

where

B_e	Equivalent width of the foundation [m]
L_e	Equivalent length of the foundation [m]

The bearing capacity factor, N_γ, for plane strain and drained conditions is calculated from Equation (9.6).

$$N_\gamma = 2\,(N_q - 1)\,\tan\left(\varphi'_d\right) \qquad N_q = e^{\pi \tan\left(\varphi'_d\right)}\,\frac{1 + \sin\left(\varphi'_d\right)}{1 - \sin\left(\varphi'_d\right)} \tag{9.6}$$

where

φ'_d	Design value of effective friction angle [°]

The shape factor, s_γ, is expressed by Equation (9.7).

$$s_\gamma = 1 - 0.3\,\frac{B}{L} \tag{9.7}$$

where

L | Length of the foundation [m]

For circular foundations the shape factor, s_γ, is seen to be 0.7. Finally the inclination factors, i_i, are calculated from the expression given in Equation (9.8).

$$i_q = i_c = \left(1 - \frac{H_d}{V_d + A'\, c'\, \cot\left(\varphi'_d\right)}\right)^2 \qquad i_\gamma = i_q^2 \tag{9.8}$$

where

H_d | Horizontal design load [kN]

After the calculation of the vertical bearing capacity it will additionally be controlled if the foundation is subjected to strong eccentric loading. This is done by applying the formula in Equation (9.9).

$$e \leq 0.3\, D \tag{9.9}$$

where

D | Diameter of foundation [m]

If the eccentricity exceeds the demand stated in Equation (9.9) an alternative bearing capacity formula for strong eccentric loading should be respected as well. This is presented in Equation (9.10).

$$R_d = \left(\gamma'\, B'\, N_\gamma\, s_\gamma\, i_\gamma^e + c'\, N_c\, s_c\, i_c^e \left(1.05 + \tan^3\left(\varphi'_d\right)\right)\right) A' \tag{9.10}$$

where

i_γ^e and i_c^e | Load inclination factors for strong eccentric loading [-]

This bearing capacity formula is known as Rupture 2 and it takes the possibility of failure of the soil under the unloaded part of foundation into consideration. The new inclination factors i_c^e and i_γ^e are stated in Equation (9.11).

$$i_c^e = 1 + \frac{H_d}{V_d + A'\, c\, \cot\left(\varphi'_d\right)} \qquad i_\gamma^e = \left(i_c^e\right)^2 \tag{9.11}$$

For extremely eccentric loaded foundations it is the bearing capacity formula, either Equation (9.1) or Equation (9.10), which results in the lowest bearing capacity, that will drive the design.

In the ongoing analysis for frictional soils a foundation height of 3 m will be assumed, as it seems realistic compared to the found width. [Ibsen, 2012]

9.1.2 Results

A MATLAB programme containing the calculations can be seen in CD Appendix A. The diameter of the wind turbine is presented in Table 9.1.

Table 9.1: *Dimensions of the foundation.*

Parameter	Symbol	Value	Unit
Foundation diameter	D	18.38	m

The found dimension of the foundation has resulted in a total self-weight of the structure presented in Table 9.2.

Table 9.2: *Characteristic self-weight of entire structure.*

Parameter	Symbol	Value	Unit
Self-weight of wind turbine	$G_{wt,c}$	5,000	kN
Self-weight of foundation	$G_{f,c}$	19,541	kN
Total self-weight	G_c	24.541	kN

The total self-weight of the structure combined with the resulting moment leads to the eccentricity given in Table 9.3.

Table 9.3: *Eccentricity of the foundation.*

e	$0.3\,D$
[m]	[m]
4.07	5.54

From Table 9.3 it is seen that the eccentricity does not exceed the requirement stated in Equation (9.4), and therefore is it only Equation (9.1) that should be respected.

This foundation design will form the basis for the comparison with the probabilistic approach, which is the topic of Chapter 11. Before the probabilistic approach is considered a model uncertainty will be found for the scenario of interest. This is the topic of the following chapter.

Chapter 10

Determination of Model Uncertainty

Physical phenomenas are hard to describe by the use of mathematical and theoretical models, as the nature is very complex. Therefore it is important to introduce a model uncertainty, which will be expressed in the following. Before being able to appoint a model uncertainty for the analytical expression described by Terzaghi in Equation (9.2) a base of comparison is needed. For this purpose it has been chosen to compare the analytical obtained results with numerical simulations of the same situation using the commercial programme LimitState:Geo. Therefore this chapter will start by describing the model defined in LimitState:Geo and the results obtained from the simulations. In order to perform a proper comparison, a validation of the use of the programme has been performed in Appendix H. A convergence analysis has additionally been performed and a suitable size of the elements used in the numerical programme has been determined in connection to that. The convergence analysis is presented in Appendix I.

10.1 Numerical Model in LimitState:Geo

The numerical model made in LimitState:Geo can be found in CD Appendix A.
Before the results from LimitState:Geo can be found the model needs to be defined and a simulation plan should be presented as well. These two issues are the topics of the present section, which will end with a presentation of the final simulated results.

10.1.1 Construction of the Model

Firstly the construction of the model will be described in details. The base of the model is a surface footing as depicted in Figure 10.1 and 10.2.
The dimensions indicated in Figure 10.2 are presented in Table 10.1.

Table 10.1: *Dimensions for the model.*

Parameter	Symbol	Value	Unit
Horizontal dimension	x_{min}	-50	m
Horizontal dimension	x_{max}	75	m
Vertical dimension	y_{min}	0	m
Vertical dimension	y_{max}	30	m
Footing height	h_f	3	m
Footing width	b_f	20	m
Tower height	h_t	100	m

From Figure 10.1 it should be noted that the boundaries for the soil are modelled as fixed. This is done due to the limited options in LimitState:Geo where only free, symmetric and fixed boundaries can be modelled. None of the mentioned boundaries represent the real conditions. By modelling the boundaries as fixed, constrainment of the soil

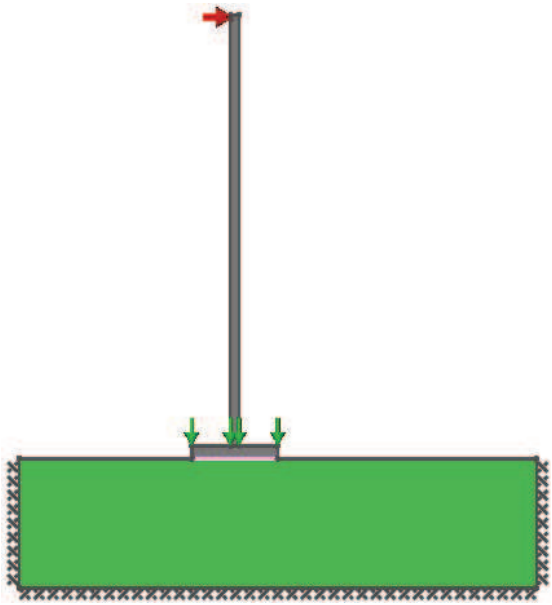

Figure 10.1: *Screenshot of the model constructed in LimitState:Geo.*

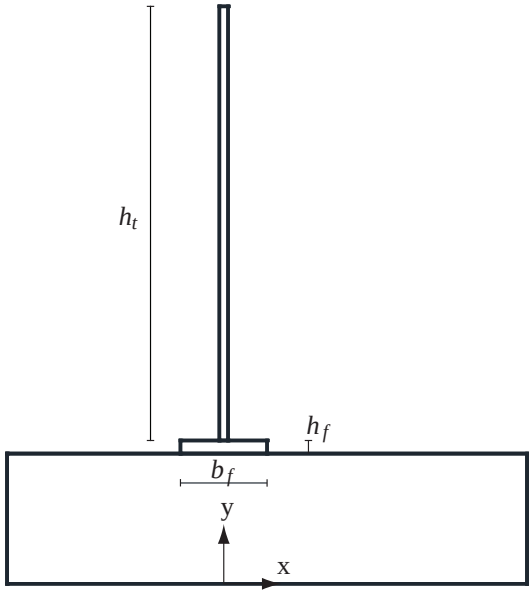

Figure 10.2: *Dimensions for the LimitState:Geo model.*

volume is ensured. Also the domain of the model has been made sufficiently large in order to make sure that the failure mechanism has enough space to develop. As the soil at the location is saturated a pheatric water level is defined at the top of the soil layer. From Figure 10.1 it is further observed that the vertical and the horizontal loads are assigned different colors. The green arrows symbolise loads that are not connected to the adequacy factor calculated by the programme, and the red arrows symbolise the loads connected to the adequacy factor. The adequacy factor is a measure of the relative change of the appointed loads, that will lead to failure. As the vertical loads are not connected to the adequacy factor it is ensured that the footing will be exposed to the entire vertical load. The adequacy factor will then describe the relative bearing capacity of the applied horizontal and moment load caused by the horizontal load.

As indicated in Figure 10.1 the horizontal load only affects the tower at the upper meter of the tower. This is done in order to provide a more realistic modelling of the actual loads on a wind turbine where the majority of the horizontal load will be caused by the wind force on the blades.

In the model both the tower and the footing are modelled as rigid objects. Also no friction is allowed between the footing and the soil. This is done as the numerical model is to replicate the behaviour described by the analytical expression in the best possible way. Therefore the assumptions made for the expression in Equation (9.2) are to be fulfilled for the numerical model as well. These can be reviewed in Section 9.1.1.

The soil volume in the model has been modelled to represent the characteristics from the location at Vulkanvej. For this purpose the mean value of the characteristics found in Section 5.1.4 has been chosen, as it provides a description of the actual conditions. This and the remaining definitions defined for the soil used in the model are listed in Table 10.2.

Table 10.2: *Properties for the soil.*

Parameter	Symbol	Value	Unit
Soil model	-	Mohr-Coulomb	-
Drainage behaviour	-	Always drained	-
Effective friction angle	φ'	33.19	$^\circ$
Unit weight	γ	16	kN/m^3
Saturated unit weight	γ_s	19	kN/m^3

10.1.2 Simulation Plan

In order to simulate the failure surface different scenarios for simulation has to be chosen. For this purpose the simulations will be done for predefined vertical load/self-weight of the construction along with different combinations of horizontal and moment loads. The different combinations will be created by varying the height of the tower/the attack point for the horizontal load. This will ensure the right stress paths for the simulations. The concept of choosing different stress paths is illustrated in Figure 10.3. As the drainage type for the simulations are set as *Always drained* no consolidation phase needs to be modelled, as the soil will be drained from the beginning.

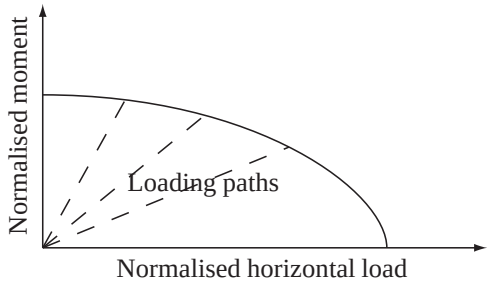

Figure 10.3: *Concept of different load paths for predefined vertical loads.*

It has been chosen to make the vertical load correspond to 50% of the ultimate vertical bearing capacity, V_0, and this value only. The value is a typical design value for foundations, whereas it has been chosen to concentrate the simulations around this very value [Ibsen, 2012]. For the attack point of the horizontal load various heights have been selected for simulation as mentioned earlier. From catalogues from the danish wind power firm Vestas it has been found, that typical hub-heights for onshore wind turbines are in the range of 70 to 90 m [Vestas, 2012]. Therefore the simulations are concentrated within these heights, as the main horizontal load is expected to occur at hub-height. Therefore a simulation has been performed for each meter within the mentioned range. In order to produce values for the entire failure surface additional simulations have been performed for each 5 m below the described range and 2 simulations have been performed for higher attack points in order to obtain values for low H/M values. To summarize a total of 36 simulations is chosen to represent the numerical yield envelope.

10.1.3 Results

In the following the results from the simulations will be presented. Firstly the values will be shown in a table, after which the failure domains will be commented upon. In the following section the results will be compared to the analytical expression presented in Section 9.1.1.

Before the simulations are performed, the ultimate vertical bearing capacity is found. For this purpose no horizontal force is applied to the model, and the vertical load is assigned an adequacy factor. The results from the simulation is presented in Table 10.3.

Table 10.3: *Simulation results of the ultimate vertical bearing capacity.*

Parameter	Symbol	Value	Unit
Ultimate vertical bearing capacity	V_0	90,432	kN/m

From this the simulations describing the different stress paths are performed. The results obtained from the 36 simulations are as presented in Table 10.4.

Table 10.4: *Simulation results from LimitState:Geo. The loads presented are the loads at failure. The arm indicates the height of the attack point of the horizontal load.*

Arm [m]	Vertical load [kN/m]	Horizontal load [kN/m]	Moment [kNm/m]	Arm [m]	Vertical load [kN/m]	Horizontal load [kN/m]	Moment [kNm/m]
5	45,216	9,506	47,530	75	45,216	2,372	177,900
10	45,216	9,500	95,000	76	45,216	2,344	178,144
15	45,216	8,038	120,570	77	45,216	2,316	178,332
20	45,216	6,810	136,200	78	45,216	2,289	178,542
25	45,216	5,874	146,850	79	45,216	2,262	178,698
30	45,216	5,146	154,380	80	45,216	2,236	178,880
35	45,216	4,568	159,880	81	45,216	2,211	179,091
40	45,216	4,103	164,120	82	45,216	2,186	179,252
45	45,216	3,719	167,355	83	45,216	2,162	179,446
50	45,216	3,401	170,050	84	45,216	2,138	179,592
55	45,216	3,131	172,205	85	45,216	2,115	179,775
60	45,216	2,900	174,000	86	45,216	2,092	179,912
65	45,216	2,700	175,500	87	45,216	2,070	180,090
70	45,216	2,526	176,820	88	45,216	2,048	180,224
71	45,216	2,494	177,074	89	45,216	2,027	180,403
72	45,216	2,462	177,264	90	45,216	2,006	180,540
73	45,216	2,432	177,536	3,000	45,216	64.19	192,570
74	45,216	2,402	177,748	5,000	45,216	38.54	192,700

From Table 10.4 the general tendency is quite obvious. As the moment increases the horizontal bearing capacity is reduced and vice versa. For the results obtained for the arms within the smallest and the two highest arms the tendencies deviates slightly from the general tendencies. This is reasoned by the meshing of the model, as a refinement of the mesh would have indicated slightly different horizontal loads for the simulations.

10.1.4 Failure Domains

In the following section the failure domains observed in LimitState:Geo during the simulations will be commented upon shortly.

It has been chosen to include two figures for a brief comparison, which are shown in Figure 10.4 and 10.5. Figure 10.4 shows a failure domain with a point of attack for the horizontal load which is 5 m above the ground, and Figure 10.5 shows the failure domain, when the point of attack is 100 m above the ground.

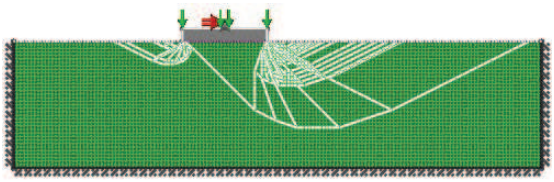

Figure 10.4: *Failure domain for the footing with a point of attack 5 m above the ground.*

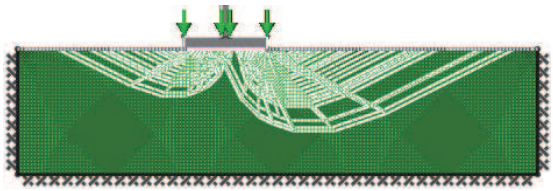

Figure 10.5: *Failure domain for the footing with a point of attack 100 m above the ground.*

From the figures it is quite obvious that the H/M ratio is important for the shape of the failure domain. The higher H/M ratio the more the failure domain tends to develop in the direction to which the horizontal load is directed. For the low H/M ratio depicted in Figure 10.5 it is observed, that the horizontal force is less dominant.

The failure domains for the simulations are similar to those of Figure 10.4 and 10.5. It should be noted that all the zones in the figures are passive, which is reasoned by the vertical load applied in all the simulations.
From Figure 10.4 and 10.5 it is also observed, that the failure domains run close to the geometrical boundaries of the numerical models. To enlighten which influence this might have on the obtained results a small study of the edge effects are presented in Appendix J.

10.2 Calculating the Model Uncertainty

After having run the needed numerical simulation, the found loading that caused failure will be used in the bearing capacity formula by Terzaghi. The two results will be compared and a model uncertainty will be determined for the analytical expression. The simulated results obtained from LimitState:Geo in Section 10.1.3 will be regarded as the exact results although they have not been verified from real life measurements.

The method used to determine the model uncertainty is from Eurocode 0 - Annex D. The method is also explained in [Sørensen, John D., 2011], which forms the basis for the described method.

10.2.1 Method and Assumptions

The model uncertainty is assumed to be LogNormal distributed and has to be multiplied with the mathematical model in order to obtain a result including the model uncertainties. This is described in Equation (10.1).

$$Y = b\,\Delta\,h(\underline{X}) \tag{10.1}$$

where

Y	Model included model uncertainties [-]
b	Constant [-]
Δ	Model uncertainty with $\mu_\Delta = 1$ and σ_Δ [-]
$h(\underline{X})$	Mathematical model [-]
$\underline{X}$	Set of stochastic variables included in mathematical model [-]

The mathematical model will correspond to the expression for R_d, cf. Equation (9.1), normalised with respect to 50% of the ultimate vertical bearing capacity, V_0, found in Table 10.3. This provides a relative measure of the calculated bearing capacity, that is directly comparable to the simulated values. Hereby the mathematical model can be expressed as shown in Equation (10.2).

$$h(\underline{X}) = \frac{R(\underline{X})}{0.5\,V_0} \tag{10.2}$$

The constant, b, describes the mean deviation between the mathematical model and the simulated results. The constant can be estimated by the use of the LSM, cf. Equation (10.3).

$$b = \frac{\sum y_i\, h(\underline{x}_i)}{\sum h(\underline{x}_i)^2} \tag{10.3}$$

where

y_i	Value obtained from the simulations [-]
$\underline{x}_i$	Values of the stochastic variable corresponding to y_i [kN/m or kNm/m]

In the considered situation the value of y_i will be 1, which indicate failure in the simulation. At this point the load combination will correspond to a point at the failure envelope.

By using the constant, b, a realisation of Δ can be calculated using Equation (10.4).

$$\Delta_i = \ln\left(\frac{y_i}{b\,h(\underline{x}_i)}\right) \tag{10.4}$$

where

Δ_i	Realisation of the LogNormal model uncertainty [-]

The realisation is used to determine the characteristics of the model uncertainty. The mean is known to be 1 and an estimate of the standard deviation and the corresponding coefficient of variation is calculated from Equation (10.5).

$$\sigma_\Delta = \sqrt{\frac{1}{N-1}\sum_{i=1}^{n}\left(\Delta_i - \overline{\Delta}\right)^2} \qquad V_\Delta = \sqrt{\exp\left(\sigma_\Delta^2\right) - 1} \tag{10.5}$$

where

σ_Δ	Standard deviation of the model uncertainty [-]
N	Number of comparisons [-]
$\overline{\Delta}$	Mean value of the LogNormal stochastic uncertainty [-]
V_Δ	Coefficient of variation for the model uncertainty [-]

The mean value of the LogNormal realisations are calculated from Equation (10.6).

$$\overline{\Delta} = \frac{1}{N}\sum_{i=1}^{n}\Delta_i \tag{10.6}$$

It should be noted, that by applying the above mentioned method, it is assumed that the simulations provide the exact results. It would be appropriate to assign an additional uncertainty describing the model uncertainty between measurements from real life models and the results obtained from the simulations. By doing this the mathematical model will be able to describe the real life model with the associated uncertainties. The last described aspect is out of the scope of this thesis.

10.2.2 Results

A MATLAB programme containing the calculations for the model uncertainty can be seen in CD Appendix A. The comparison of the simulated and mathematical results are shown in Figure 10.6 for illustrative purpose.

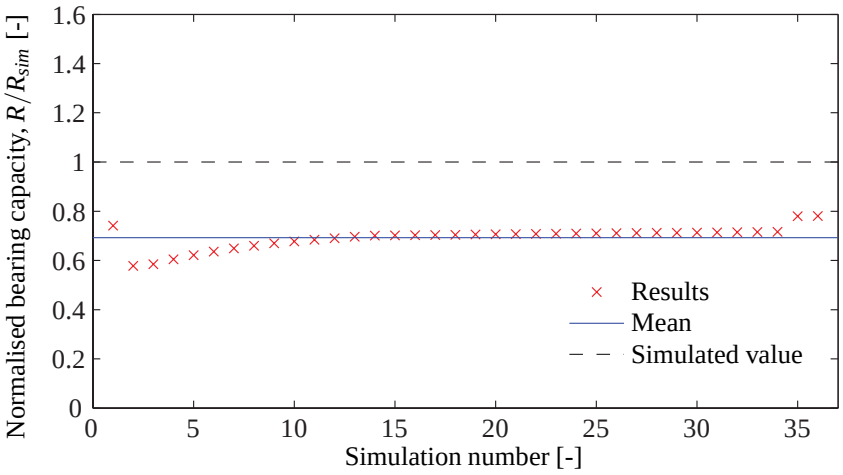

Figure 10.6: *Comparison of simulated and calculated vertical bearing capacities.*

From Figure 10.6 it can be observed, that the results from the mathematical model in general are around 30% lower than those observed from the simulations. This is in good agreement with the expectation of the analytical expressions to be a lower bound calculation compared to the simulations, that are based on upper bound algorithms. Therefore the value of the constant, b, is expected to be higher than 1. An overall trend is observed in Figure 10.6 for the calculated results. The only deviations of the general trend are found at the first and the last simulation numbers corresponding to low and high points of attack of the horizontal force. The deviations are expected to be due to the change in failure domains as explained in Section 10.1.4 and due to limitations regarding the mesh for the simulated

models explained in Section 10.1.3. As the deviating points represent extreme and unrealistic scenarios (points of attack of 5, 3,000 and 5,000 m above the ground), these points will be regarded as outliers and will therefore be excluded from further calculations.
The remaining calculated results moves toward an asymptotic line. From this it can be concluded, that the mathematical expression is somewhat dependent on the M/H ratio. Therefore the constant, b, could be expressed as a function dependent of the M/H ratio. This has been omitted in this thesis. Instead it has been chosen to focus on the simulations, that have arms to the horizontal point of attack within the interval 70 - 90 m, as these are considered to be in best agreement with real scenarios. By doing this only simulation 14 - 34 in Figure 10.6 will be considered, when the parameters describing the model uncertainty are to be determined. The calculated parameters are presented in Table 10.5.

Table 10.5: *Determined parameters for describing the model uncertainty.*

Parameter	Symbol	Type	Mean [-]	Standard deviation [-]
Model uncertainty	Δ	LogNormal	1	0.0066
Constant	b	Deterministic	1.41	-

As the last 20 results in Figure 10.6 are deviating by approximately the same factor, a very low measure for the standard deviation is obtained. The calculated value of b of 1.41 seems rather high, as an agreement between the upper bound solution and the calculated bearing capacities. An explanation for the deviation is thought to be the complicated load scenario treated with a high eccentricity. The two methods are known to produce similar results for simple scenarios, but might deviate as the scenario and thereby failure domain changes significantly. The results will be used, when the reliability of the foundation is to be considered.

Chapter 11

Probabilistic Approach

In this chapter the wind turbine foundation will be designed using a probabilistic approach for the frictional soil. A limit state function on the same form as the bearing capacity formula presented in Section 9.1.1, will be setup in order to determine the reliability of the foundation. From this analysis a partial safety factor for the effective friction angle will be calibrated and compared to the one given in [Eurocode 7-1, 2007]. Additionally a sensitivity analysis will be performed in order to identify, which variables that has the greatest influence on the reliability index.

11.1 Reliability Analysis

The reliability of the structure will be evaluated on the basis of a reliability index obtained by FORM. At first a design and limit state equation will be stated.

11.1.1 Limit State Function and Design Equation

In order to determine the safety level of the foundation the procedure described in the following will be used. At first a design equation will be setup, see Equation (11.1).

$$\frac{R_c}{\gamma_m} \geq z\, Q_c\, \gamma_f \tag{11.1}$$

where

R_c	Characteristic resistance [-]
Q_c	Characteristic load [-]
γ_m	Partial safety factor for the resistance [-]
γ_f	Partial safety factor for the load [-]
z	Design parameter [-]

From Equation (11.1) it is seen that the design equation contains characteristic values with appertaining partial safety factors. The partial safety factors used in the design equation can be seen in Table 11.1.

Table 11.1: *Partial safety factors used in the project.*

Parameter	Symbol	Value
Partial safety factor for aerodynamic loads	γ_Q	1.35
Partial safety factor for self-weight	γ_G	1.0
Partial safety factor for effective friction angle	$\gamma_{\varphi'}$	1.25

The design parameter, z, will be calibrated until the characteristic load and characteristic resistance with their appertaining partial safety factors are identical.
The design parameter, z, will then be used in a limit state function, which can be written on the form shown in Equation (11.2).

$$g = R - z\,Q \tag{11.2}$$

R	Stochastic resistance [-]
Q	Stochastic load [-]

In the considered case the Terzaghi bearing capacity formula from Equation (9.2) will form the basis for the design equation with the associated uncertainty defined in the previous chapter. The result is shown in Equation (11.3).

$$G = b\,R_d - V_d\,z = 0 \tag{11.3}$$

where

G	Design equation [-]
b	Constant, cf. Table 10.5 [-]
R_d	Design value of the bearing capacity [kN]
V_d	Design value of the vertical load [kN]
z	Design parameter [-]

The dimensions of the foundation given in Table 9.1 will be maintained, and z will therefore be a measure of how much the loads should be modified before the design limit is reached.
The limit state function is shown in Equation (11.4).

$$g = \Delta\,b\,R - V\,z \tag{11.4}$$

where

g	Limit state equation [-]
Δ	Model uncertainty [-]
R	Stochastic variable describing the bearing capacity [kN]
V	Stochastic variable describing the vertical load [kN]
z	Design parameter [-]

11.1.2 Stochastic Variables

When a probabilistic approach is used for design the uncertainties regarding the strength parameters and the loads for the limit state function should by modelled carefully. This is done through stochastic variables, which are characterized by their mean value, standard deviation and distribution type. The correlation between each stochastic variable

should furthermore be defined, as it influences the reliability of the structure. The abbreviations defined in Table 11.2 will be used throughout this project.

Table 11.2: *The abbreviation of the different distributions.*

Type	Abbreviation
Deterministic	D
Normal	N
LogNormal	LN
Gumbel	G

Stochastic Models for Loads

The uncertainties regarding the loads are the same for the drained and the undrained case and will therefore only be presented once.
The wind turbine is exposed to a wind load, which will induce a horizontal load and an overturning moment. Since both the horizontal load and overturning moment origins from the wind load they will be modelled as fully correlated stochastic variables.

The wind speed is a stochastic process that varies in time and space. This might induce difficulties when the exact magnitude of the wind load are to be determined. In order to determine the wind loads for design situation DLC 1.1, it would be ideal to perform a wind speed measurement at the given site over a time period of minimum one year, in order to get measurements from a whole season. The wind loads should be extrapolated in order to get a representative value for the given design period. Since it is out of the scope of this project to determine the exact wind loads, the estimates presented in Section 3.2 will provide the design basis. In the probabilistic approach these loads should be transformed into stochastic variables.
The characteristic 98% quantile loads from Section 3.2 is calculated on the basis of different uncertainty factors connected to the magnitude of the wind load. In Equation (11.5) these model uncertainties is presented for the horizontal load, but the procedure is identical for the wind induced moment load. [Tarp-Johansen et al., 2002]

$$H = H_b \, X_{exp} \, X_{st} \, X_{aero} \, X_{dyn} \, X_{sim} \, X_{ext} \tag{11.5}$$

where

H	Stochastic variable describing the horizontal wind load [kN]
H_b	Stochastic variable describing the basic horizontal wind load [kN]
X_{exp}	Stochastic variable describing the terrain uncertainty [-]
X_{st}	Stochastic variable describing the climate statistics uncertainty [-]
X_{aero}	Stochastic variable describing the aerodynamic uncertainty [-]
X_{dyn}	Stochastic variable describing the structural uncertainty [-]
X_{sim}	Stochastic variable describing the simulation uncertainty [-]
X_{ext}	Stochastic variable describing the extrapolation uncertainty [-]

The mean values, coefficient of variations, COV, and types of distribution for the model uncertainties are given in Table 11.3.

Table 11.3: *Uncertainties regarding the aerodynamic load effect. [Tarp-Johansen et al., 2002]*

Name	Type	μ	COV Normal	COV Low
X_{exp}	LN	1	**20%**	10%
X_{st}	LN	1	10%	**5%**
X_{aero}	G	1	20%	**10%**
X_{dyn}	LN	1	20%	**5%**
X_{sim}	N	1	5%	**5%**
X_{ext}	LN	1	5%	**5%**

Regarding Table 11.3 it is observed that two proposals for the COV's are listed. The COV's in the *Normal* column is what is used in common practice, whereas the COV's in the *Low* column is reasoned by the fact that most computational models are calibrated to full scale tests. The only exception to this is X_{exp}, where it is recommended to use a COV from the normal uncertainty model due to the natural randomness of the topography in nature[Tarp-Johansen et al., 2002]. In the probabilistic approach it is the COV's with bold font that will be used.

The basic wind load, H_b, is assumed Gumbel distributed, with a COV_{wind} in the range of 5 - 15% [Sørensen, 2012]. It could be argued for to use a Weibull distribution instead, as design situation DLC 1.1 is for normal wind conditions. A Weibull distribution is suggested by [IEC, 2005]. The reliability index will be calculated for two situations, with COV_{wind} = 5% and COV_{wind} = 15% respectively in order to determine the influence of this parameter.
The 98% quantile for the wind load is given in Table 3.2. By using this, μ_{h_b} is the only unknown from Equation (11.5) and can therefore be determined.
In Table 11.4 μ_{hb} and μ_{mb} is shown for the two situations of COV_{wind}.

Table 11.4: *Mean value of basic wind loads.*

Description	Abbreviation	COV_{wind} = 5%	COV_{wind} = 15%	Unit
Horizontal load	μ_{hb}	445	415	kN
Moment	μ_{mb}	44,500	41,500	kNm

As seen from Table 11.4 the mean value of the load is largest for the situation with COV_{wind} = 5%. This is reasoned by the fact that a Gumbel distribution with a COV_{wind} = 15% has a greater tail than a Gumbel distribution with COV_{wind} = 5%.

Stochastic Strength Parameters

The stochastic variables appertaining the bearing capacity formula for the drained case are the effective friction angle, φ', and the effective specific weight of the soil, γ'. The specific weight and effective friction angle are presented in

Table 4.1 and 5.4 and the mean value and COV are presented in Table 11.5, where a normal distribution and a COV = 2.5% for the specific weight is assumed. [Look, 2007]

Table 11.5: *Mean value and COV for effective friction angle and specific weight of the soil.*

Description	Symbol	Distribution type	μ	COV
Effective friction angle	φ'	LN	33.19°	5.5%
Effective specific weight	γ'	N	9.37 kN/m^3	2.5%

11.1.3 Results

A Fortran programme containing the calculations for the reliability index can be found in CD Appendix A.
In order to be able to evaluate the potential of probabilistic design, the target reliability index, β_T, for wind turbines should be considered. Since there is an ongoing discussion about what the desired reliability index for onshore wind turbines should be, the target reliabilities given in Table 11.6 will be investigated in this project in order to evaluate the probabilistic approach.

Table 11.6: *Investigated target reliability indices.*

Target reliability index, β_T	Annual probability of failure
3.09	10^{-3}
3.72	10^{-4}

A target reliability index, β_T, of 3.09 is proposed by [Tarp-Johansen et al., 2002]. A β_T of 3.72 is provided by [Sørensen, 2012].
The results from the reliability analysis can be seen in Table 11.7. The method for calculating the reliability index can be found in Appendix K.

Table 11.7: *Reliability index for different COV's.*

Description	Symbol	COV$_{wind}$ = 5%	COV$_{wind}$ = 15%
Reliability index	β	4.72	4.25
Annual probability of failure	p_f	$1.20 \cdot 10^{-6}$	$1.07 \cdot 10^{-5}$

When comparing the results from Table 11.7 with the target reliabilities from Table 11.6, it is seen that the safety of the structure is larger than what is prescribed by common standards. A way to minimise this gap is by calibrating the partial safety factor, $\gamma_{\varphi'}$, which is connected to the effective friction angle.
In Table 11.8 $\gamma_{\varphi'}$ is calibrated towards a target reliability index of 3.72 for the two situations of COV$_{wind}$.

Table 11.8: *Calibrated* $\gamma_{\varphi'}$.

Situation	$\gamma_{\varphi'}$	β_T
COV$_{wind}$ = 15%	1.04	3.72
COV$_{wind}$ = 5%	1.00	3.72

From Table 11.8 it is seen that there is a large potential in probabilistic design, when the calibrated $\gamma_{\varphi'}$ is compared with what is prescribed by the Eurocodes. The partial safety factor, $\gamma_{\varphi'}$, is highly dependent on the target reliability index, and therefore could $\gamma_{\varphi'}$ be reduced further if a reliability index equal to 3.09 is targeted instead. It shall be mentioned that the results obtained through this reliability analysis are determined on the basis of number of assumptions regarding the probabilistic models. Therefore the results are influenced by subjective opinions, and should therefore only be regarded as a measure for comparison.
The COV for the sand used in this reliability analysis is 5.5%. It is known that COV for the effective friction angle for sands lie in the range 5 - 15% [Look, 2007]. Therefore a COV of 5.5% could explain some of the high structural safety obtained in this analysis.
In order to investigate the influence of $COV_{\varphi'}$, two analyses with $COV_{\varphi'}$ = 10% and $COV_{\varphi'}$ = 15% respectively are performed. The results can be seen in Table 11.9.

Table 11.9: *Reliability index for COV_{wind} = 15% for different $COV_{\varphi'}$.*

Description	Symbol	$COV_{\varphi'}$ = 10%	$COV_{\varphi'}$ = 15%
Reliability index	β	4.12	3.57
Annual probability of failure	p_f	$1.85 \cdot 10^{-5}$	$1.78 \cdot 10^{-4}$

It is observed that the reliability indices obtained with a higher $COV_{\varphi'}$ lies closer to the target reliability indices presented in Table 11.6. This result emphasizes the importance of determining the standard deviation of the effective friction angle with great accuracy as the reliability index is highly dependent hereof.

Sensitivity Analysis

In order to get a measure of the relative importance of each stochastic variable, a sensitivity analysis is performed. At first the omission sensitivity factor, ζ, will be determined. The omission sensitivity factor, ζ, gives a measure for how much the reliability index would change if the investigated stochastic variable is considered as a deterministic parameter. The method for calculating ζ can be found in Appendix K.
In Table 11.10 ζ for the situation with COV_{wind} = 15% is presented.

Table 11.10: *Omission sensitivity factor for COV_{wind} = 15%*

Variable	H_b	M_b	X_{exp}	X_{st}	X_{aero}	X_{dyn}	X_{sim}	X_{ext}	V	φ'	γ'	Δ
ζ	1.00	1.26	1.22	1.01	1.01	1.01	1.01	1.01	1.00	1.02	1.00	1.00

From Table 11.10 it can be seen that the effect of setting the basic moment, M_b, to a deterministic parameter would be an increase of the reliability index of 26%. From the omission sensitivity factor it can be seen that the influence of the basic horisontal wind load, H_b, is minimal. It is furthermore seen that the reliability index will increase by 22% by setting the uncertainty factor, X_{exp}, to a deterministic parameter. From these results it is therefore recommended to increase the effort in determining the COV of M_b and X_{exp} more precisely in order to remove some uncertainty. It is furthermore seen that the effect of determining the effective friction angle more precisely would be minimal. This is due to the relatively low COV on φ'.

Another sensitivity measure is the elasticity coefficient, e, which gives a measure for how much the reliability index would change if the given parameter is increased by 1%. The method for determining e can be found in Appendix K.

The results can be seen in Table 11.11.

Table 11.11: *Elasticity coefficient e_μ and e_σ for COV_{wind} = 15%*

Variable	H_b	M_b	X_{exp}	X_{st}	X_{aero}	X_{dyn}	X_{sim}	X_{ext}	V	φ'	γ'	Δ
e_μ	-0.03	-0.42	-0.38	-0.66	-0.56	-0.66	-0.66	-0.66	0.43	0.95	0.31	0.18
e_σ	-0.00	-0.24	-0.30	-0.02	-0.12	-0.02	-0.02	-0.02	-0.01	-0.17	-0.00	-0.00

From Table 11.11 it is seen that effective friction angle, φ', is the most important parameter regarding the mean values. The reliability index will increase by 0.95% if $\mu_{\varphi'}$ is increased by 1%. It is once again observed that the influence of H_b is minimal. It is furthermore seen that the magnitudes of e_μ for the uncertainty parameters, X_i, and the basic moment, M_b, are in the same order of magnitude. This is explained by the fact that they are mutually connected by Equation (11.6).

$$M = M_b \, X_{exp} \, X_{st} \, X_{aero} \, X_{dyn} \, X_{sim} \, X_{ext} \tag{11.6}$$

where

M | Wind induced moment [kNm]

By examining e_σ it is seen that M_b and X_{exp} are the variables with the greatest influence, which also is seen from Table 11.10.
The omission sensitivity factor, ζ, and elasticity coefficient, e, for COV_{wind} = 5% can be seen in Table 11.12 and Table 11.13.

Table 11.12: *Omission sensitivity factor for COV_{wind} = 5%*

Variable	H_b	M_b	X_{exp}	X_{st}	X_{aero}	X_{dyn}	X_{sim}	X_{ext}	V	φ'	γ'	Δ
ζ	1.00	1.02	1.35	1.01	1.21	1.01	1.01	1.01	1.01	1.04	1.00	1.00

By comparing the results from Table 11.10 and 11.12 it is seen that effect of setting M_b to a deterministic parameter is decreased significantly. This is reasoned by the fact that COV_{wind} is equal to 5% in the later analysis. It is furthermore seen that the relative importance of the uncertainty factors X_{exp} and X_{aero} are increased in this analysis. All the other variables have COV's equal to 5.5% and below, whereas X_{exp} and X_{aero} have a COV of 20% and 10% respectively. Therefore the relative importance of X_{exp} and X_{aero} have increased.

Table 11.13: *Elasticity coefficient e_μ and e_σ for COV_{wind} = 5%*

Variable	H_b	M_b	X_{exp}	X_{st}	X_{aero}	X_{dyn}	X_{sim}	X_{ext}	V	φ'	γ'	Δ
e_μ	-0.05	-0.64	-0.30	-0.69	-0.51	-0.69	-0.69	-0.69	0.46	1.08	0.36	0.20
e_σ	-0.00	-0.07	-0.41	-0.03	-0.20	-0.03	-0.03	-0.03	-0.01	-0.26	-0.00	-0.00

By comparing Table 11.11 and 11.13 it is seen that the general picture is the same. Therefore the comments connected to the results for the situation with COV_{wind} does also apply here. Though, it is seen that the influence of e_σ for the basic moment, M_b, is reduced, which is due to the fact that the uncertainty regarding M_b is reduced in this analysis.

11.1.4 Discussion

From the results obtained through the reliability analysis, it can be concluded that the reliability index, β, is highly depended on $COV_{\varphi'}$. Therefore it is suggested that the partial safety factor for the effective friction angle, φ', should depend on $COV_{\varphi'}$ for the given site. CPTu measurements are already performed for all larger construction projects, which means that no additional measurements needs to be done in order to gain information about $COV_{\varphi'}$. The potential of lowering the costs of the foundation is on the other hand large and should therefore be considered. The partial safety factor for the effective friction angle could for instance be stated in the following way.

Table 11.14: *Partial safety factor for the effective friction angle for the situation with COV_{wind} = 15%.*

$COV_{\varphi'}$	5%	10%	15%
$\gamma_{\varphi'}$	1.04	1.13	1.28

In Table 11.14 the situation with COV_{wind} = 15% is shown.

It shall once again be mentioned that these results is obtained on the basis of subjective assumptions, and should therefore only be regarded as a measure of comparison.

The reliability analysis performed for the frictional soil is under the assumption of a homogeneous soil, which can be described by a mean value and a standard deviation. This assumption corresponds to a infinite long correlation length. In Chapter 8 the vertical correlation length for the frictional soil was determined to 0.1 - 0.5 m, whereas the horizontal correlation length was determined to 2.5 m. These correlation lengths are considerable smaller than the extent of the failure domain. Therefore it should be considered, which quantile of the effective friction angle, that should be governing the bearing capacity of the foundation, which will be discussed in the following.

With correlation lengths in the order of magnitude determined in Chapter 8, it seems as a good assumption to let the mean value of the effective friction angle govern the bearing capacity. This corresponds to setting the stochastic value φ' to a deterministic parameter and then perform another reliability analysis. The change in the reliability index by doing this, can also be determined by multiplying the reliability index with the omission sensitivity factor determined in Table 11.10 and 11.12. The effect of this for COV_{wind} = 15% can be seen in Table 11.15.

Table 11.15: *Effect of letting the mean value of the effective friction angle govern the bearing capacity.*

Situation	β	Annual probability of failure	Calibrated $\gamma_{\varphi'}$
$COV_{\varphi'}$ = 0%	4.34	$7.15 \cdot 10^{-6}$	1.01

The last column shows the necessary value of the partial safety factor $\gamma_{\varphi'}$ in order to obtain a reliability index equal to 3.72. If Table 11.14 and Table 11.15 are compared, it can be seen that $\gamma_{\varphi'}$ can be reduced if the mean value governs the bearing capacity. The reduction potential depends on the value of $COV_{\varphi'}$ for the given problem.

The situation where the mean value governs the bearing capacity represents an upper bound solution for the problem. The situation where the soil is assumed to be homogeneous, on the other hand, represents a lower bound solution. The real reliability index lies in between the two bounds, but it is believed that the upper bound represents the best guess due the small correlation lengths.

A way to implement the correlation lengths in the analysis is described in [Fenton and Griffiths, 2003]. In here the problematic regarding the determination of the right failure path is dealt with by approximating the extend of the failure domain. Then the value of the effective friction angle is determined as an geometric average over this failure domain. By doing this the effect of the correlation lengths can be determined. It shall be mentioned that this method ignores the weakest path issue and therefore only gives a qualified estimate of the problem. A method similar to this, where the correlation length is considered, will be presented for the cohesive soil in the following chapters.

Part IV

Calculations of two Approaches for Cohesion Soil

At first the dimensions of the foundation will be determined according to a deterministic approach suggested by [DNV/Risø, 2010]. After having calculated the necessary width of the foundation a simulation will be run in LimitState:Geo with the strength parameters found for the clay and the calculated dimension of the foundation. The analysis will be based on a strip foundation, which is done since the geometry of the failure domain will be extracted from a 2D numerical model created in LimitState:Geo. The geometry is then implemented into a stochastic field made in MATLAB. 10,000 realisations of the stochastic field will be generated. For each realisation a mean undrained shear strength is calculating by integration over the failure domain. The undrained shear strengths are measures of the bearing capacity by the use of bearing capacity formulas. The undrained shear strengths determined from the stochastic field form the basis for a reliability analysis, which will be performed using asymptotic sampling.

Chapter **12**

Deterministic Approach

In the following chapter the dimensions of the strip foundation will be determined according to the guideline by [DNV/Risø, 2010]. The foundation is designed to withstand the loads presented in Section 3.2.

12.1 Transformation of the Loads

The loads in Section 3.2 needs to be transformed into being loads acting on a strip foundation, which is the subject of this section. For this purpose some simplification needs to be performed, which will be shortly presented along with the results.

12.1.1 Method and Assumptions

The loads presented in Section 3.2 are assumed to be describing a wind turbine placed on a circular footing with a radius of 10 m [Andersen, 2012]. From this assumption it is possible to transform the foundation into a quadratic foundation with equivalent area by applying the expression in Equation (12.1).

$$L_{equi} = \sqrt{R^2\,\pi} \tag{12.1}$$

where

L_{equi}	Equivalent side length of a quadratic foundation [m]
R	Radius for the circular foundation [m]

Furthermore considerations about the transformation from 3D to 2D needs to be taken into consideration. This will be done by considering the shape factor used in the formulation for the bearing capacity presented by Terzaghi, cf. Equation (12.2).

$$s_\gamma = 1 - 0.3\,\frac{B}{L} \qquad s_q = s_c = 1 + \frac{B}{L}\sin(\varphi_d) \tag{12.2}$$

where

s_γ, s_q, s_c	Shape factors [-]
B	Width of the foundation [m]
L	Length of the foundation [m]

From Equation (12.2) it is seen, that only the term concerning the unit weight of the soil is affected by the transformation from 3D to 2D, when soil with no friction is considered. Therefore only the equal areal transformation will be performed in the following, as s_γ is not a part of the Terzaghi formulation for undrained conditions.

12.1.2 Results

By applying the above described method the equivalent side length of a quadratic foundation, L_{equi}, has been calculated as presented in Table 12.1.

Table 12.1: *Calculated equivalent side length.*

Description	Abbreviation	Value	Unit
Equivalent side length	L_{equi}	17.72	m

By the use of the result obtained in Table 12.1 the transformed loads are as presented in Table 12.2.

Table 12.2: *Design loads before and after transformation.*

	Before		After	
Load	Value	Unit	Value	Unit
V_d	5,000	kN	282.1	kN/m
H_d	1,000	kN	56.4	kN/m
M_d	100,000	kNm	5,642	kNm/m

The loads presented in Table 12.2 per meter length are those used for the dimensioning of the strip foundation in the following.

12.2 Deterministic Calculation for Clay

The necessary width of the foundation will be calculated in accordance to [DNV/Risø, 2010]. The bearing capacity formulas given in [DNV/Risø, 2010] is a refined version of the classical bearing capacity theory for a strip foundation stated by Terzaghi. It will be investigated if the foundation is exposed to a strong eccentric loading. In that case an additional bearing capacity formula should be followed. Besides the vertical bearing capacity, the foundation is furthermore tested for failure due to sliding.

12.2.1 Method and Assumptions

The method is very similar for that of sand described in Section 9.1.1. The method described in the following will assume undrained conditions, which corresponds to a short term calculation. It is furthermore assumed that the soil is a pure cohesive material. The bearing capacity formula for undrained conditions is expressed in Equation (12.3).

$$R_d = \left(N_c \, c_{u,d} \, s_c^0 \, i_c^0 + q'\right) \, B' \tag{12.3}$$

where

R_d	Design bearing capacity [kN/m]
N_c	Bearing capacity factor, (π + 2) for undrained conditions [-]
$c_{u,d}$	Design undrained shear strength [kPa]
q'	Effective overburden pressure at the bottom of the foundation [kPa]
s_c^0	Shape factor for undrained conditions [-]
i_c^0	Inclination factor for undrained conditions [-]
B'	Effective width of the foundation [m]

This bearing capacity formula is known as Rupture 1. As the considered situation is a surface footing the overburden pressure at the bottom of the foundation, q', is zero. The shape factor for undrained conditions, s_c^0, for a strip footing assuming undrained conditions is given by Equation (12.4).

$$s_c^0 = s_c = 1 \tag{12.4}$$

The inclination factor for undrained conditions, i_c^0, is calculated in accordance with Equation (12.5).

$$i_c^0 = \frac{1}{2}\left(1 + \sqrt{1 - \frac{H_d}{B'\, c_{u,d}}}\right) \tag{12.5}$$

Furthermore it will be investigated whether the foundation is subjected to strong eccentric loading. This is the case if the inequality in Equation (12.6) is not fulfilled.

$$e \leq 0.3\, B \qquad e = \frac{M_d}{V_d} \tag{12.6}$$

In case of strong eccentric loading the second bearing capacity is given by Equation (12.7).

$$R_d = \left(c_{u,d}\, N_c\, s_c\, i_c^{e,0}\left(1.05 + \tan^3(\varphi_d)\right)\right) B' \tag{12.7}$$

where

$i_c^{e,0}$	Inclination factor for strong eccentric loading under undrained conditions [-]
φ_d	Design friction angle [°]

This bearing capacity is known as Rupture 2 and it takes the possibility of failure of the soil under the unloaded part into consideration. For undrained conditions the friction angle is 0, and therefore Equation (12.7) can be reduced to Equation (12.8).

$$R_d = \left(c_{u,d}\, N_c\, s_c\, i_c^{e,0}\, 1.05\right) B' \tag{12.8}$$

The inclination factor for the strong eccentric undrained case, $i_c^{e,0}$, is given by Equation (12.9).

$$i_c^{e,0} = \sqrt{\frac{1}{2} + \frac{1}{2}\sqrt{1 + \frac{H_d}{B' \, c_{u,d}}}} \tag{12.9}$$

The design horizontal load, H_d, needs to fulfill the sliding criteria in Equation (12.10).

$$H_d \leq B' \, c_{u,d} \tag{12.10}$$

As for the method used to describe the bearing capacity for drained conditions, it is assumed that only the horizontal surfaces of the foundation contributes to the bearing capacity.

As a final assumption the height of the foundation has been estimated to be approximately 2 m which will be used, when calculating the necessary dimension of the foundation.

12.2.2 Results

The calculations for the deterministic design of the foundation installed on clay can be found in CD Appendix A. The presented scenario has been investigated regarding the vertical load bearing capacity. At first the strip foundation was attempted designed without strong eccentricity. The obtained results are presented in Table 12.3.

Table 12.3: *Results obtained from standard design methods.*

V_d	R_d	B	e	e_{crit}	H_d	$B' \, c_{u,d}$
[kN/m]	[kN/m]	[m]	[m]	[m]	[kN/m]	[kN/m]
960.65	962.54	13.82	5.87	4.15	56.42	202.46

In Table 12.3 different results are observed. The vertical load bearing capacity is sufficient for a width of the foundation of 13.82 m and no problems will be observed when sliding of the foundation is concerned. Although the eccentricity demands cause problems. The criterion described in Equation (12.6) yields 4.15 m whereas the actual eccentricity is calculated to be approximately 1.7 m above this result. Therefore the foundation qualifies as a footing subjected to strong eccentric loading. Therefore will it be investigated if the Rupture 2 failure mechanism provides a lower bearing capacity. The values for the Rupture 2 bearing capacity is presented in Table 12.4.

Table 12.4: *Results obtained from design method for strong eccentric loading.*

V_d	R_d	B	e	e_{crit}	H_d	$B' \, c_{u,d}$
[kN/m]	[kN/m]	[m]	[m]	[m]	[kN/m]	[kN/m]
960.65	1,128.19	13.82	5.87	4.15	56.42	202.46

By comparing the bearing capacities from Rupture 1 and Rupture 2, it is observed that Rupture 1 failure mode provides the most critical result. The foundation width of 13.82 m has been found acceptable and will be used in the further calculations.

Chapter 13

Probabilistic Approach

After having presented the deterministic calculation for the scenario on clay, the following chapter will treat the probabilistic calculation of the same topic. The dimensions of the footing used in this chapter will be based on the results from Section 12.2, in order to have a proper base for comparison.
After determining the geometry of the failure beneath the footing and implementing the geometry into stochastic fields, 10,000 simulations will be run to gain input to the reliability analysis, which will be performed through asymptotic sampling.

13.1 Extraction of Failure Domain

The LimitState:Geo model used for failure domain extraction can be found in CD Appendix A.
In the following the model used for extracting the failure domain from LimitState:Geo will be presented followed by the geometric description of the domain, which will be implemented in a MATLAB code programmed to estimate the soil strength through the failure by the use of stochastic fields, see CD Appendix A.

13.1.1 Building the Model and Assumptions

The model is very similar of that described in Section 10.1 only with a few modifications. As presented previously the foundation is modelled as a surface footing. The visualisation and dimensions of the model are presented in Figure 13.1 and 13.2.

Figure 13.1: *Screenshot of the model constructed in LimitState:Geo.*

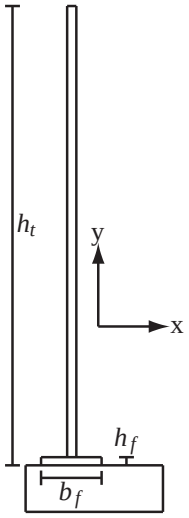

Figure 13.2: *Dimensions for the LimitState:Geo model.*

The dimensions indicated in Figure 13.2 are presented in Table 13.1 for clarification.

Table 13.1: *Dimensions for the model.*

Parameter	Symbol	Value	Unit
Horizontal dimension	x_{min}	0	m
Horizontal dimension	x_{max}	30	m
Vertical dimension	y_{min}	0	m
Vertical dimension	y_{max}	10	m
Footing height	h_f	2	m
Footing width	b_f	13.82	m
Tower height	h_t	100	m

As for the model used for convergence analysis, the boundaries are modelled as fixed. If the model is compared to that of Section 10.1 it is noted, that the soil domain is much smaller. This is done as the failure domain tends to move under the foundation as the eccentricity increases. The eccentricity has increased slightly compared to the model presented for the convergence analysis. A phreatic surface has been defined at the bottom of the foundation in order to ensure undrained conditions. In Figure 13.1 it is observed that both the vertical and the horizontal loads are assigned a red colour, which indicates that they are increased simultaneous as the adequacy factor is to be calculated. By doing so, it is ensured that the right failure domain is emphasised as the ratio between the different loadings are kept constant.

As for the model in Section 10.1 it is observed that the horizontal load only affects the tower at the upper meter of the tower for the same reasons mentioned earlier. The foundation and the tower are modelled as rigid objects and no adhesion is modelled between the foundation and the soil.

The soil in the model has been modelled by the use of the characteristics found in Section 6.1.2, which describes the strength parameters from the measurements at Suderbovej. The input parameters used in LimitState:Geo to describe the clay are presented in Table 13.2.

Table 13.2: *Properties for the soil at Suderbovej.*

Parameter	Symbol	Value	Unit
Soil model	-	Mohr-Coulomb	-
Drainage behaviour	-	Always undrained	-
Undrained shear strength	c_u	184.7	kPa

From here it is only left to extract the failure domain found from the simulation in LimitState:Geo, which will be presented in the following section.

13.1.2 Results

The model has been run and the failure domain is illustrated in Figure 13.3.

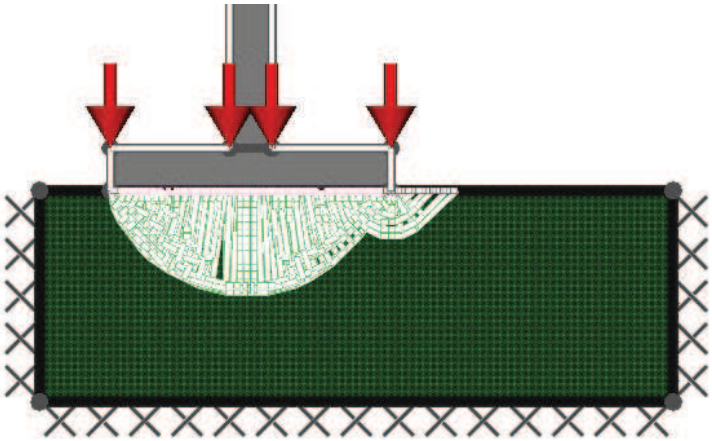

Figure 13.3: *Result output from LimitState:Geo. An illustration of the failure domain for the treated scenario.*

From Figure 13.3 it is seen that the expectation of the failure domain to develop primarily under the footing due to the strong eccentricity, is satisfied. Furthermore, it is observed that the geometry of the failure under the foundation mainly consist of a circle, which also is expected for cohesive soils. Additional study of the failure domain supports the failure generated through LimtState:Geo, see Appendix L.
The surrounding geometry will shortly be described in the following. The main geometry is presented in Figure 13.4.

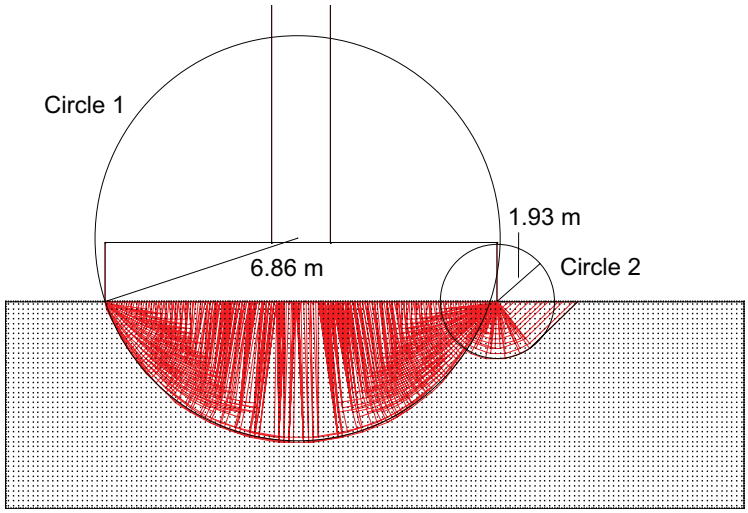

Figure 13.4: *Geometry of failure beneath the surface footing.*

The numerical model shows the failure line in the soil, which is interpreted as shown in Figure 13.5. The eccentric loading causes a soil volume to displace in downward direction causing a shear fan to develop to the right pushing another soil volume upwards. To the left the failure develops as a circular slip line.

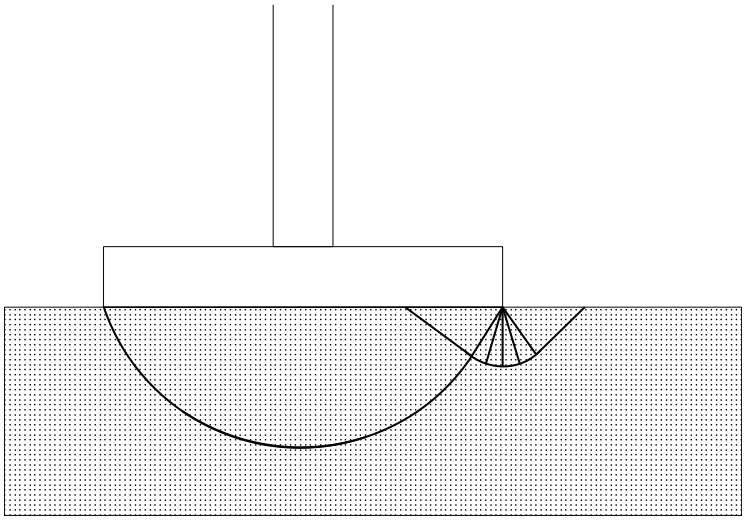

Figure 13.5: *Geometry of failure beneath the surface footing.*

The presented failure will be incorporated in the stochastic field, which will be presented in the following.

13.2 Stochastic Field Modelling

In order to take the correlation of the undrained shear strength in different points into account, a stochastic field will be generated. A 2D situation with plane strain will be considered. An example of a 2D stochastic field can be seen in Figure 13.6.

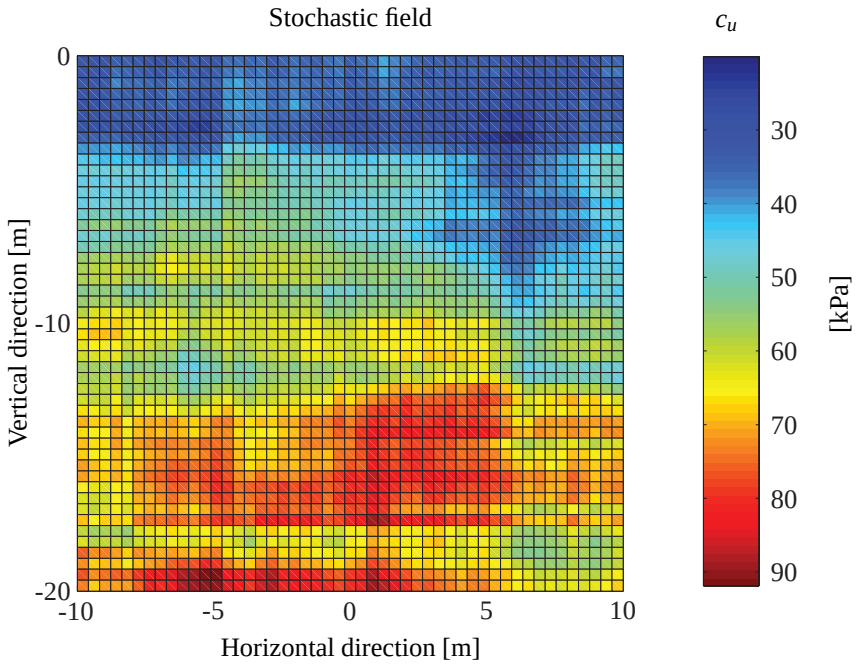

Figure 13.6: *Example of a random field that varies in space.*

The field is divided into a suitable number of elements in the x- and z-direction, where each element will be allocated a random c_u-value. In order to incorporate the correlation length, it is important that the considered correlation

lengths are larger than the element sizes. From Figure 13.6 it can be seen that there is a trend in the z-direction, whereas no trend is modelled in the x-direction. The trend in the z-direction is due to the increasing overburden pressure, which will influence the strength of the soil.

13.2.1 Method and Assumptions

The method for generating a stochastic field for the cohesion soils is described in the following. The stochastic field parameter is the undrained shear strength, c_u, which can be modelled by Equation (13.1).

$$\underline{c_u} = \underline{\mu} + \underline{\underline{D}}\,\underline{\underline{T}}\,\underline{u} \tag{13.1}$$

where

$\underline{c_u}$	Vector containing outcome from the stochastic field [kPa]
$\underline{\mu}$	Vector containing the mean value of c_u [kPa]
$\underline{\underline{D}}$	Diagonal matrix containing the standard deviation of c_u [kPa]
$\underline{\underline{T}}$	Lower triangular matrix containing the correlation of c_u [-]
$\underline{u}$	Vector of random normal distributed numbers [-]

In the case presented in the thesis the mean value will be calculated with a trend in the vertical direction. The diagonal matrix, $\underline{\underline{D}}$, containing the standard deviation will be calculated by Equation (13.2).

$$\underline{\underline{D_{i,i}}} = \underline{\mu_i}\,\underline{\underline{\mathrm{COV}}} \tag{13.2}$$

where

$\underline{\underline{\mathrm{COV}}}$	Coefficient of variation for the undrained shear strength [kPa]

$\underline{\underline{\mathrm{COV}}}$ is assumed to be constant with depth and it is equal to 0.18, which was determined in Chapter 6.
The lower triangular matrix, $\underline{\underline{T}}$, is determined by doing a Cholesky transformation on the correlation matrix, $\underline{\underline{\rho}}$, see Equation (13.3).

$$\underline{\underline{\rho}} = \underline{\underline{T}}\,\underline{\underline{T}}^T \tag{13.3}$$

where

$\underline{\underline{\rho}}$	Correlation coefficient matrix [-]

The correlation between the strength in two points can according to [Baker, J. and Calle, E, 2006] be determined by Equation (13.4).

$$\underline{\underline{\rho}} = \exp\left(-\frac{|\tau_x|}{D_x} - \frac{|\tau_z|}{D_z}\right) \tag{13.4}$$

$$\text{where} \quad \tau_x = x_2 - x_1$$

$$\text{where} \quad \tau_z = z_2 - z_1$$

where

D_x	Correlation length in x-direction [m]
D_z	Correlation length in z-direction [m]

In Section 13.1 it is described how the soil failure is extracted. This failure is implemented in a stochastic field as shown in Figure 13.7.

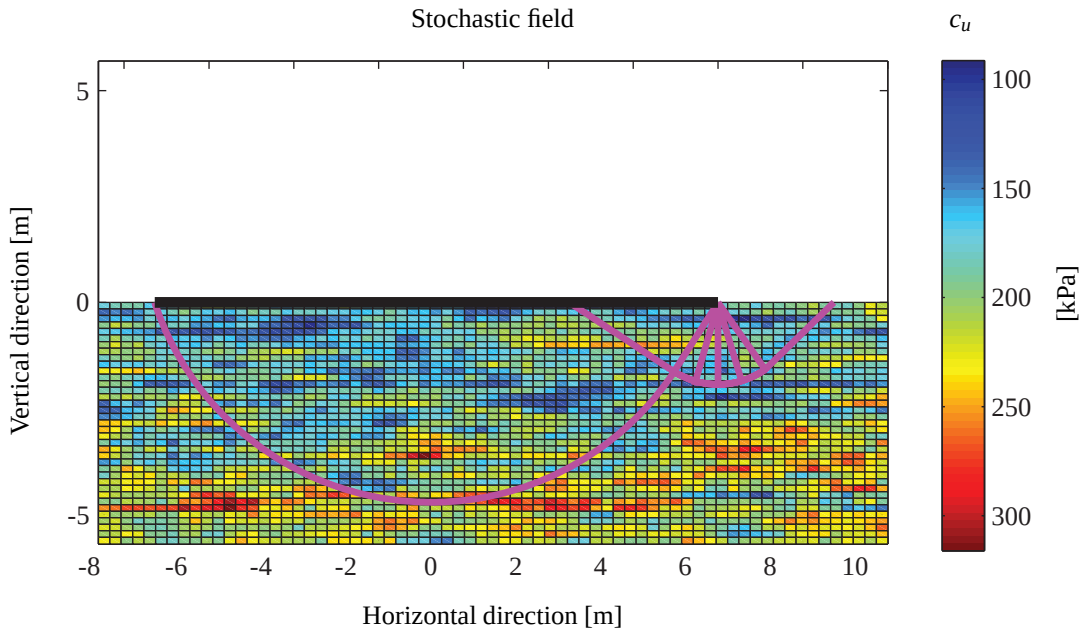

Figure 13.7: *Geometry implemented in the stochastic field.*

By running 10,000 realisations of the stochastic field, and integrating over the failure domain each time, 10,000 mean values for the undrained shear strength over the failure domain are produced. These mean values are a measure of the bearing capacity and by using the realisations of the mean c_u in the limit state expression in Equation (13.6) and asymptotic sampling, the reliability index can be determined. This is described further in the following chapter.

13.3 Reliability Analysis

In the following section the reliability of the foundation will be evaluated, which is done through asymptotic sampling. The mean values of the undrained shear strengths determined through the stochastic field will be used in the limit state function that is used in the asymptotic sampling. The partial safety factor on the undrained shear strength, γ_{c_u}, will be calibrated against the target reliabilities stated in Table 11.6. At first the design equation and limit state function will be presented.

13.3.1 Limit State Function

The design equation and limit state function for the cohesive soil will be based on Equation (12.3). The foundation is exposed to a strong eccentric loading, but it is shown, that Equation (12.3) provides the lowest bearing capacity compared to Equation (12.7) and therefore Equation (12.3) will represent the most critical situation.
The design equation can be seen in Equation (13.5).

$$G = \left(N_c \, c_{u,d} \, s_c^0 \, i_{c,d}^0\right) \, B' - V_d \, z = 0 \tag{13.5}$$

where

G	Design equation [-]
N_c	Bearing capacity factor, (π + 2) for undrained conditions [-]
$c_{u,d}$	Design value of undrained shear strength [kPa]
s_c^0	Shape factor for undrained conditions [-]
$i_{c,d}^0$	Design value of inclination factor for undrained conditions [-]
B'	Effective width of the foundation [m^2]
V_d	Design value of vertical load [kN]
z	Design parameter [-]

The corresponding limit state function can be seen in Equation (13.6).

$$g = \left(N_c \, c_u \, s_c^0 \, i_c^0\right) \, B' - V \, z \tag{13.6}$$

where

c_u	Stochastic variable describing the undrained shear strength [kPa]
V	Stochastic variable describing the vertical load [kN]

The inclination factor, i_c^0, and the effective area, A', are furthermore variables, as they depend on the stochastic loads, V, M_b, and H_b.

13.3.2 Models for Stochastic Loads

The stochastic loads are determined in a similar way as described in Section 11.1.2, and they can be seen in Table 13.3.

Table 13.3: *Mean value of basic wind loads.*

Description	Abbreviation	COV$_{wind}$ = 5%	COV$_{wind}$ = 15%	Unit
Horizontal load	μ_{hb}	24.8	23.0	kN/m
Moment	μ_{mb}	2,480	2,300	kNm/m

The uncertainty factors presented in Table 11.3 will be also be used in this reliability analysis.

13.3.3 Stochastic Strength Parameters

The mean value and standard deviation for the undrained shear strength was determined in Chapter 6 and is presented once again to set the record straight, see Table 13.4.

Table 13.4: *Mean value and COV for the undrained shear strength.*

Description	Distribution type	μ	COV
Undrained shear strength	LN	Realisations from stochastic field	15.9%

13.3.4 Method and Assumptions for Asymptotic Sampling

The main idea of asymptotic sampling is to increase the standard deviation, σ, by dividing σ with a scale factor denoted f. The scale factor f lies between 0 and 1 and σ is therefore increased. By doing this, the number of events in D_f increases. This is illustrated in Figure 13.8 and Figure 13.9.

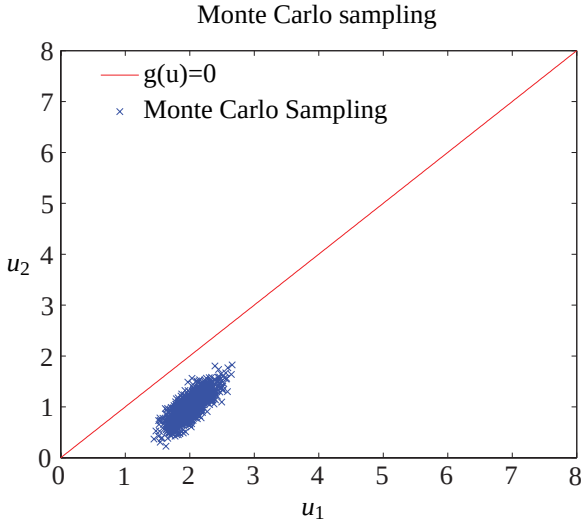

Figure 13.8: *Crude Monte Carlo sampling.*

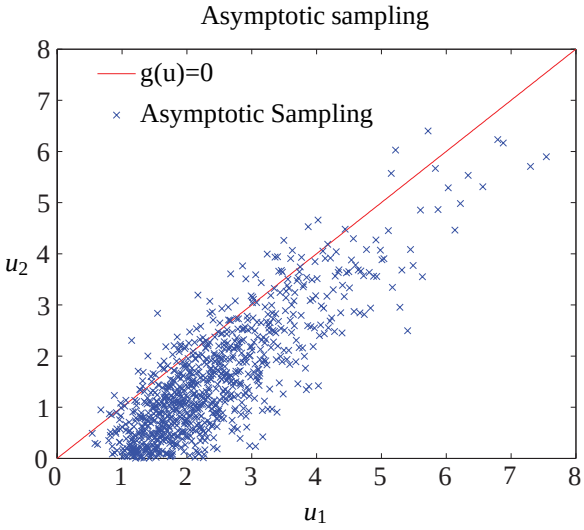

Figure 13.9: *Asymptotic sampling.*

In Figure 13.8 a crude Monte Carlo simulation with 1,024 simulations is shown. Figure 13.9 shows the same scenario with asymptotic sampling applied. The number of events in D_f is increased by setting the scale factor, $f = 0.20$.

The procedure for asymptotic sampling is given in Figure 13.10.

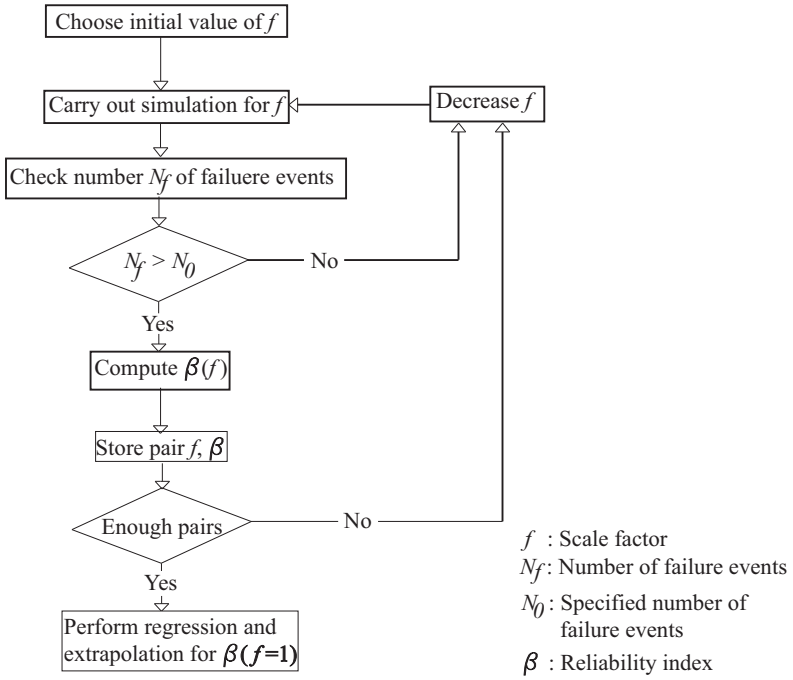

Figure 13.10: *The procedure for asymptotic sampling. [Bucher, 2009] - edited*

As seen from Figure 13.10 a number of pairs of f and β should be collected, after which a regression can be performed. In this thesis the least square method is used for fitting the curve to the estimated points. In order to ensure asymptotic behaviour the collected pairs of f and β are fitted to Equation (13.7).

$$\frac{\beta}{f} = A + \frac{B}{f^2} \tag{13.7}$$

where

β	Reliability index [-]
A, B	Fitting parameters [-]
f	Scale factor [-]

An example of such a fit is shown in Figure 13.11.

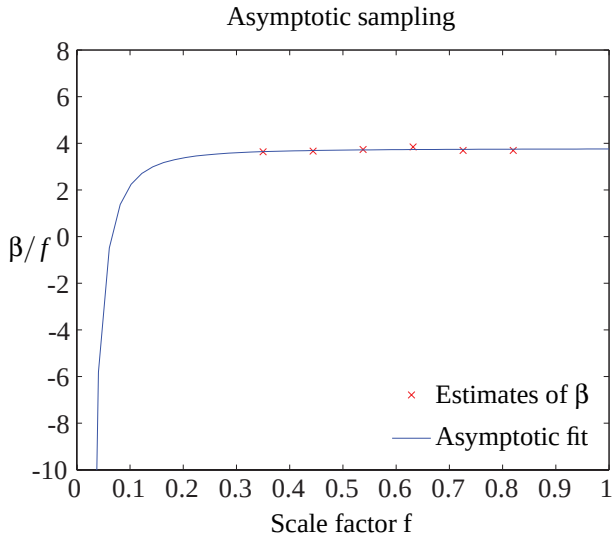

Figure 13.11: *An example of asymptotic sampling.*

In [Bucher, 2009] it is shown that a reliable measure of the reliability index is determined faster, when quasi random numbers are used compared to pseudo random numbers. In particular it is shown that quasi random numbers following a randomized Sobol sequence have the fastest convergence rate. Therefore is it chosen to use a randomized Sobol sequence for the asymptotic sampling. In Figure 13.12 and Figure 13.13 the difference between pseudo random numbers and quasi random numbers can be seen.

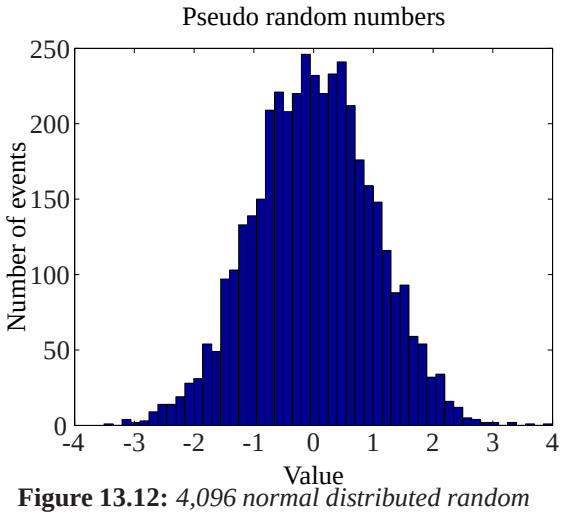

Figure 13.12: *4,096 normal distributed random numbers.*

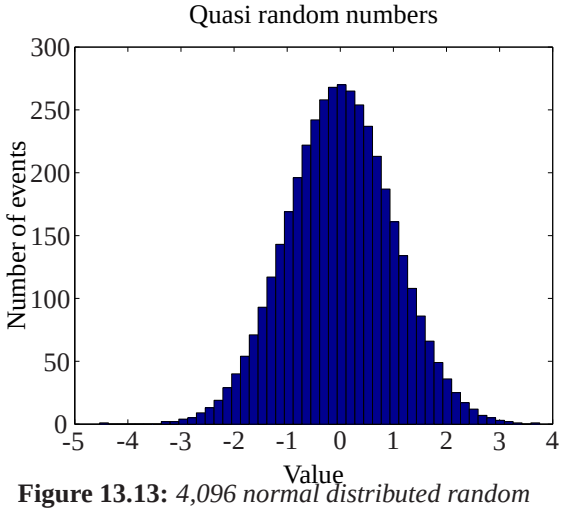

Figure 13.13: *4,096 normal distributed random numbers following a Sobol sequence.*

Both histograms are made on the basis of 4,096 normal distributed random numbers, with mean value, $\mu = 0$, and standard deviation, $\sigma = 1$. The only difference is that the histogram in Figure 13.12 is generated from pseudo random numbers, whereas the histogram in Figure 13.13 is generated from numbers following a randomized Sobol sequence. From Figure 13.12 and Figure 13.13 it can be seen that there are less scatter in the histogram following a Sobol sequence, which is the reason for the faster convergence rate. A convergence analysis for the method is described in Appendix M.

13.3.5 Results

A MATLAB programme containing the calculations for asymptotic sampling can be seen in CD Appendix A.
In the following section the results from the asymptotic sampling will be presented. The partial safety factor for the undrained shear strength will be calibrated against the target reliabilities stated in Table 11.6. Furthermore a sensitivity analysis will be performed in order to determine the relative importance of the different stochastic variables.
In Table 13.5 the reliability indices for two situations of COV_{wind} is seen.

Table 13.5: *Reliability index for different COV's.*

Description	Symbol	COV_{wind} = 5%	COV_{wind} = 15%
Mean reliability index	$\bar{\beta}$	3.55	3.33
Annual probability of failure	p_f	$1.89 \cdot 10^{-4}$	$4.41 \cdot 10^{-4}$

By comparing the results in Table 13.5 with the target reliabilities in Table 11.6, it is seen that safety of the structure lies between the two bounds stated. Therefore the partial safety factor for the undrained shear strength, γ_{c_u}, should be increased in order to obtain a target reliability index of 3.72, which is shown in the following discussion.

Sensitivity Analysis

In Table 13.6 the omission sensitivity factor, ζ, for COV_{wind} = 15% can be seen.

Table 13.6: *Omission sensitivity factor for COV_{wind} = 15%.*

Variable	H_b	M_b	V	c_u	X_{exp}	X_{st}	X_{aero}	X_{dyn}	X_{sim}	X_{ext}
ζ	1.00	1.27	1.01	1.00	1.24	1.01	1.08	1.01	1.01	1.01

From Table 13.6 it is observed that the basic moment, M_b, and the uncertainties connected with it are the variables that provides the biggest uncertainties to the reliability index. Therefore is it these variables that should be investigated further in order to increase the reliability index. It is more surprising to see that the effect of setting the undrained shear strength to a deterministic parameter does not have any influence on the result. The reason for this will be discussed later.

In Table 13.7 the elasticity coefficients, e, for the mean values and standard deviations for COV_{wind} = 15%, are presented.

Table 13.7: *Elasticity coefficients, e_μ and e_σ, for COV_{wind} = 15%.*

Variable	H_b	M_b	V	c_u	X_{exp}	X_{st}	X_{aero}	X_{dyn}	X_{sim}	X_{ext}
e_μ	0.00	-0.64	0.85	0.08	-0.58	-0.88	-0.79	-0.88	-0.88	-0.88
e_σ	0.00	-0.26	-0.02	-0.00	-0.32	-0.02	-0.11	-0.02	-0.02	-0.02

The result shows that the effect of changing the mean value of the undrained shear strength is of minor importance. Therefore a change of the partial safety factor for the undrained shear strength, γ_{c_u}, would only have a little effect,

and it is therefore expected that a large γ_{c_u} is needed in order to obtain a target reliability index equal to 3.72.

The omission sensitivity factor, ζ, and elasticity coefficient, e, for COV_{wind} = 5% can be seen in Table 13.8 and Table 13.9.

Table 13.8: *Omission sensitivity factor for COV_{wind} = 5%.*

Variable	H_b	M_b	V	c_u	X_{exp}	X_{st}	X_{aero}	X_{dyn}	X_{sim}	X_{ext}
ζ	1.00	1.02	1.01	1.00	1.43	1.02	1.18	1.02	1.02	1.02

Table 13.9: *Elasticity coefficient e_μ and e_σ for COV_{wind} = 5%.*

Variable	H_b	M_b	V	c_u	X_{exp}	X_{st}	X_{aero}	X_{dyn}	X_{sim}	X_{ext}
e_μ	-0.01	-0.98	0.96	0.09	-0.54	-0.99	-0.82	-0.99	-0.99	-0.99
e_σ	0.00	-0.08	-0.03	-0.01	-0.48	-0.03	-0.20	-0.03	-0.03	-0.03

In Table 13.8 and 13.9 the same observations as for the situation with COV_{wind} = 15% is made, and therefore the same comments apply here.

13.3.6 Discussion

From the sensitivity analysis it is clear that the undrained shear strength's relative importance is small. The reason for this is the strong eccentric loading of the foundation. From the deterministic analysis made in Chapter 12 the width of the foundation was determined to 13.82 m. From Table 12.3 it is seen that the eccentricity was determined to 5.87 m. This leads to an effective width of the foundation equal to 2.08 m. in accordance to Equation (13.8).

$$B' = B - 2\,e \tag{13.8}$$

B'	Effective width of foundation [m]
B	Width of foundation [m]
e	Eccentricity [m]

This strong eccentric loading leads to a small effective area of the foundation, and therefore the relative importance of the moment will be undesirable large. This means that even a small variation in the moment load could result in a great reduction of the effective area. The great importance of the moment is also shown through the sensitivity analysis performed.

The minor importance of the undrained shear strength for this situation is also emphasised by the calibrated partial safety factor shown in Table 13.10.

Table 13.10: *Calibrated γ_{c_u} for COV_{wind} = 5%.*

Situation	γ_{c_u}	β
COV_{wind} = 5%	2.71	3.72

From this result it is seen, that the reliability analysis is strongly dependent on the eccentricity of the foundation. In order to emphasise this dependency, a similar foundation installed on the same soil conditions is designed in Appendix N. The only difference is an increase of the self-weight of the structure, in order to reduce the eccentricity.

Part V

Additional Study

Further analyses are made, which follows from the next two parts. First, a case study on the correlation lengths' effect on a vertically loaded surface footing is treated. A stochastic field is modelled to describe the soil randomness, and specifying the soil strength with a linear trend in the depth direction. An integration over a Prandtl failure is used for calculating the bearing capacity. This is done for 10,000 realisations of the stochastic field for various combinations of the horizontal and vertical correlation lengths. The bearing capacity distribution is compared with a deterministic calculation for the same soil strength for each combination of correlation length. Lastly, partial safety factors are calibrated for all combinations of correlation lengths.

Chapter 14

Effects of the Correlation Length

As stated previously the soil strength is governed by varying quantiles dependent on the correlation length of the given soil. This chapter will shed light on this issue through a case study of stochastic field modelling.

14.1 Vertically Loaded Surface Footing

The bearing capacity under a vertical loaded surface footing is evaluated by implementing a stochastic field using different combinations of horizontal and vertical correlation lengths. Distributions of the bearing capacities for each combination of correlation lengths are made on the basis of 10,000 simulations, where the bearing capacity is evaluated by integration over the failure mechanism. Lastly the 5% quantile is used for comparison between the different combinations of correlation length.

14.1.1 Scenario Description and Assumptions

The case is a simple vertical loaded surface footing on clay. The soil deposit is assumed to have an undrained shear strength of 60 kPa under the footing and a strength increase of 1.5 kPa/m in the vertical direction. For analysis setup, see Figure 14.1.

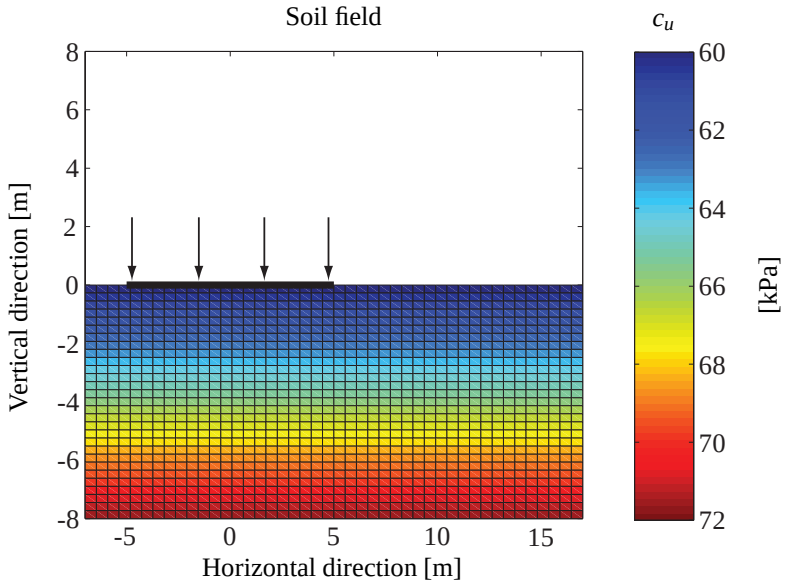

Figure 14.1: *Soil modelled with a strength increase of 1.5 kPa/m in vertical direction. No randomness included.*

In nature the soil strength is attached to a great portion of randomness. This randomness is taken into account by applying the theory described in Section 13.2 when modelling the stochastic field. This is illustrated in Figure 14.2 and 14.3 with different correlation lengths. At the same time the failure mechanism is shown.

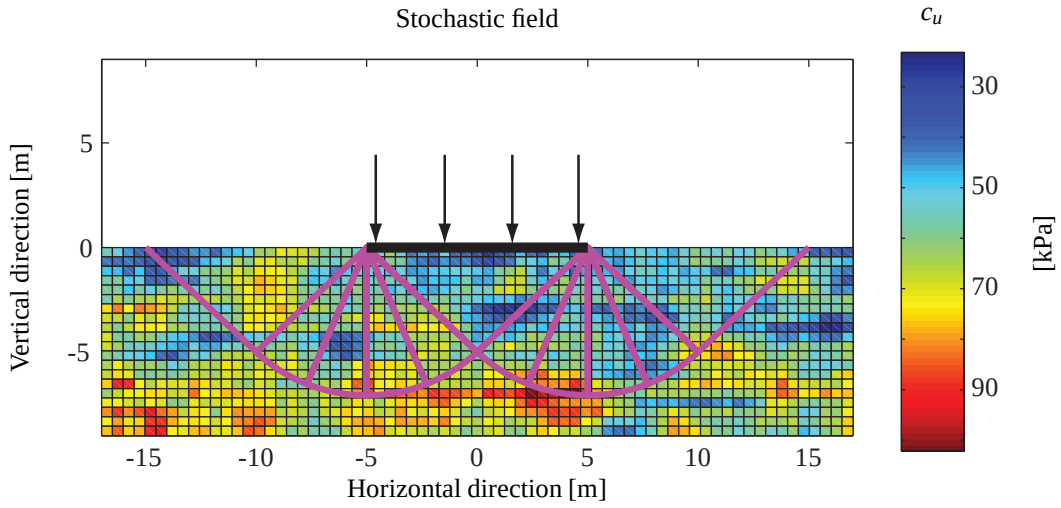

Figure 14.2: *Stochastic soil field realisation. Horizontal and vertical correlation length equals 3 and 1 m respectively.*

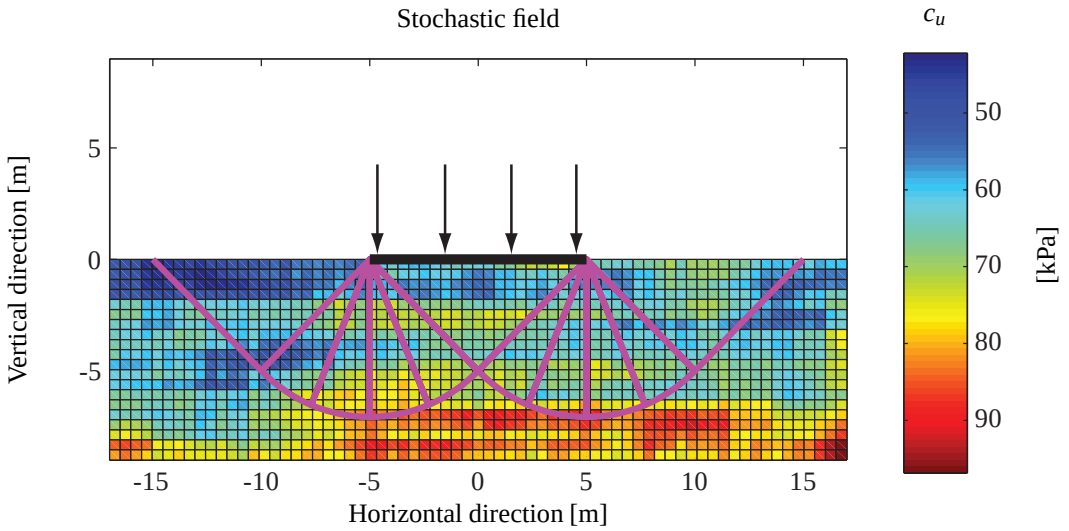

Figure 14.3: *Stochastic soil field realisation. Horizontal and vertical correlation length equals 15 and 3 m respectively.*

The bearing capacity is determined by integrating over the failure line that expands to both sides of the foundation. The bearing capacity will be governed by the elements with the lowest strength and the failure will therefore seek toward the side with the lowest bearing capacity. Therefore will the side with the lowest bearing capacity of the two opportunities be chosen for further calculation in each scenario. The failure line used is the Prandtl solution for vertically loaded shallow foundations [Azizi, 2000]. This provides a coinciding lowest upper bound and highest lower bound solution for the problem.

10,000 realisations of the stochastic field is being executed for each combination of correlation lengths. Each time the bearing capacity is determined by integrating over the failure mechanism and lastly the bearing capacities are fitted to a LogNormal cumulative distribution function. The influence of the correlation will be compared by analysing the cumulated distribution functions provided by different sets of correlation lengths, which are assumed to be between 0.5 - 50 m in horizontal direction and 0.5 - 5 m in vertical direction.

It is assumed that the horizontal correlation length at all time is equal to or larger than the vertical correlation length.

The 5% quantiles used for comparison are calculated using the expression given in Equation (14.1), which can be used if the coefficient of variation is small [Sørensen, 2011]. The coefficient of variation is assumed to be 0.16.

$$R_{0.05} = \mu_R \exp\left(-1.645\,\mathrm{COV}_R\right) \tag{14.1}$$

where

$R_{0.05}$	5% quantile of the bearing capacity [kN/m]
μ_R	Mean value of the bearing capacity [kN/m]
COV_R	Coefficient of variation of the bearing capacity [-]

After having determined the characteristics of the bearing capacities for the different combinations of correlations lengths, a partial safety factor will be calibrated for each case. In order to calibrate the partial safety factor, a target reliability has to be defined. The target reliability index investigated is listed in Table 14.1.

Table 14.1: *Investigated target reliability [Sørensen, 2012].*

Target reliability index, β_T	Annual probability of failure
3.72	10^{-4}

The vertical load on the foundation is assumed to originate from self-weight and it is set equal to the 5% quantile of the bearing capacity found from the deterministic calculation. The design equation and limit state equation used to calibrate the partial safety factors follows from Equation (14.2) and (14.3).

$$\begin{aligned} &G = R_d - V_d\, z = 0 \Leftrightarrow \\ &G = N_c\, \frac{c_{u,c}}{\gamma_{c_u}}\, B - V_c\, \gamma_{V_c}\, z = 0 \end{aligned} \tag{14.2}$$

where

G	Design equation [-]
R_d	Design value of the bearing capacity [kN/m]
V_d	Design value of the vertical load [kN/m]
z	Design parameter [-]
N_c	Bearing capacity factor [-]
$c_{u,c}$	Characteristic value of the undrained shear strength [kPa]
γ_{c_u}	Partial safety factor for the undrained shear strength [-]
B	Width of foundation [m]
V_c	Characteristic vertical load [kN/m]
γ_{V_c}	Partial safety factor for the vertical load [-]

The partial safety factors used in the calculations are shown in Table 14.2.

Table 14.2: *Partial safety factor for the undrained shear strength and self weight of the structure [Eurocode 7-1, 2007] and [Eurocode 1-1-1, 2007].*

γ_c	1.4
γ_{V_c}	1.0

In Table 14.2 it should be noted, that γ_c is only used for comparison as this is the partial safety factor that should be calibrated in the different scenarios. The limit state equation is as presented in Equation (14.3).

$$g = R - V\,z \tag{14.3}$$

where

g	Limit state equation [-]
R	Stochastic variable describing the bearing capacity [kN/m]
V	Stochastic variable describing the load [kN/m]

The distributions of the stochastic variables describing the bearing capacity, R, are calculated from the 10,000 simulations run for each combination of the correlation length. Values will follow in the results section. Furthermore it has been chosen to set the stochastic variable describing the load, V, equal to the 5% quantile of the bearing capacity calculated from a situation where no randomness is included in the field. By doing so the calculations will have an common base for comparison. This also entails that V will be set as a deterministic parameter.

14.1.2 Results

A MATLAB programme containing the calculations can be seen in CD Appendix A.
The simulations results in a number of bearing capacities for different correlation lengths. In Figure 14.4 the influence of the change in correlation lengths on the bearing capacity is clear. It is noted, that the distributions tend to have an decreasing standard deviation as the correlation lengths decreases. From this it is observed that the bearing capacity is more and more dominated by the mean value as the correlation lengths goes toward zero.

Further the LogNormal fitted distribution is considered acceptable, but for larger correlation lengths the distribution tends to diverge in the tails. For a more accurate estimate of the lower quantiles a tail fit is executed for all combinations of correlation lengths. Figure 14.5 to 14.8 shows the tail fit for horizontal and vertical correlation lengths equal to 3 and 1 meter and 15 and 3 meter, respectively. A change of bearing capacity is present for changes in the correlation length.

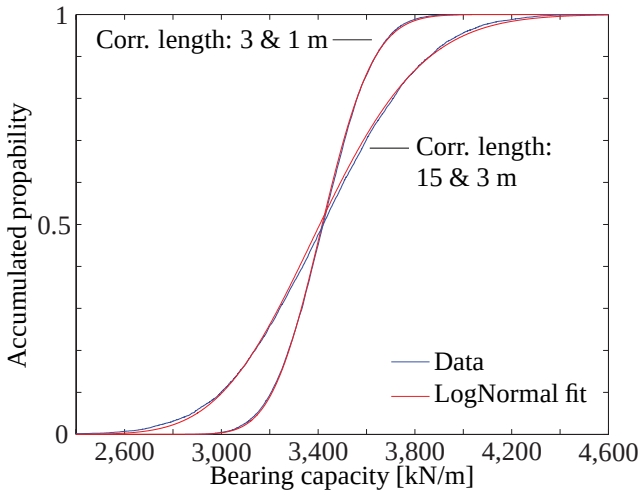

Figure 14.4: *LogNormal cumulative distribution function of simulated bearing capacities with different correlation lengths.*

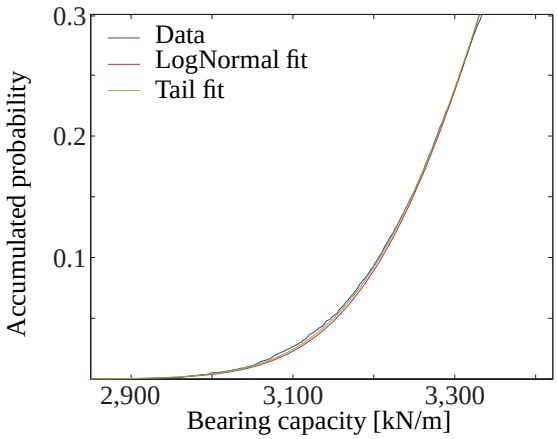

Figure 14.5: *Tail fit for correlation lengths equal to 3 and 1 meter.*

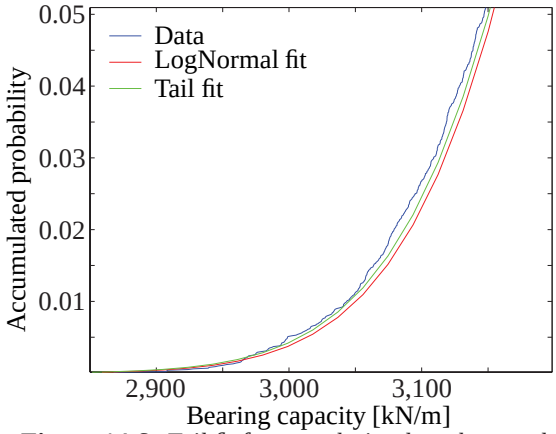

Figure 14.6: *Tail fit for correlation lengths equal to 3 and 1 meter. Zoomed in.*

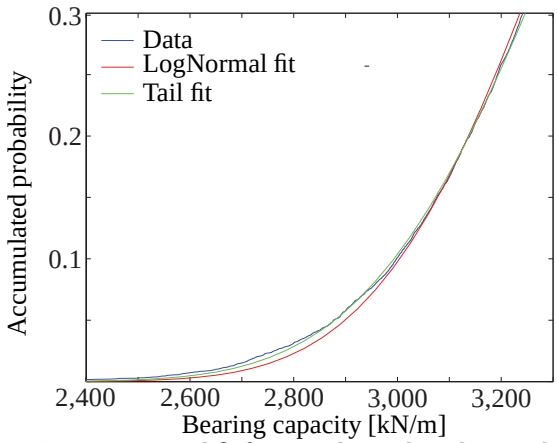

Figure 14.7: *Tail fit for correlation lengths equal to 15 and 3 meter.*

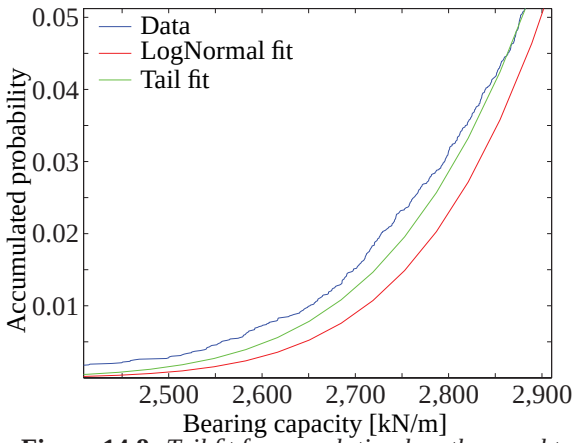

Figure 14.8: *Tail fit for correlation lengths equal to 15 and 3 meter. Zoomed in.*

As a point of reference for the calculated bearing capacities, the results are compared to the 5% quantile normally used for design. The deterministic bearing capacity is calculated from a mean c_u knowing that the failure reach a depth of $1/\sqrt{2}B$ and assuming a coefficient of variation of 0.16. This leads to a mean of 65.3 kPa and a 5% quantile of 2,580 kN/m for the bearing capacity. The characteristics of the bearing capacity are calculated and presented in Table 14.3.

Table 14.3: *Characteristic values of the bearing capacity calculated for the deterministic approach.*

	μ_R [kN/m]	σ_R [kN/m]	$R_{5\%}$ [kN/m]	COV [-]
Bearing capacity, R	3,357	537	2,580	0.16

The results from the different simulations and fitted curves are shown in Table 14.4, where a schematic overview of the influence of the correlation lengths is presented.

Table 14.4: *5% quantile of the bearing capacity [kN/m].*

Vertical correlation length [m]	Horizontal correlation length [m] 1	3	15	50
0.5	3,236	3,172	3,087	3,071
1	3,201	3,109	2,989	2,966
3	-	3,006	2,826	2,781
5	-	-	2,756	2,725

From Table 14.4 it is seen that the bearing capacity tends towards the mean value of the bearing capacity for small correlation lengths.

Figure 14.9 shows a plotted overview of the same results. Here the red line illustrates the 5% quantile of the deterministic bearing capacity normally used in design.

As the correlation lengths increase, so does the standard deviation and the 5% quantile of the bearing capacity decreases. It is noted that the normally used 5% quantile and coefficient of variation equal to 16% highly underestimate the bearing capacity in the range of normally depicted correlation lengths. For instance for very small correlation lengths, of 1 and 0.5 m in horizontal and vertical direction respectively, the standard deterministic method will underestimate the bearing capacity by approximately 20%. This indicates that there is a huge potential of savings when dimensioning foundations, if a spatial analysis of the strength parameters is carried out prior to the calculations - well-knowing that costs regarding the CPTu tests needed in order to perform the analysis have not been included. Typically an estimate of the correlation length can be found from the normally used mappings of the soil investigations.

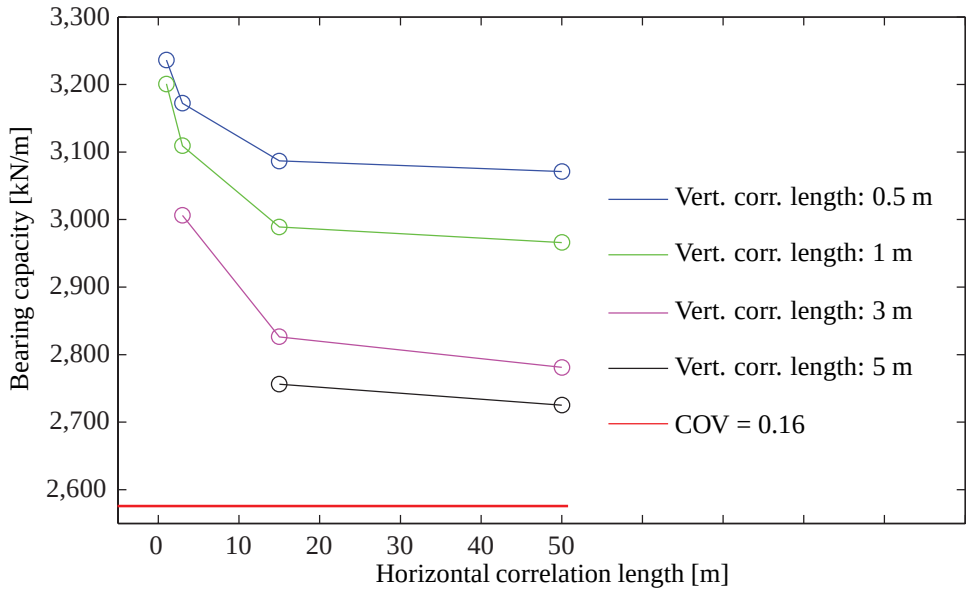

Figure 14.9: *The correlation length's influence on the 5% quantile of the bearing capacity. The red line indicates the 5% quantile for coefficient of variation equal to 0.16 normally used for design.*

In Table 14.5 the correlation lengths influence on the coefficient of variation for the bearing capacity is investigated.

Table 14.5: *Coefficient of variation derived from the simulations [%].*

Vertical correlation length [m]	Horizontal correlation length [m]			
	1	3	15	50
0.5	2.47	3.47	5.14	5.80
1	2.97	4.42	6.80	7.66
3	-	6.08	9.67	11.11
5	-	-	10.89	12.30

As expected the overall tendency of the coefficient of variation is rather clear. As the correlation lengths are increased the coefficient of variation describing the strength parameter is increasing. This is in good accordance with the fact, that small correlations leads to a dominating mean value of the soil. That is, the failure runs through heavily varying soil strengths, which adds up close to the mean value, instead of running through a majority of either high or low soil strengths.

The mean values for the bearing capacity from the simulations are as follows from Table 14.6, which are used for partial safety factor calibration.

Table 14.6: *Mean bearing capacity derived from the simulations [kN/m].*

Vertical correlation length [m]	Horizontal correlation length [m]			
	1	3	15	50
0.5	3,400	3,422	3,494	3,470
1	3,215	3,371	3,410	3,288
3	-	3,149	3,642	3,617
5	-	-	3,402	3,406

At this point all the information needed for calibrating the partial safety factors for each situation is present. The Stochastic variables used in Equation (14.3) are presented in Table 14.7 to set the record straight.

Table 14.7: *Stochastic variables for the limit state function.*

Name	Type	μ [kN/m]	COV [%]
V	D	2,580	0
R	LN	See Table 14.6	See Table 14.5

An iterative process has been executed for each of the combinations of the mean values and coefficients of variation in order to find the partial safety factors needed to obtain the target reliability, β_T, of 3.72. The results are presented in Table 14.8.

Table 14.8: *Partial safety factors, γ_{c_u}, for combinations of correlation lengths [-].*

Vertical correlation length [m]	Horizontal correlation length [m]			
	1	3	15	50
0.5	0.83	0.86	0.90	0.92
1	0.90	0.90	0.98	1.05
3	-	1.03	1.02	1.08
5	-	-	1.14	1.20

From Table 14.8 it is observed, that the partial safety factor possesses a great reduction potential compared to the current used value of 1.4. For small correlation lengths the partial safety factor obtain values lower than 1. These partial safety factors should be seen in connection with the 5% quantile determined from the deterministic design, which explains why it is lower than 1 for some combinations. The low values in Table 14.8 are good for stating an example of the potential reduction. From the results it is found that an investigation of the correlation lengths prior to the design could lead to large savings. One way of incorporating the correlation lengths could be to make partial safety factors dependent on the correlation lengths or make the 5% quantile depend on the correlation length, when considering a design situation.

The analysis has furthermore shown that the integrated 5% quantile of the bearing capacity tends towards the mean value of the bearing capacity for small correlation lengths. This is also indicated by the low COV on the bearing capacity for small correlation lengths.
It should be mentioned that the results are obtained on the basis of a simple example and should therefore only be regarded as a measure of comparison.

Part VI

Additional Study II

In the following part an advanced analytical model for shallow foundations will be used for design of the wind turbine foundation. At first the necessary diameter of the foundation will be determined from a deterministic design. The model uncertainty will be found by a comparison with simulations performed in the 2D numerical programme LimitState:Geo. At last the potential of probabilistic design will be evaluated.

Chapter **15**

Deterministic Approach for Frictional Soils

In the following chapter a deterministic approach for calculating the bearing capacity of the gravity based foundation will be presented. The method will be based on an advanced method suggested by [Randolph and Gourvenec, 2011].

15.1 Analytical Expression for Frictional Soil

In the following section a yield envelope will be described for frictional soil given by [Randolph and Gourvenec, 2011]. The yield envelope will be used later as the comparison between a deterministic and a probabilistic approach is carried out.
It should be noted that the expression for the yield envelope is adopted in contrast to failure envelope that is used, when describing clay. The difference is found in the behaviour and stress dependency between the two types of soil. The shear strength of sands are stress dependent whereas the shear strength for clay is independent of the stress state, as outlined in Equation (15.1) describing Mohr Coulomb's failure criteria for cohesive and frictional materials respectively.

$$\tau_f = c_u \qquad \tau_f = c' + \sigma'_f \tan\left(\varphi'\right) \tag{15.1}$$

where

τ_f	Shear strength leading to failure [kPa]
c_u	Undrained shear strength [kPa]
c'	Effective cohesion [kPa]
σ'_f	Effective normal stress leading to failure [kPa]
φ'	Effective friction angle [°]

Therefore an increasing displacement will lead to both increased yielding and hardening for a frictional soil, whereas for clay only an increase in yielding will occur. Therefore the use of a yield envelope is encouraged.

15.1.1 Method and Assumptions

The yield envelope for a surface footing in drained conditions is described by the expression in Equation (15.2).

$$f = \left(\frac{m_n}{m_0}\right)^2 + \left(\frac{h_n}{h_0}\right)^2 - 2\,a\,\left(\frac{h_n\,m_n}{h_0\,m_0}\right) - 1 = 0 \tag{15.2}$$

where

f	Failure envelope [-]
m_n	Dimensionless moment, cf. Equation (15.3) [-]
m_0	Dimensionless constant, 0.09 [-]
h_n	Dimensionless horizontal load, cf. Equation (15.3) [-]
h_0	Dimensionless constant, 0.12 [-]
a	Dimensionless constant, -0.22 [-]

The dimensionless forces, m_n and h_n, in Equation (15.2) are calculated as described in Equation (15.3).

$$m_n = \frac{M/(D\,V_0)}{4\,v\,(1-v)} \qquad h_n = \frac{H/V_0}{4\,v\,(1-v)} \tag{15.3}$$

where

M	Moment loading [kNm]
D	Diameter of foundation [m]
V_0	Uniaxial vertical yield load [kN]
v	Dimensionless vertical load, cf. Equation (15.4) [-]
H	Horizontal load [kN]

The dimensionless vertical load is calculated as described in Equation (15.4).

$$v = \frac{V}{V_0} \tag{15.4}$$

where

V	Vertical load [kN]

In order to calculate the ultimate vertical bearing capacity, V_0, Terzaghi's bearing capacity formula for drained conditions has been chosen, which is shown in Equation (15.5).

$$V_0 = \left(c'\,N_c\,s_c\,i_c + q'\,N_q\,s_q\,i_q + \frac{1}{2}\gamma'\,b'\,N_\gamma\,s_\gamma\,i_\gamma\right)A' \tag{15.5}$$

where

c'	Effective cohesion [kPa]
N_c, N_q, N_γ	Bearing capacity factors [-]
s_c, s_q, s_γ	Shape factors [-]
i_c, i_q, i_γ	Factors taking the inclination of the load into account [-]
q'	Effective overburden pressure at the bottom of the foundation [kPa]
γ'	Effective specific weight of the soil [kN/m^3]
b'	Effective or equivalent width of the foundation [m]
A'	Effective area of the foundation [m^2]

For the considered situation, some simplifications can be done for the expression in Equation (15.5). The term including the effective cohesion can be excluded, as it is assumed that no cohesion is present. Also it should be noted that no overburden pressure will be considered, as the considered foundation is a surface footing. A further simplification of Equation (15.5) can be done, as V_0 is calculated for a uniaxial stress state. Therefore the inclination factors can all be set to 1 and thereby ignored. Also the effective area will be the total area and the effective width will be the total width, as no eccentricity will be present. Hereby Equation (15.5) can be reduced to Equation (15.6).

$$V_0 = \frac{1}{2}\gamma' \, b \, N_\gamma \, s_\gamma \, A \tag{15.6}$$

where

b	Width of the foundation [m]
A	Total area of the foundation [m^2]

For a description of the remaining of the parameters in Equation (15.6) reference is made to Section 9.1.1.

Studies have shown that the expression in Equation (15.2) is in compliance with typical friction materials. The expression has shown good results whether the soil has been modelled with or without density and with or without dilant behaviour. [Randolph and Gourvenec, 2011]

15.1.2 Shape of Yield Envelope

In the present section the general shape for the yield envelope will be described and illustrated. The expression in Equation (15.2) has been evaluated, and the appertaining plot is shown in Figure 15.1.

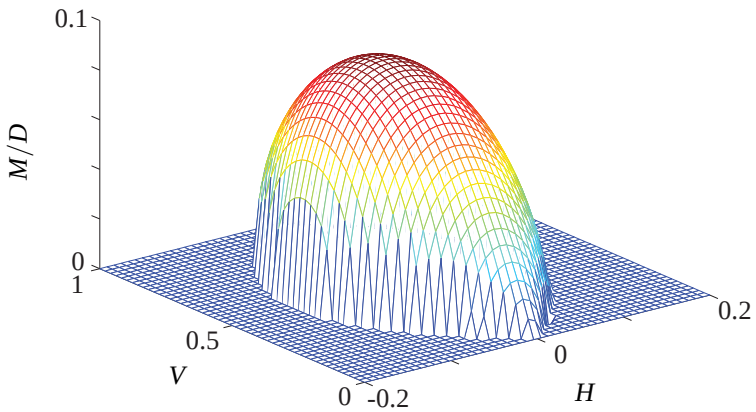

Figure 15.1: *3D plot of the yield surface.*

In Figure 15.1 only half the yield surface is shown, as a rotation around the V-axis will provide the other half. As the expression is for a surface footing it is observed, that no moment and no horizontal load will be absorbed by the footing, when no vertical load is applied.
The expression in Equation (15.2) needs to be compared with results obtained from real model measurements, in order to determine the uncertainties associated with the mathematical model. As no such measurements are available

at the given time, a comparison to values obtained from numerical simulations will be presented in the following chapter.

15.2 Design of Foundation

In the following section the necessary diameter of the foundation will be determined from Equation (15.2) and the loads given in Section 3.2.

15.2.1 Method and Assumptions

The self-weight of the structure will be determined by the criteria given in Equation (15.7). [Ibsen, 2012]

$$G = 0.5\, V_0 \tag{15.7}$$

where

G	Self-weight [kN]

The reason for this criteria can be seen in Figure 15.1, where it is shown that the maximum horizontal and moment bearing capacity is obtained at 50% of the uniaxial vertical bearing capacity. Therefore the self-weight will be determined by an iterative process, which can be seen in Figure 15.2.

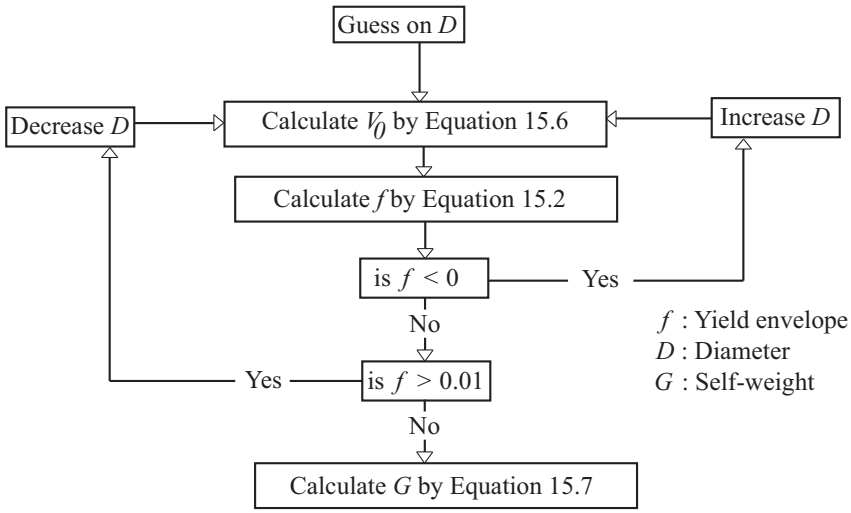

Figure 15.2: *The iterative process for determining the self-weight of the structure.*

15.2.2 Results

This iterative process has lead to the self-weight presented in Table 15.1.

Table 15.1: *Characteristic self-weight of entire structure.*

Description	Abbreviation	Value	Unit
Self-weight of wind turbine	$G_{wt,c}$	5,000	kN
Self-weight of foundation	$G_{f,c}$	27,739	kN
Total self-weight	G_c	32,739	kN

From Table 3.1 it is seen that the characteristic self-weight, G_c, is identical to the design self-weight, G_d, as the partial safety factor, γ_G, is equal to 1.

The self-weight from Table 15.1 has lead to a foundation with the diameter presented in Table 15.2.

Table 15.2: *Diameter of the foundation.*

Description	Abbreviation	Value	Unit
Foundation diameter	D	17.8	m

This foundation will be used in the probabilistic approach in order to compare the two approaches.

Chapter **16**

Determination of Model Uncertainty

As was the case for the analysis performed in Chapter 10, a model uncertainty will be appointed to the considered advanced expression in the following chapter.

16.1 Model Uncertainty for the Advanced Expression

The considered situation is still the same, whereas the simulation results presented in Table 10.4 are applicable for describing the model uncertainty associated with the expression in Equation (15.2) as well.

16.1.1 Method and Assumptions

The method is very similar to that of Section 10.2.1, why only the differences will be described in the following. The main difference is found in the formulation of the mathematical model, which, of course, differs significantly. To set the record straight the mathematical model is presented again with a small modification, cf. Equation (16.1). [Randolph and Gourvenec, 2011]

$$f = \left(\frac{m_n}{m_0}\right)^2 + \left(\frac{h_n}{h_0}\right)^2 - 2\,a\,\left(\frac{h_n\,m_n}{h_0\,m_0}\right) \tag{16.1}$$

where

f	Failure envelope [-]
m_n	Dimensionless moment, cf. Equation (15.3) [-]
m_0	Dimensionless constant, 0.09 [-]
h_n	Dimensionless horizontal load, cf. Equation (15.3) [-]
h_0	Dimensionless constant, 0.12 [-]
a	Dimensionless constant, -0.22 [-]

If the expression in Equation (16.1) is compared to that of Equation (15.2) it is noted, that the final term subtracting 1 is missing. This is done in order to facilitate the later calculations. This also implies that failure is obtained for a value of f equal to 1 instead of 0.

Except for the new expression of the mathematical model, the procedure is exactly the same as stated in Section 10.2.1. Once again it is important to note, that by applying the numerical simulations for the method, it is assumed that the simulations provide the exact results. An additional model uncertainty should be applied for the differences between the simulated results and real life measurements.

16.1.2 Results

The method has been applied to the advanced analytical expression and the obtained results will be commented upon in the following. The comparison of the simulated and mathematical results is shown in Figure 16.1 for illustrative purpose.

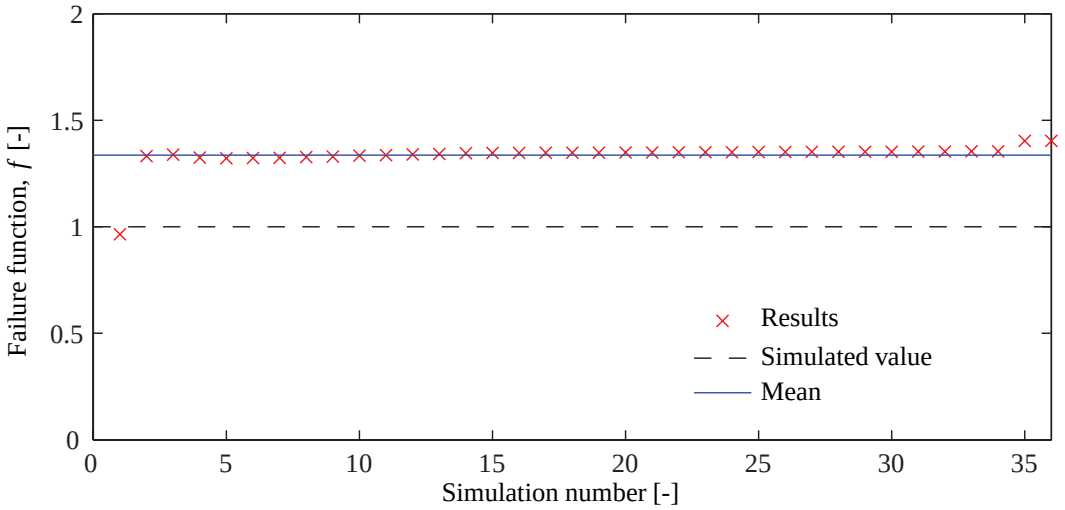

Figure 16.1: *Illustration of the mismatch between the mathematical model and the simulated results.*

From Figure 16.1 it can be observed, that the results from the mathematical model in general are 30 - 40% higher than those observed from the simulations. Due to the contruction of the failure envelope, this implies that the bearing capacity is largest from the numerical simulations, which also was expected. Therefore the value of the constant, b, is expected to be lower than 1, as this is multiplied with the loads, see Equation (16.2). Additionally it it observed, that there is an overall trend of the calculated results. The outliners for arms equal 5, 3,000 and 5,000 meters have been omitted again due to the same reasons as explained in Section 10.2.2. The calculated parameters are presented in Table 16.1.

Table 16.1: *Determined parameters for describing the model uncertainty.*

Parameter	Symbol	Type	Mean [-]	Standard deviation [-]
Model uncertainty	Δ	LogNormal	1	0.008
Constant	b	Deterministic	0.744	-

As the values all are very close to the mean value, as seen in Figure 16.1, a very low measure for the standard deviation is obtained. The results will be used, when the reliability of the failure envelope is to be considered.

For further illustrative purpose the simulated results are plotted against the modified analytical expression of the yield envelope, which can be rewritten as in Equation (16.2) in order to take the constant, b, into consideration.

$$f = b \left(\left(\frac{m_n}{m_0} \right)^2 + \left(\frac{h_n}{h_0} \right)^2 - 2\,a \left(\frac{h_n\, m_n}{h_0\, m_0} \right) \right) - 1 \tag{16.2}$$

By doing this, the difference seen in Figure 16.2 and 16.3 can be obtained. For the figures it has been chosen to show the 2D values corresponding to 50% of the ultimate bearing capacity, as it is difficult to see how well it fits, when plotting the entire 3D failure envelope.

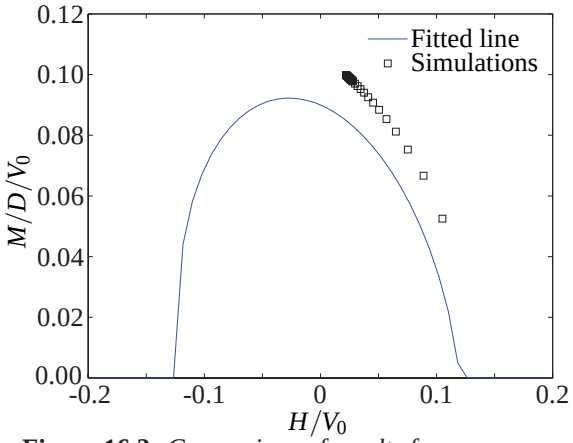

Figure 16.2: *Comparison of results from mathematical model and simulated values.*

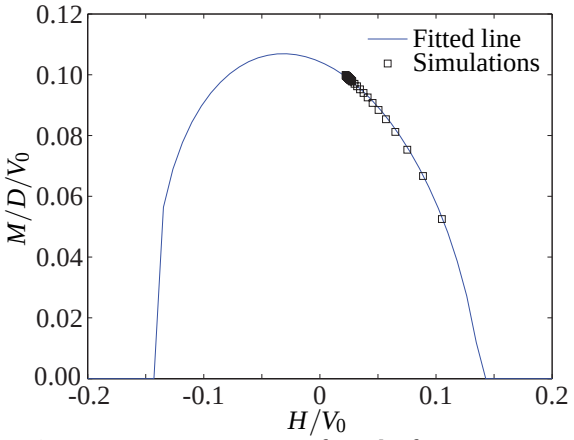

Figure 16.3: *Comparison of results from mathematical model and simulated values with b.*

As it can be observed from the figures, a very good agreement between the mathematical model and the simulated results are achieved, when the model uncertainties are included. The obtained values will therefore form the basis of the reliability analysis performed in Chapter 17.

Chapter **17**

Probabilistic Approach

The procedure for determining the reliability index is the same as described in Chapter 11. Furthermore the stochastic variables regarding the load and strength parameters are the same. The only exception to this is the mean value of the self-weight, which has changed due to the change of foundation dimensions. The limit state function will be described before the results will be presented, as this is the only element that has changed.

17.1 Limit State Function

In the considered case the calibrated yield envelope from Equation (16.2) will form the basis for the design equation, which can be seen in Equation (17.1).

$$G = 1 - \left(\left(\frac{m_{n,d}}{m_0} \right)^2 + \left(\frac{h_{n,d}}{h_0} \right)^2 - 2\,a\,\left(\frac{h_{n,d}\,m_{n,d}}{h_0\,m_0} \right) \right) b\,z = 0 \tag{17.1}$$

where

G	Design equation [-]
$m_{n,d}$	Dimensionless design moment [-]
m_0	Dimensionless constant, 0.09 [-]
$h_{n,d}$	Dimensionless horizontal design load [-]
h_0	Dimensionless constant, 0.12 [-]
a	Dimensionless constant, -0.22 [-]
b	Deviation between mathematical model and simulated results [-]

If Equation (17.1) is compared to Equation (16.2) it is seen that the signs have changed, which is due to the fact that failure of the structure will be considered for G < 0. The partial safety factors are connected to the design equation by Equation (17.2).

$$m_{n,d} = \frac{M_c\,\gamma_w/(D\,V_{0,d})}{4\,v_d\,(1-v_d)} \qquad h_{n,d} = \frac{H_c\,\gamma_w/V_{0,d}}{4\,v_d\,(1-v_d)} \qquad V_{0,d} = \frac{1}{2}\gamma'\,b\,N_{\gamma,d}\,s_\gamma\,A \qquad v_d = \frac{G_c\,\gamma_G}{V_{0,d}} \tag{17.2}$$

where

M_c	Characteristic moment load [kNm]
D	Diameter of foundation [m]
$V_{0,d}$	Design uniaxial vertical yield load [kN]
v_d	Dimensionless design vertical load, cf. Equation (15.4) [-]
H_c	Characteristic horizontal load [kN]
γ'	Effective specific weight of the soil [kN/m^3]
b	Equivalent width of the foundation [m]
$N_{\gamma,d}$	Design bearing capacity factor [-]
s_γ	Inclination factor [-]
A	Area of the foundation [m^2]
γ_w	Partial safety factor for the aerodynamic loads [-]
G_c	Characteristic self-weight [kN]
γ_G	Partial safety factor for the self-weight [-]

The corresponding limit state function can be seen in Equation (17.3).

$$g = 1 - \left(\left(\frac{m_n}{m_0} \right)^2 + \left(\frac{h_n}{h_0} \right)^2 - 2\,a\,\left(\frac{h_n\,m_n}{h_0\,m_0} \right) \right) b\,\Delta\,z \tag{17.3}$$

where

g	Limit state function [-]
Δ	Model uncertainty [-]

For the intermediate calculations reference is made to Section 15.1.

The self-weights of the wind turbine and foundation result in a vertical load. The vertical load will be assumed to be centrally loaded, and will therefore not induce an extra moment due to eccentricities. The self-weight of the structure can be determined with rather high accuracy. Therefore COV is set to 5% for the self-weight. The self-weight is Normal distributed and therefore the mean value can be found from Equation (17.4).

$$\mu_G = -\left(\Phi^{-1}\left(0.5\right)\,\sigma_G - G_{0.5}\right) = G_{0.5} \tag{17.4}$$

where

μ_G	Mean value of self-weight [kN]
σ_G	Standard deviation of self-weight [kN]
$G_{0.5}$	50% quantile of self-weight [kN]

This leads to the self-weight presented in Table 17.1.

Table 17.1: *Mean value of self-weight.*

Description	Abbreviation	Value	Unit
Self-weight	μ_G	32,739	kN

17.2 Results and Discussion

The results from the reliability analysis can be seen in Table 17.2.

Table 17.2: *Reliability index for different COV's.*

Description	Symbol	$COV_{0.15}$	$COV_{0.05}$
Reliability index	β	5.02	5.59
Annual probability of failure	p_f	$2.55 \cdot 10^{-7}$	$1.09 \cdot 10^{-8}$

When the results from Table 17.2 are compared to the target reliabilities from Table 11.6, it is seen that the safety of the foundation is quite large, which could result in rather conservative design of the foundation.
It should be mentioned that the reliability indices from Table 17.2 are obtained in connection with the demand stated in Equation (15.7). From Figure 15.1 it is seen that the moment and horizontal bearing capacities are at their maximum, when the self-weight of the structure is at 50% of the uniaxial vertical bearing capacity. When this is implemented in the probabilistic approach the distance to the yield envelope, would be greater compared to a design situation, where the demand in Equation (15.7) is not considered. This could be the explanation for the high reliability indices obtained in the analysis.

Additionally it is observed from Equation (17.2), that $V_{0,d}$ is present in both the numerator and the denominator, which has an unstabilising effect on the reliability analysis. Therefore it is found, that the used advanced expression is not suited for reliability analysis with the applied method.

Part VII

Conclusion

Chapter 18

Conclusion

The purpose of the thesis was to investigate the possible gaining of designing a gravitational foundation by the use of probabilistic methods compared to design following standards. In order to reach the specified goal preliminary works were carried out.

CPTu tests were performed at two different test locations in order to gather data for both a cohesive and a frictional soil. At the test site in Aalborg sand was analysed and expressions by both Mayne and Bolton was used to determine the characteristics. As the theory presented by Bolton allowed incorporation of the reduced effective friction angle, which is in best compliance with the used bearing capacity formulas, this method was preferred. The resulting sand was found to have a mean value of 33.2°, COV of 0.05 and a resulting 5% quantile of 30.3°. The values were found to be very low and concerns about the used method were outlined. Nonetheless, the results were used for further analysis, as the influence of the following analysis was of minor importance.
The test results from the clay site in Frederikshavn provided several challenges regarding the interpretation of the soil. Especially because no laboratorial investigations had been performed at the time of the interpretations. The characteristics of the clay were found to be consistent of a mean value of the undrained shear strength of 195 kPa, COV of 0.18 with a resulting 5% quantile of 144 kPa.
A spatial analysis was performed for both the test sites as well. Here it was found that the soil was hard to describe by the use of known tools for describing the spatial variation. In general dissatisfactory results were obtained. Although a general tendency of the spatial variation could be estimated from the results. The correlation lengths for the sand were found to be 0.1 - 0.5 and 2.5 m in vertical and horizontal directions respectively. For the clay slightly smaller correlation lengths were detected of 0.15 and 1.5 m respectively for vertical and horizontal direction.

From the characteristics of the soils it was possible to perform a deterministic design of the given wind turbine foundation. In the frictional soil a simple design situation was presented with the use of the Terzaghi bearing capacity formula. In spite of the large moment affecting the foundation, no problems were observed with the eccentricity of the foundation, and a resulting diameter of 18.38 m was found sufficient. From the deterministic design of the foundation, a probabilistic evaluation of the result was sought. In order to do so a model uncertainty was appointed to the bearing capacity formula. For this purpose a model was build in LimitState:Geo and the resulting simulated values of the loads leading to failure were regarded as exact results of the problem. A total of 36 simulations were run for the purpose, from which 20 was selected for the determination of the model uncertainty. It was found that the Terzaghi formulas in general underestimated the bearing capacity of the foundation by 40%, which was corrected for by appointing a bias and model uncertainty to the expression by Terzaghi. From here a probabilistic analysis of the found design was performed. It was found that the expression by Terzaghi provided large reliability indices compared to the target reliability index of 3.72 suggested by [Sørensen, 2012]. The reliability index was found to be 4.72 and 4.25 for a COV of 5% and 15% for the aerodynamic loads, respectively. For calibration of the partial safety factors of the strength parameters a partial safety factor of 1.35 for the load is used. It was found that for the problem treated the normally used partial safety factor of 1.25 for the effective friction angle could be reduced to 1.00 and

1.04 for a COV of 5% and 15% for the aerodynamic loads, respectively. Further it was observed that the COV for the effective friction angle plays an important part in the analysis as well. By increasing COV the reliability index of the design will decrease significantly. Therefore it is proposed, that the partial safety factor for the soil strength should depend on the characteristics of the loading and the soil if such information are available prior to design. In the sensitivity analysis of the Terzaghi bearing capacity formula it was found, that the expression was very sensitive toward changes in the characteristics of the moment loading, as this is dominant in the bearing capacity formula through the expression of the eccentricity. Therefore it was found, that for similar scenarios caution should be taken when describing the aerodynamic loads in particular.

The same scenario was investigated for the cohesive soil found at the location in Frederikshavn. For the cohesive material the scenario was transformed into a 2D case, as an implementation of a stochastic field was desired. By applying the Terzaghi formula for cohesive materials a needed width of a strip footing was found to be 13.82 m. The surface footing was found to be exposed to strong eccentric loading, which was taken into account in the dimensioning. The probabilistic approach for analysing the found deterministic design was rather different compared to that of sand. A failure domain was subtracted from LimitState:Geo, from which an integration of the undrained shear strength took place. The found values were used to determine the reliability of the Terzaghi bearing capacity formula through asymptotic sampling. For this case reliability indices of 3.55 and 3.33 were found for a COV of 5% and 15% for the aerodynamic loads respectively. These are seen to be lower than the target reliability of 3.72, which is why the partial safety factors should be increased to fulfil the given demands. In the sensitivity analysis, it was found that changing the undrained shear strength would have a minor effect on the reliability index. Therefore an unrealistic high partial safety factor of 2.71 on the undrained shear strength for a COV of 5% for the aerodynamic loads was observed, and the analysis is thought to be case sensitive. This was furthermore confirmed by the sensitivity analysis, where the moment was found to be the overriding parameter, when the reliability was to be determined. This was additionally confirmed from a case study in Appendix N, where the eccentricity was reduced and a potential reduction of the partial safety factor was spotted.

In connection to the probabilistic design situations it was investigated how much the correlation length influenced the bearing capacity for a vertically loaded strip footing. The bearing capacities were found by integrating over a Prandtl solution. It was found that the partial safety factor for the undrained shear strength could be reduced to be in the range 0.83 - 1.20, when the vertical correlation length ranged from 0.5 - 5 m and the horizontal ranged from 1 - 50 m. Again it was suggested, that a partial safety factor dependent on the soil characteristics could be introduced, as great savings could be found by performing soil investigations regarding the correlation length prior to design.

As a second additional study, it was investigated how well the used method, for describing the reliability of bearing capacities, performed for more advanced models describing a 3D yield envelope for drained conditions. Although the proceeding was identical to that for the Terzaghi bearing capacity formula, it was found, that complications emerged due to use of the strength parameters in the expression. Therefore this method is not always applicable but relies on the limit state equation.

In general it is concluded, that significant gaining could be obtained from probabilistic dimensioning of gravity based foundations. This is both the case for frictional and cohesive soils, but it highly depends on the load case. Investigation of the spatial variation of soils prior to design is expected to sum up as an economical beneficial investigation.

Chapter 19

Discussion

Through this thesis it is sought to describe the potential gainings from a probabilistic approach when calculating a gravitational foundation exposed to typical onshore wind turbine loading. Also the importance of determining the correlation length prior to a design is handled.

To gain input for the analyses CPTu tests are analysed with different methods. The choice of methods used to interpreting the CPTu data are shown to have great influence on the result for the effective friction angle. It is important to keep in mind that the general physical behaviour of the material should be respected before results are used for design. Due to low friction angles that verge on the loosest sand deposits obtained, the applied methods used in this thesis is considered to underestimate the strength of the frictional material, which could lead to conservative results. For the reliability analysis made in this thesis it did not have any influence, but for use in practical design it is of great importance to consider the physical behaviour.

Due to great uncertainties regarding the strength of soil, mathematical models often provides a conservative estimate of the strength in order to provide a hidden safety. From a probabilistic point of view it is of greater interest to get the best estimate, in contrary to a conservative model with a hidden safety.

It shall furthermore be mentioned that including sand stripes in cohesive soils and cohesive material in frictional soil is a must in a design situation, where this soil content can have significant influence on the bearing capacity. Including this the method will get undesirable complex.

When analysing the spatial correlation among the strength parameter of the soil, difficulties are found. Both applied methods are acting unintended as the CPTu tests are analysed. Great uncertainty is attached to the results in the thesis, but the presented analyses still treat the effect of the observed correlation lengths. It is considered, that guidelines to or a refinement of the methods are needed for treatment of CPTu tests of soils with significant fluctuation around the trend or clear inhomogeneity.

Eurocode 0 suggest that either the 5% quantile of the strength parameter or 5% quantile of the bearing capacity is used for design. A simple study shows that there is significant difference in up to 15% in using both methods. This difference is present for design on frictional soil, whereas the situation is unchanged for analyses on cohesive soil. This is due to how the strength parameters, φ' and c_u, are included in the bearing capacity formulas. The formulation in Eurocode 0 is considered loose and a clarification is desirable as the result influences the level of safety.

Model uncertainty is throughout the thesis treated by making a numerical model describing the problem as accurate as possible. Assuming the results from the numerical model as exact values and determining the model uncertainty from this assumption, gives a false impression of the actual model uncertainty. Nonetheless, it is a better estimate, compared to disregarding the model uncertainty completely. Analytical expressions works well for simple scenarios,

but as the problem gets more complex, numerical models provide more accurate estimates. For determining the correct model uncertainty, real life measurements should be available, which was not the case for this thesis.

It is found in the probabilistic analysis of frictional soil, that a great reduction of the partial safety factor for the effective friction angle, $\gamma_{\varphi'}$, can be obtained. Therefore it is considered, that a cost reduction is possible if the partial safety factor for the effective friction angle, $\gamma_{\varphi'}$, is made dependent of the COV for the soil strength. For large construction projects a number of CPTu tests are already required, wherefore no additional test are needed in order to take this effect into account.

The loading situation entails that the most important stochastic variable is the basic moment. This has a much greater influence on the safety than the strength parameters. This is due to a very small effective area, which causes a minor change in the loading to cause a greater change in the safety. Therefore much attention should be given in determining the characteristics of the wind load and the uncertainty parameters connected with it in order to reduce the uncertainty.

The reliability analysis made for the foundation installed on the cohesive soil has shown that the foundation is very sensitive to moment loads. This was due to the strong eccentric loading, which made it difficult to calibrate the partial safety factor for the undrained shear strength. In general it is believed that there is a large reduction potential when probabilistic design is considered, which also was observed for a vertically loaded foundation installed on cohesive soil.

The study of the effect of the correlation length clearly shows that the bearing capacity is highly influenced by the correlation length. As the correlation lengths decrease, the bearing capacity is governed by a quantile that approaches the mean value for the soil strength. If this aspect could be implemented in construction projects and the correlation lengths could be determined with a high degree of accuracy, a huge reduction potential is available within this topic.

Bibliography

Andersen, **2012**. Morten Søgaard Andersen. *Design Loads for Wind Turbine Foundation*. Mail corrospondance d. 7/3-2012, 2012.

Andersen and Sjørring, **1992**. Steen Andersen and Steen Sjørring. *Geologisk set: Det nordlige Jylland*. ISBN: 87-7702-055-3, Vol. 1. Geografforlaget, Miljøministeriet, 1992.

Azizi, **2000**. Fethi Azizi. *Applied Analyses in Geotechnics*. Taylor and Francis, 2000.

Baker, J. and Calle, E, **2006**. Baker, J. and Calle, E. *JCSS Probalistic Model Code*, 2006.

Berthelsen, **1987**. Ole Berthelsen. *Geologi i Aalborg området*. ISBN: 87-421-0752-0, Vol. 1. Dansk Geologisk Undersøgelse, Miljøministeriet, 1987.

Bolton, **1986**. M. D. Bolton. *The Strength and Dilantancy of Sands*. Géotechnique, 36, 1986.

Bucher, **2009**. Christian Bucher. *Asymptotic sampling for high dimensional reliability analysis*. Probabilistic Engineering Mechanics, no. 24, p. 504–510, 2009.

Chr. Jensen, **2009**. Bjarne Chr. Jensen. *Teknisk Ståbi*. ISBN: 978-87-571-2685-3, 20. udgave. Nyt Teknisk Forlag, 2009.

DNV, **2010**. DNV. *STATISTICAL REPRESENTATION OF SOIL DATA*, 2010.

DNV/Risø, **2010**. DNV/Risø. *Guidelines for Design of Wind Turbines*, 2010.

Eurocode 0, **2007**. Eurocode 0. *DS/EN 1990: Eurocode 0: Projekteringsgrundlag for bærende konstruktioner*. ICS: 91.070.10; 91.080.01, 2. udgave. Dansk Standard, 2007.

Eurocode 1-1-1, **2007**. Eurocode 1-1-1. *DS/EN 1991-1-1: Eurocode 1: Last på bærende Konstruktioner - Del 1-1: Generelle laster - Densitet, egenlast og nyttelast for bygninger*. DS/EN 1991-1-1, 2. udgave. Erhvervs og Byggestyrelsen, 2007.

Eurocode 7-1, **2007**. Eurocode 7-1. *DS/EN 1997-1: Eurocode 7: Geoteknik - Del 1: Generelle regler*. ICS: 91.070.70; 93.020, 2. udgave. Dansk Standard, 2007.

Eurocode 7-1 DK NA, **2008**. Eurocode 7-1 DK NA. *EN 1997-1 DK NA: Nationalt Anneks til Eurocode 7: Geoteknik - Del 1: Generelle regler*. 4. udgave. Dansk Standard, 2008.

Fenton and Griffiths, **2003**. Gordon A. Fenton and D. V. Griffiths. *Bearing Capacity Prediction of Spatially Random c-φ Soils*. Canadian Geotechnical Journal, no. 40, p. 54–65, 2003.

Geron and Iliescu, **2012**. Geremy Geron and Alexandra-Ioana Iliescu. *Seismic Cone Penetration Test. Experimental results in onshore areas of Nordjylland Denmark*. page 10, 2012.

Google, **2012**. Google. *Google Maps*. URL: `http://maps.google.dk/`, 2012. Downloadet: 23.03.2012.

Grontmij, **2012**. Grontmij. *Test Results from Suderbovej*. Per Brøndum, Raw data, 2012.

Ibsen, **2012**. Lars Bo Ibsen. *Supervision Meetings*. Supervisor, feb-jun 2012, 2012.

Ibsen, Barari, and Larsen, **2012**. L.B. Ibsen, A. Barari, and K.A. Larsen. *Modified vertical bearing capacity for circular foundations in sand using reduced friction angle*. Ocean Engineering, 39, s. 1–6, 2012.

IEC, **2005**. IEC. *IEC 61400-1 - Wind turbines - Part 1: Design requirements*. 3. Edition. International Electrotechnical Commission, 2005.

Krebs Ovesen, D. Fuglsang, Bagge, Krogsbøll, S. Sørensen, Hansen, Bødker, Thøgersen, Galsgaard, and H. Augustesen, **2007**. Niels Krebs Ovesen, Leif D. Fuglsang, Gunnar Bagge, Anette Krogsbøll, Carsten S. Sørensen, Bent Hansen, Klaus Bødker, Lotte Thøgersen, Jens Galsgaard, and Anders H. Augustesen. *Lærebog i Geoteknik*. ISBN: 978-87-502-0961-4, 1. udgave. Polyteknisk Forlag, 2007.

Look, **2007**. Burt Look. *Handbook of Geotechnical Investigation and Design Tables*. ISBN: 13:978-0-415-43038-8, 1. udgave. Taylor and Francis Group London, 2007.

Luke, **1994**. Kirsten Luke. *The use of CPTU in danish soils*, 1994.

Mayne, **2006**. P.W. Mayne. *Characterisation and Engineering Properties of Natural Soils*. Vol. 3. Geosystems Engineering Group, Georgia Institute of Technology, Atlanta, GA, USA, 2006.

NearshoreLAB Frederikshavn A/S, **2007**. NearshoreLAB Frederikshavn A/S. *Seismisk kortlægning af undersøgelsesområde*, 2007.

Nordahl, **2012**. Benjamin Nordahl. *Meetings*. Lecturer at AAU, may-jun 2012, 2012.

Pedersen, Poulsen, Roesen, Pedersen, Thomassen, and Nielsen, **2011**. Morten Lauge Pedersen, Rikke Poulsen, Hanne Ravn Roesen, Annette Næslund Pedersen, Kristina Thomassen, and Benjamin Nordahl Nielsen. *Ingeniørgeologi og geoteknik*. Forelæsning, efterår 2011, 2011.

Randolph and Gourvenec, **2011**. Mark Randolph and Susan Gourvenec. *Offshore Geotechnical Engineering*. Taylor and Francis, Inc., 2011.

Sørensen, **2012**. John Dalsgaard Sørensen. *Supervision Meetings*. Supervisor, feb-jun 2012, 2012.

Sørensen, **2011**. John Dalsgaard Sørensen. *Notes in Structural Reliability Theory*, 2011.

Sørensen, John D., **2011**. Sørensen, John D. *Modelling of Model Uncertainties*, 2011.

Tarp-Johansen, Madsen, and Frandsen, **2002**. Niels Jacob Tarp-Johansen, Peter Hauge Madsen, and Sten Frandsen. *Calibration of Partial Safety Factors for Extreme Loads on Wind Turbines*, 2002.

Vestas, **2012**. Vestas. *Turbine Overview*. URL: `http://www.vestas.com/en/wind-power-plants/procurement/turbine-overview.aspx#/vestas-univers`, 2012. Downloadet: 03.04.2012.

Part VIII

Appendix

Appendix **A**

Attached CD

Site Data

Suderbovej Pictures

Suderbovej Raw Data

Mayne Results

Bolton Results

Clay Results

Estimation of Correlation Lengths using Trend Coefficients

Estimation of Correlation Lengths using Empirical Semivariogram

Deterministic Design of Foundation Installed on Frictional Soil

LimitState:Geo Model

Model Uncertainty

Fortran Programme for Reliability Analysis

Deterministic Design of Foundation Installed on Cohesive Soil

LimitState:Geo Model used for Failure Domain Extraction

Stochastic Field

Asymptotic Sampling

Additional Study I

Bore Profiles from Suderbovej

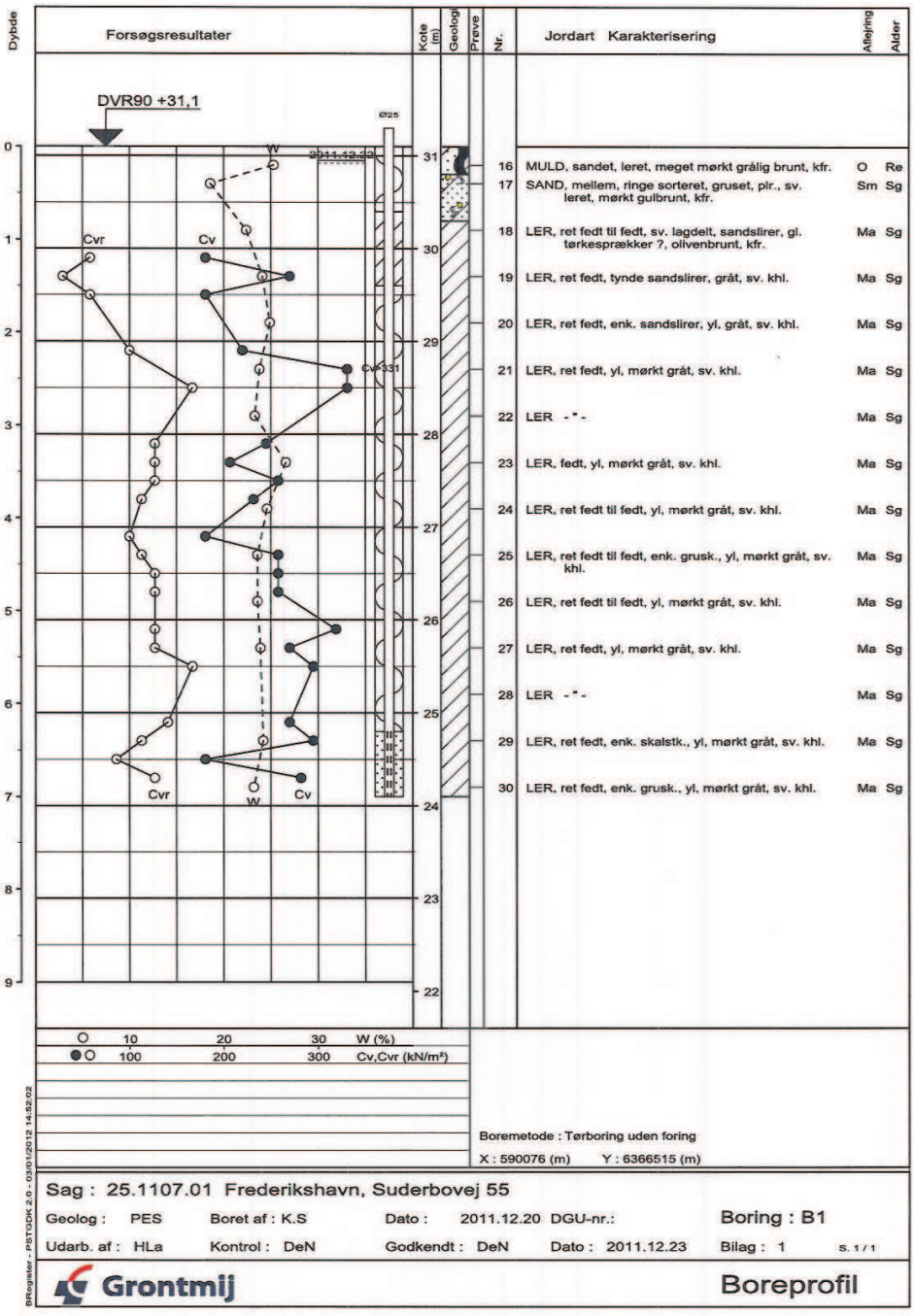

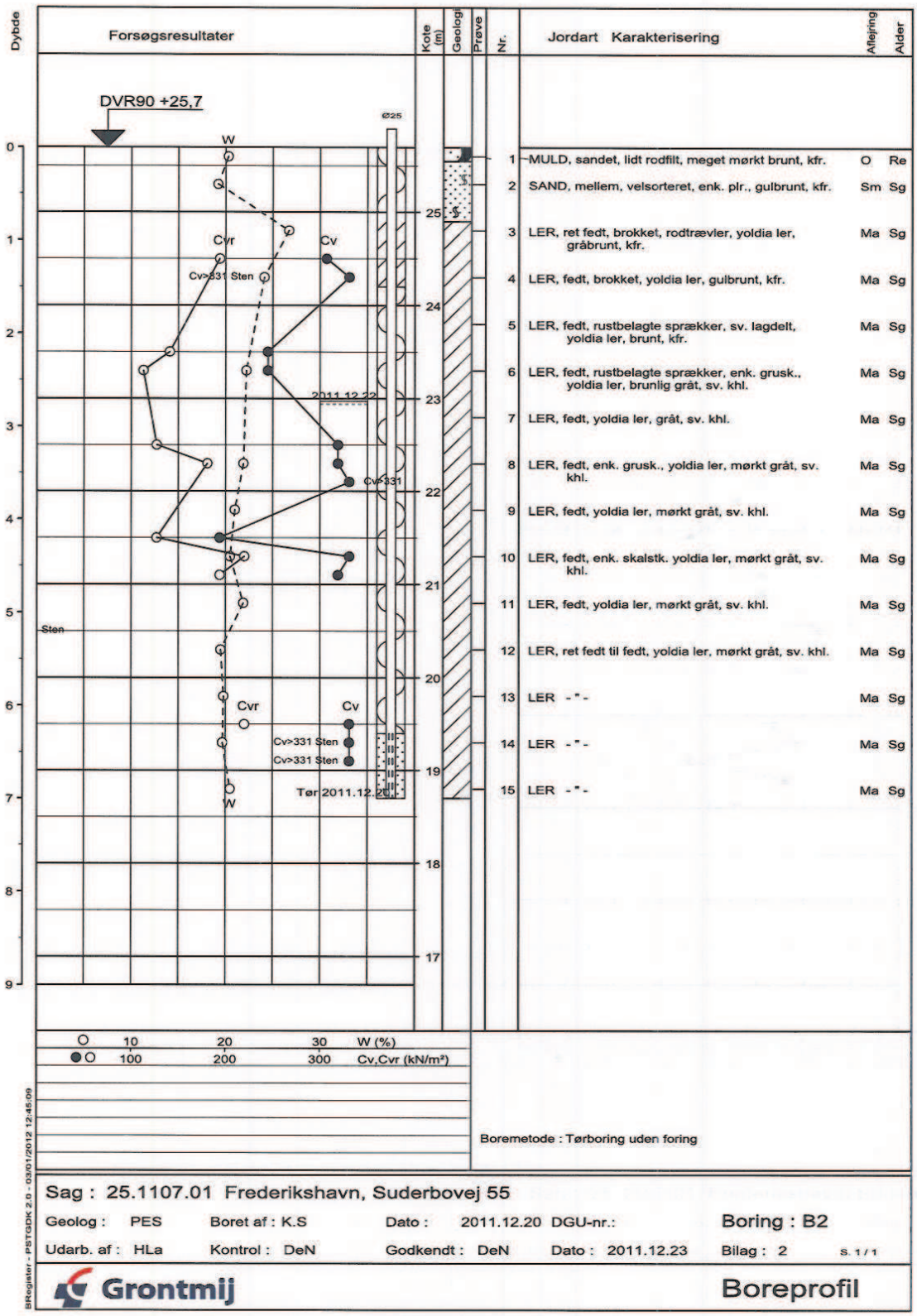
Dybde
Forsøgsresultater
Kote (m)
Geologi
Prøve
Nr.
Jordart Karakterisering
Aflejring
Alder
DVR90 +25,7
Ø25
W
Cvr
Cv
Cv>331 Sten
2011.12.22
Cv>331
Sten
Cvr
Cv
Cv>331 Sten
Cv>331 Sten
Tør 2011.12.20
W
1 MULD, sandet, lidt rodfilt, meget mørkt brunt, kfr. O Re
2 SAND, meliem, velsorteret, enk. plr., gulbrunt, kfr. Sm Sg
3 LER, ret fedt, brokket, rodtrævler, yoldia ler, gråbrunt, kfr. Ma Sg
4 LER, fedt, brokket, yoldia ler, gulbrunt, kfr. Ma Sg
5 LER, fedt, rustbelagte sprækker, sv. lagdelt, yoldia ler, brunt, kfr. Ma Sg
6 LER, fedt, rustbelagte sprækker, enk. grusk., yoldia ler, brunlig gråt, sv. khl. Ma Sg
7 LER, fedt, yoldia ler, gråt, sv. khl. Ma Sg
8 LER, fedt, enk. grusk., yoldia ler, mørkt gråt, sv. khl. Ma Sg
9 LER, fedt, yoldia ler, mørkt gråt, sv. khl. Ma Sg
10 LER, fedt, enk. skalstk. yoldia ler, mørkt gråt, sv. khl. Ma Sg
11 LER, fedt, yoldia ler, mørkt gråt, sv. khl. Ma Sg
12 LER, ret fedt til fedt, yoldia ler, mørkt gråt, sv. khl. Ma Sg
13 LER - " - Ma Sg
14 LER - " - Ma Sg
15 LER - " - Ma Sg
10 20 30 W (%)
100 200 300 Cv,Cvr (kN/m²)
Boremetode : Tørboring uden foring
Sag : 25.1107.01 Frederikshavn, Suderbovej 55
Geolog : PES Boret af : K.S Dato : 2011.12.20 DGU-nr.: Boring : B2
Udarb. af : HLa Kontrol : DeN Godkendt : DeN Dato : 2011.12.23 Bilag : 2 s. 1 / 1
Grontmij
Boreprofil
BRegister - PSTGDK 2.0 - 03/01/2012 12:45:09

Appendix **C**

Raw Data from Suderbovej

The following figures shows the uncorrected cone resistance and pore pressure along the depth for the CPTu tests from Suderbovej.

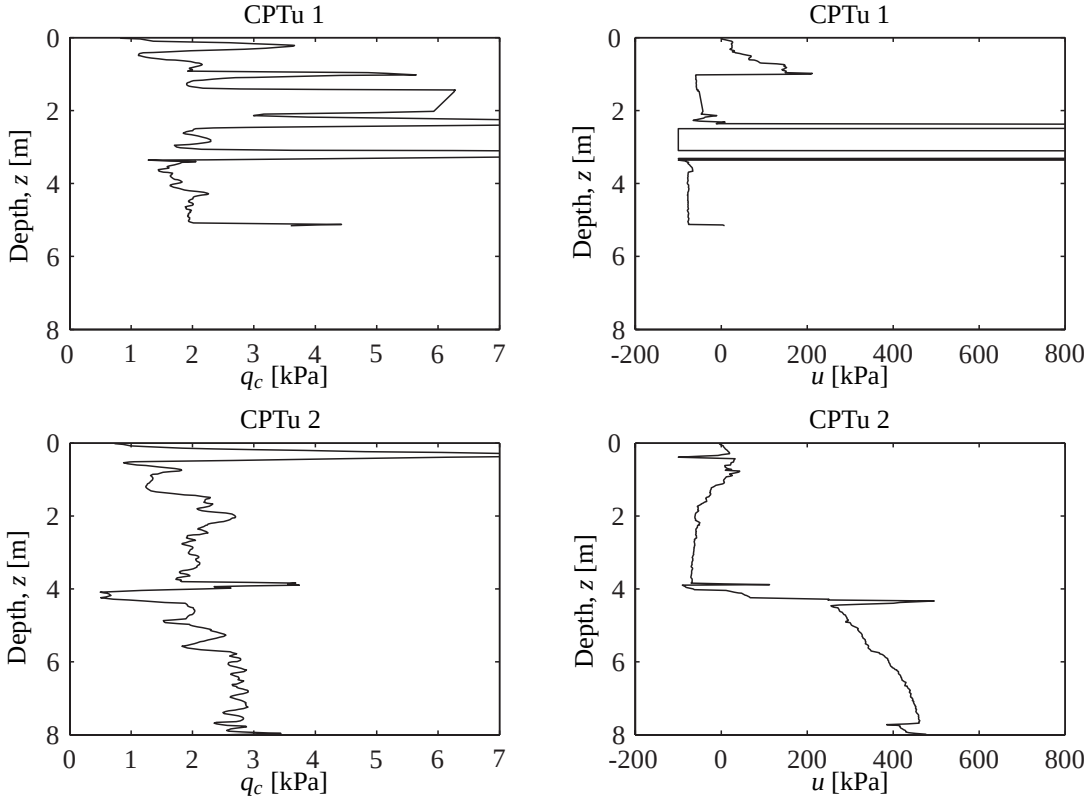

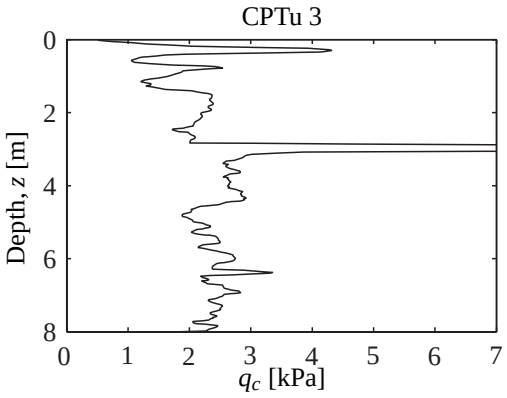
CPTu 3
Depth, z [m]
q_c [kPa]

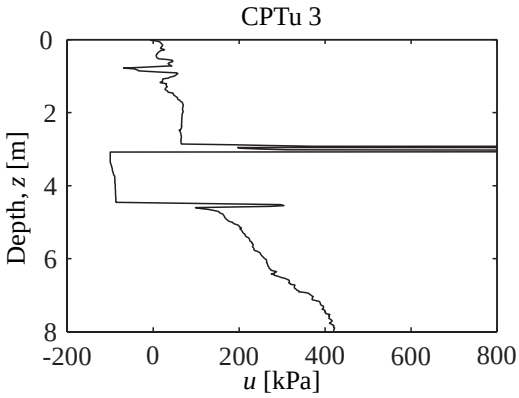
CPTu 3
Depth, z [m]
u [kPa]

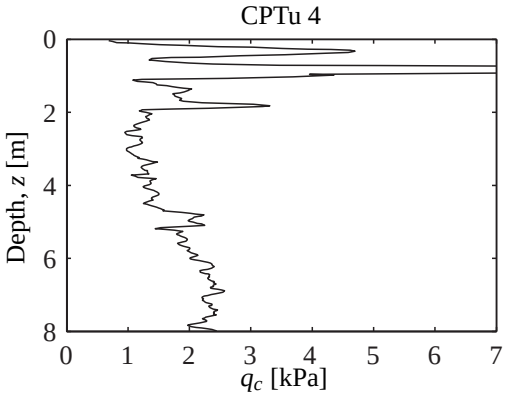
CPTu 4
Depth, z [m]
q_c [kPa]

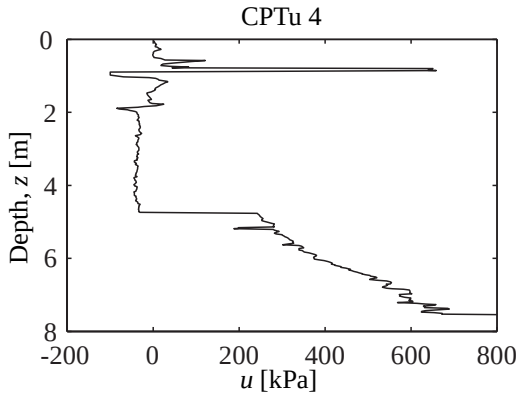
CPTu 4
Depth, z [m]
u [kPa]

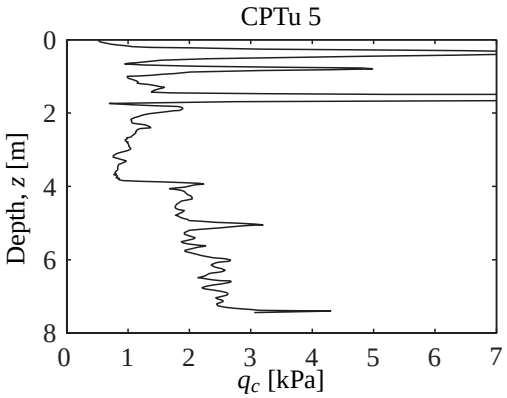
CPTu 5
Depth, z [m]
q_c [kPa]

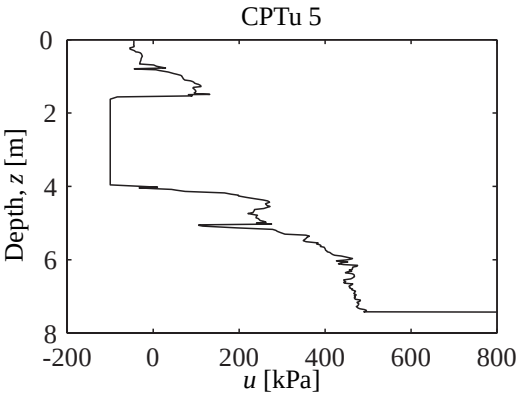
CPTu 5
Depth, z [m]
u [kPa]

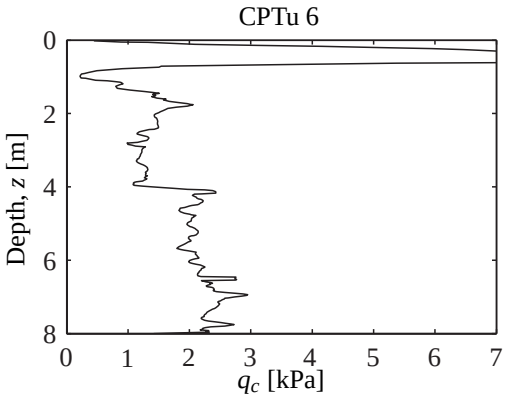
CPTu 6
Depth, z [m]
q_c [kPa]

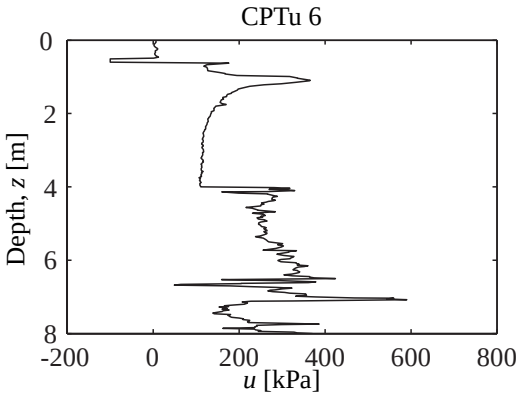
CPTu 6
Depth, z [m]
u [kPa]

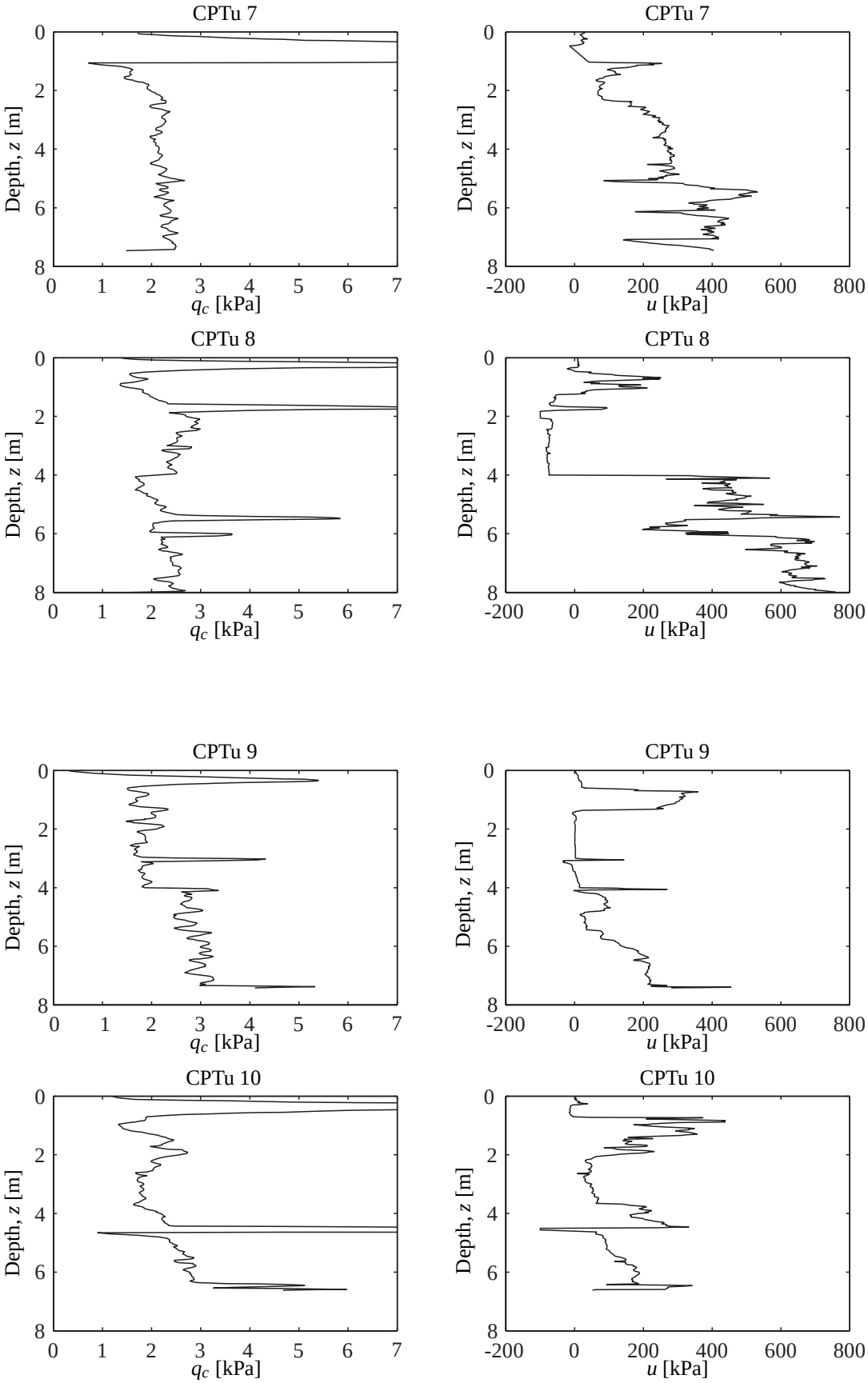
CPTu 7
Depth, z [m]
q_c [kPa]
CPTu 7
Depth, z [m]
u [kPa]
CPTu 8
Depth, z [m]
q_c [kPa]
CPTu 8
Depth, z [m]
u [kPa]
CPTu 9
Depth, z [m]
q_c [kPa]
CPTu 9
Depth, z [m]
u [kPa]
CPTu 10
Depth, z [m]
q_c [kPa]
CPTu 10
Depth, z [m]
u [kPa]

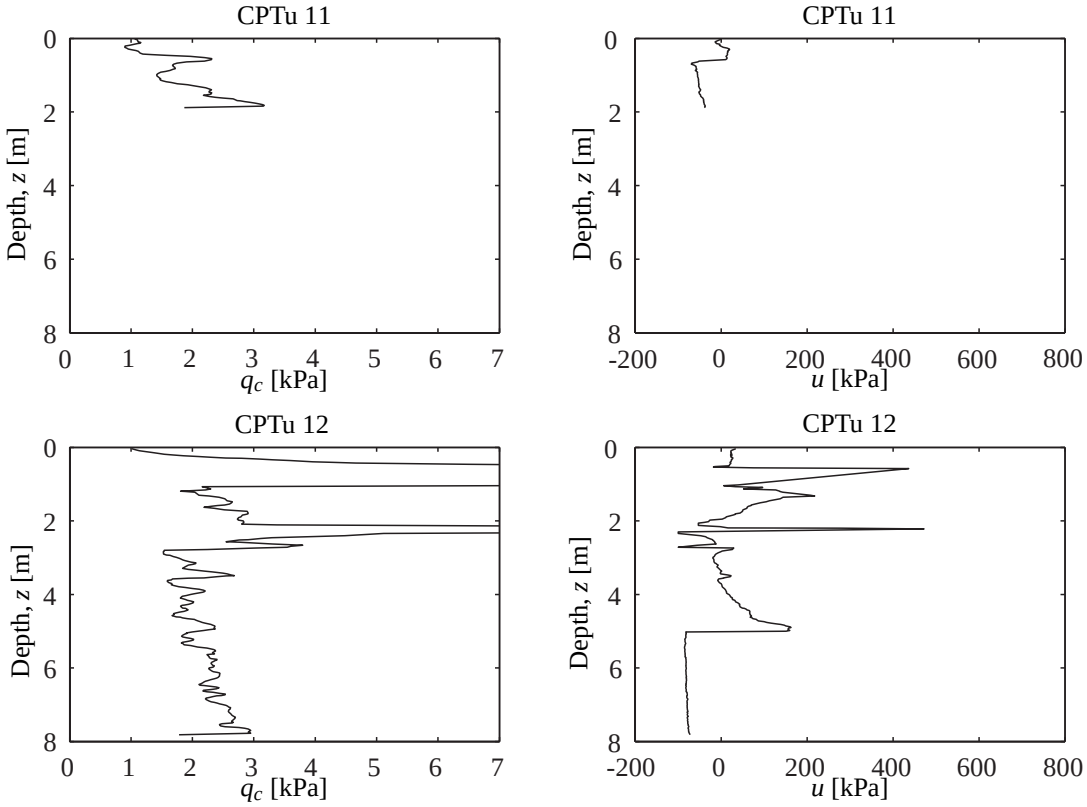
CPTu 11
Depth, z [m]
q_c [kPa]
CPTu 11
Depth, z [m]
u [kPa]
CPTu 12
Depth, z [m]
q_c [kPa]
CPTu 12
Depth, z [m]
u [kPa]

Tendencies of the Clay

The present appendix will present plots showing the tendencies of each CPTu performed at Suderbovej. The data has been sorted and the plotted data is what is used for further analysis (except for data concerning CPTu number 11). In the plots the data is shown with a black colour, the local tendency shown with blue and the general tendency is marked with a red colour.

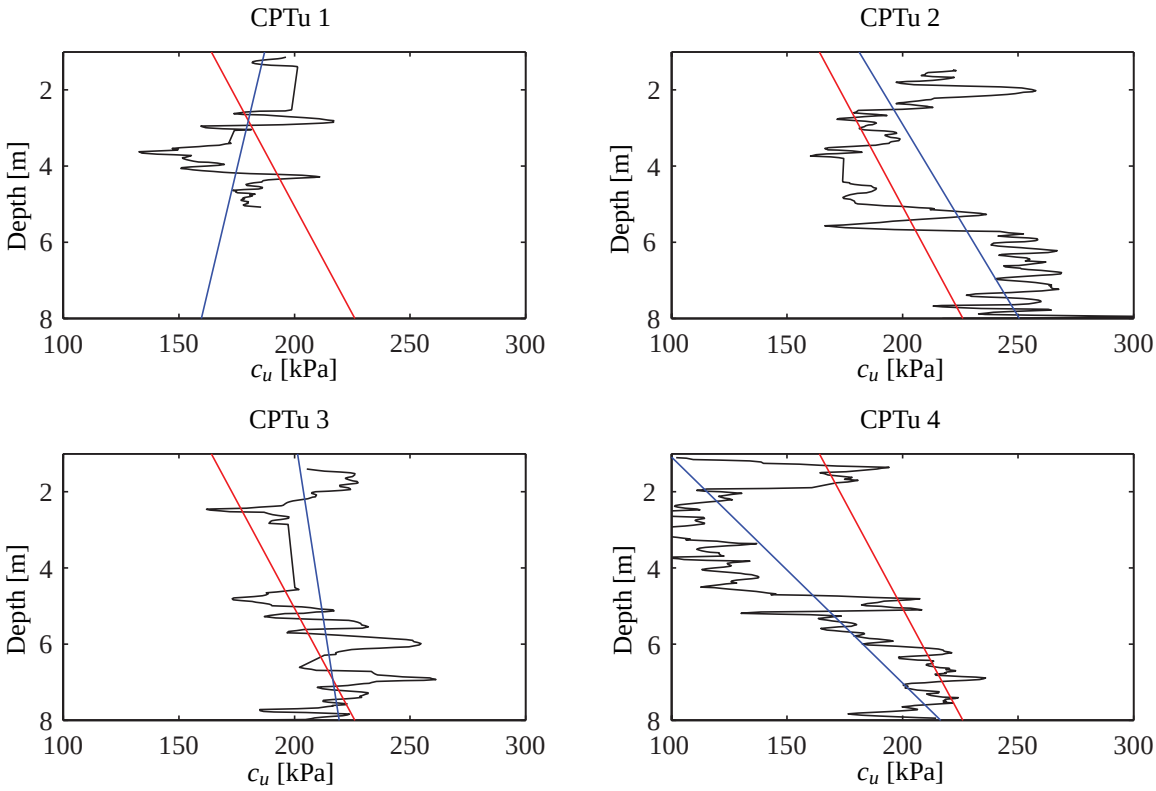

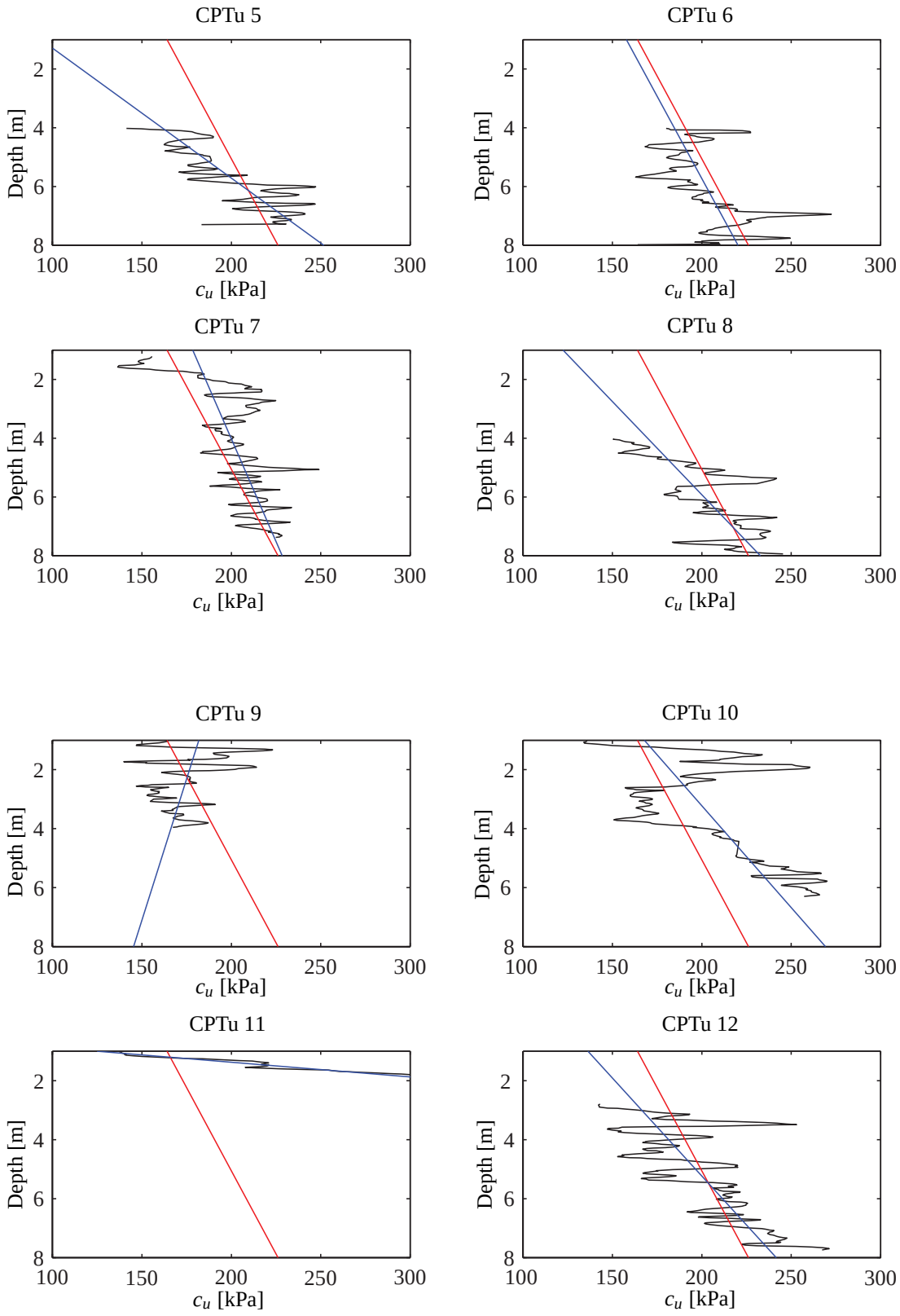
CPTu 5
CPTu 6
CPTu 7
CPTu 8
CPTu 9
CPTu 10
CPTu 11
CPTu 12
Depth [m]
c_u [kPa]
2
4
6
8
100
150
200
250
300

Appendix **E**

Parameter Estimation for Depth Dependent Soil Strength

The method described in [DNV, 2010] estimates parameters for soil subjected to depth dependency. From soil tests n observations of the soil strength, Y=[$y_1, \ldots y_n$], and the connected depth coordinate, Z=[$z_i, \ldots z_n$], are available. Assuming that the variation with depth can be reasonably modelled with a linear function and that the standard deviation is independent on depth, the coefficients a_0 and a_1 describing the surface interception and depth gradient of the soil strength, respectively, can be estimated from Equation (E.1).

$$\hat{a}_1 = \frac{\sum_{i=1}^{n} (z_i - \overline{z})(y_i - \overline{y})}{\sum_{i=1}^{n} (z_i - \overline{z})^2} \tag{E.1}$$

where

$\hat{a}_1$	Best estimate of a_1 [kPa/m]
n	Number of observations [-]
z_i	Depth coordinate [m]
y_i	Soil strength [kPa]
$\overline{z}$	Sample mean of depth coordinate, see Equation (E.2) [m]
$\overline{y}$	Sample mean of soil strength, see Equation (E.2) [kPa]

Here the sample means are calculated as in Equation (E.2).

$$\begin{aligned} \overline{y} &= \frac{1}{n} \sum_{i=1}^{n} y_i \\ \overline{z} &= \frac{1}{n} \sum_{i=1}^{n} z_i \end{aligned} \tag{E.2}$$

The value at the surface interception follows from Equation (E.3).

$$\hat{a}_0 = \overline{y} - \hat{a}_1 \overline{z} \tag{E.3}$$

Lastly, the standard deviation, σ, is found from the sample standard deviation in Equation (E.4).

$$\sigma = \sqrt{\frac{1}{n-2} \sum_{i=1}^{n} (y_i - (\hat{a}_0 + \hat{a}_1 z_i))^2} \tag{E.4}$$

Appendix **F**

Choice of 5% Quantile

In Eurocodes it is stated, that the when a characteristic bearing capacity is calculated either a 5% quantile of the bearing capacity or a 5% fractile of the strength parameter should be used [Eurocode 0, 2007]. In the present appendix, a brief investigation of the difference between the two approaches is presented.

The scenario investigated is as follows. The bearing capacity of the strip foundation presented in Figure F.1 will be subjected to the loads presented in Table F.1. No partial safety factors will be applied to the loads or the strength parameters.

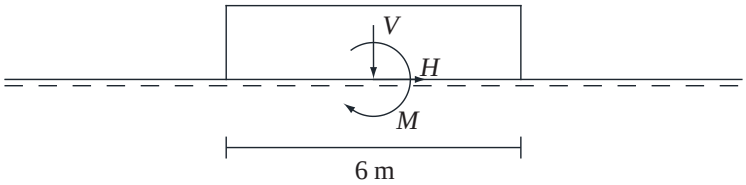

Figure F.1: *The investigated scenario.*

Table F.1: *Loads applied.*

Load	Symbol	Value	Unit
Vertical	V	1,000	kN/m
Horizontal	H	200	kN/m
Moment	M	200	kNm/m

From Figure F.1 it is observed, that the phreatic surface is defined at the surface of the soil. The following analysis will be performed for Terzaghi's bearing capacity formula. The investigated soil will be frictional soil, as the bearing capacity formula for clay has a linear link between the strength parameter and the bearing capacity as seen in Equation (F.1).

$$R = N_c \, c_u \, s_c^0 \, i_c^0 \, B' \tag{F.1}$$

where

R	Bearing capacity [kN/m]
N_c	Bearing capacity factor, (π + 2) for undrained conditions [-]
c_u	Undrained shear strength [kPa]
s_c^0	Shape factor for undrained conditions [-]
i_c^0	Inclination factor for undrained conditions [-]
B'	Effective width of the foundation [m]

As none of the factors in Equation (F.1) are dependent on the cohesion (except for itself), no difference will be found, if the 5% quantile is used for the strength parameter or the calculated bearing capacities. The characteristics for the frictional soil used for the study are defined in Table F.2.

Table F.2: *Characteristics for the frictional soil.*

Description	Symbol	Value	Unit
Mean for effective friction angle	$\mu_{\varphi'}$	37	$^\circ$
Standard deviation for effective friction angle	$\sigma_{\varphi'}$	4.0	$^\circ$
Effective unit weight	γ'	9.0	kN/m^3

From the characteristics in Table F.2 the following two procedures have been carried out:

1. 10,000 Normal distributed realisations of the effective friction angle has been found.
2. A 5% quantile of the effective friction angle has been found.
3. The 5% quantile of the effective friction angle has been used to determine the bearing capacity, using the expression in Equation (F.2).

1. 10,000 Normal distributed realisations of the effective friction angle has been found.
2. A bearing capacity is found for each of the realisations of the effective friction angle using Equation (F.2).
3. A 5% quantile of the bearing capacity has been found.

$$R = \left(\frac{1}{2}\,\gamma'\,B'\,N_\gamma\,s_\gamma\,i_\gamma\right)B' \tag{F.2}$$

where

R	Bearing capacity [kN/m]
γ'	Effective specific weight of the soil [kN/m^3]
B'	Effective width of the foundation [m]
N_γ	Bearing capacity factor [-]
s_γ	Shape factor [-]
i_γ	Factor taking the inclination of the load into account [-]

The bearing capacity factor, N_γ, for plane strain and drained conditions is calculated from Equation (F.3).

$$N_\gamma = 2\ (N_q - 1)\ \tan\left(\varphi'\right) \qquad N_q = e^{\pi\ \tan(\varphi')}\ \frac{1+\sin\left(\varphi'\right)}{1-\sin\left(\varphi'\right)} \tag{F.3}$$

where

φ'	Effective friction angle [°]
N_q	Bearing capacity factor for the overburden pressure [-]

The shape factor, s_γ, for strip footings is equal to 1. The inclination factor is found from Equation (F.4).

$$i_q = \left(1 - \frac{H}{V}\right)^2 \qquad i_\gamma = i_q^2 \tag{F.4}$$

where

i_q	Inclination factor for the overburden pressure [-]

The effective area of the foundation is found from Equation (F.5).

$$B' = B - 2\,e \qquad e = \frac{M}{V} \tag{F.5}$$

B	Total width of the foundation [m]
e	eccentricity [m]

From here the two calculated 5% quantiles are compared. The procedure is repeated 100 times in order to get a statistical qualified result. The results obtained in Table F.3 have been found from the analysis.

Table F.3: *Characteristics for the frictional soil.*

	5% of bearing capacity [kN/m]	5% of strength [kN/m]	Deviation [%]
Mean vertical bearing capacity	1,180	1,357	15

From Table F.3 it is quite clear, that it has a rather large influence which 5% quantile that is chosen for the design. In general the 5% quantile observed for the bearing capacity produces the lowest bearing capacities. The reason for the deviation is found in the calculation of the bearing capacity factor, N_γ, in Equation (F.3). From the equation it is observed that it is very sensitive toward a small change in the effective friction angle. E.g. if the effective friction angle is changed from 35 to 39° the bearing capacity factor, N_γ, will change from 45 to 89, which is approximately a factor of 2 in difference. This will result in a large coefficient of variation for the approach dealing with a 5% quantile of the bearing capacity, and therefore a resulting lower characteristic bearing capacity.

Estimation of Correlation Lengths

G.1 Semicovariance Functions for the Sand Site at Vulkanvej

In the following all the results obtained for the spatial analysis of the CPTu tests at Vulkanvej will be presented. The semicovariance functions are presented along with the calculated reduced effective friction angle. This gives an impression of how the semicovariance function is dependent on the measured results.

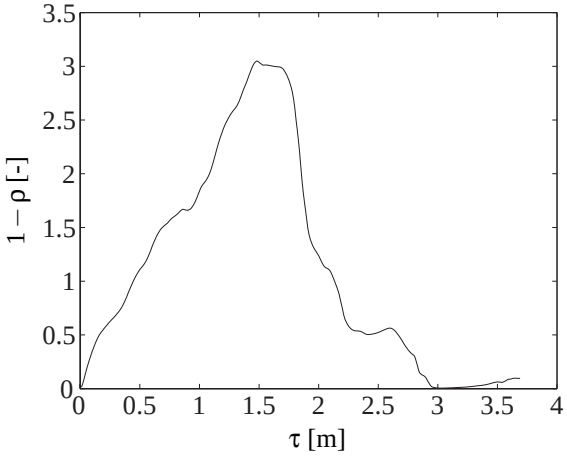

Figure G.1: *Semicovariance function for CPTu 1.*

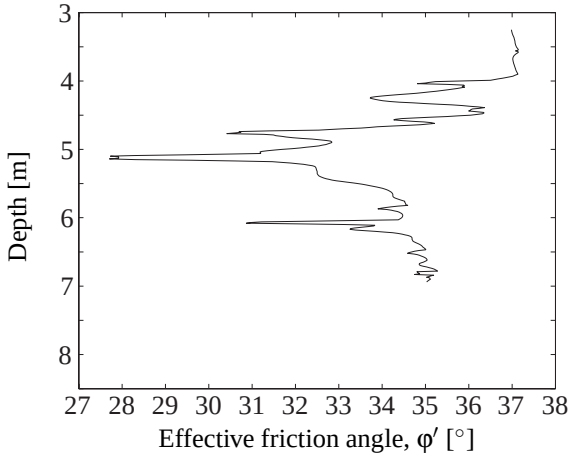

Figure G.2: *Appertaining effective friction angles.*

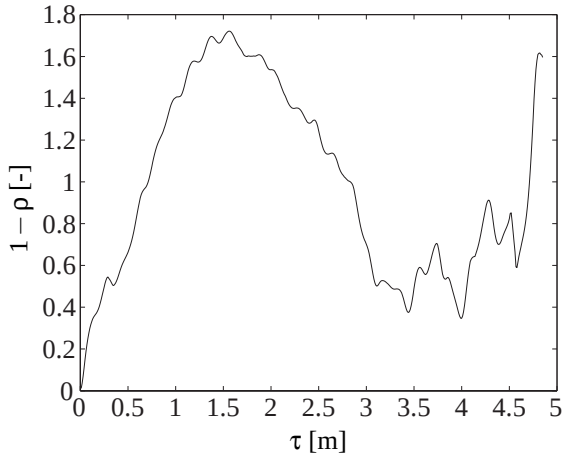

Figure G.3: *Semicovariance function for CPTu 2.*

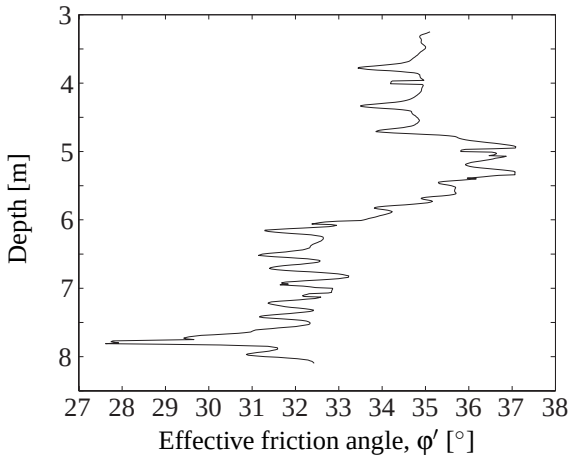

Figure G.4: *Appertaining effective friction angles.*

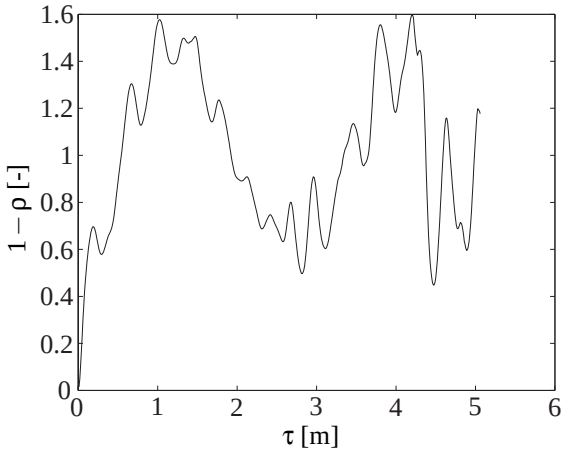

Figure G.5: *Semicovariance function for CPTu 3.*

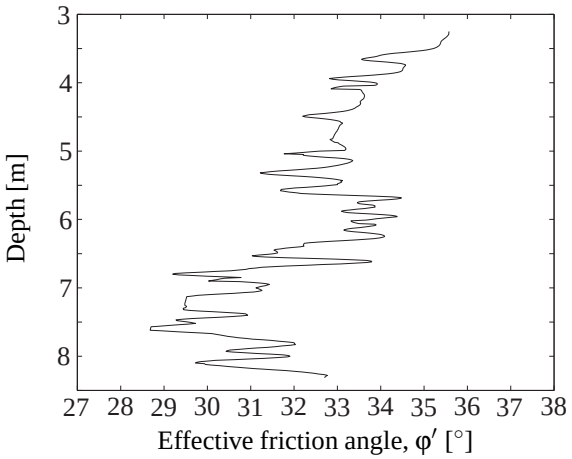

Figure G.6: *Appertaining effective friction angles.*

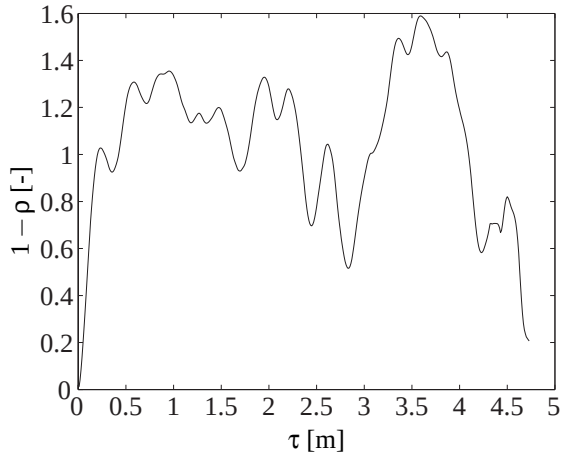

Figure G.7: *Semicovariance function for CPTu 4.*

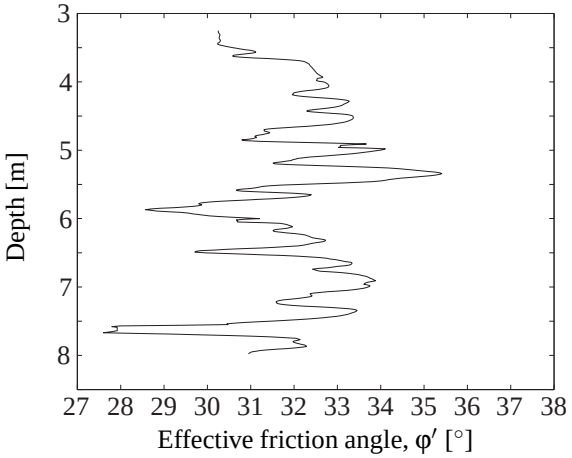

Figure G.8: *Appertaining effective friction angles.*

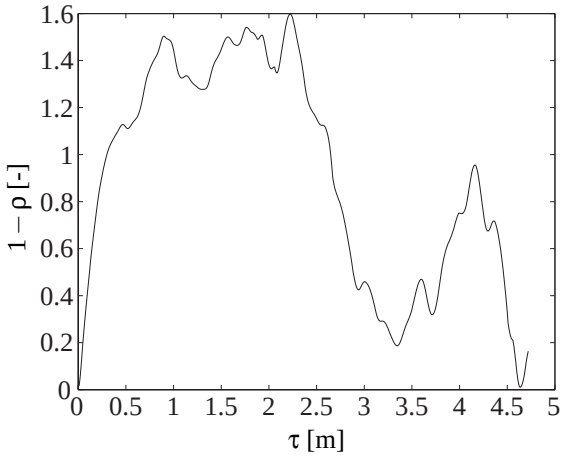

Figure G.9: *Semicovariance function for CPTu 5.*

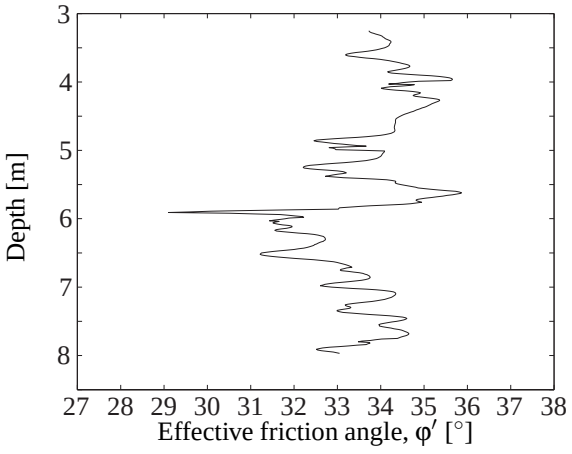

Figure G.10: *Appertaining effective friction angles.*

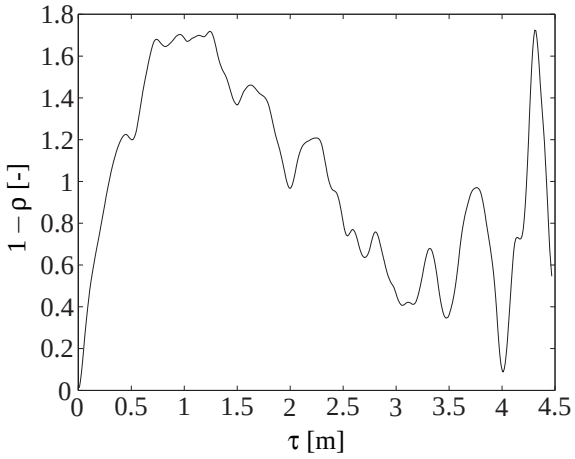

Figure G.11: *Semicovariance function for CPTu 6.*

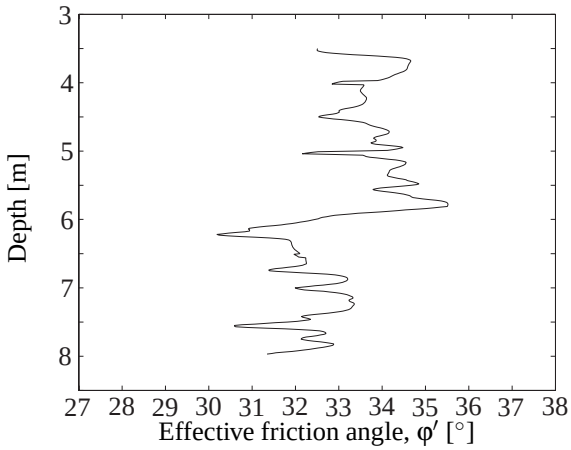

Figure G.12: *Appertaining effective friction angles.*

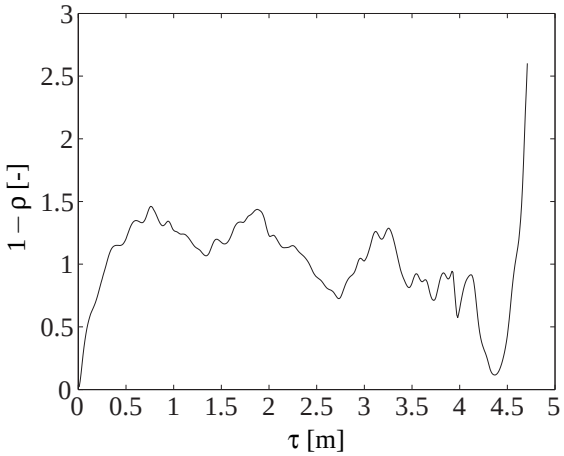

Figure G.13: *Semicovariance function for CPTu 7.*

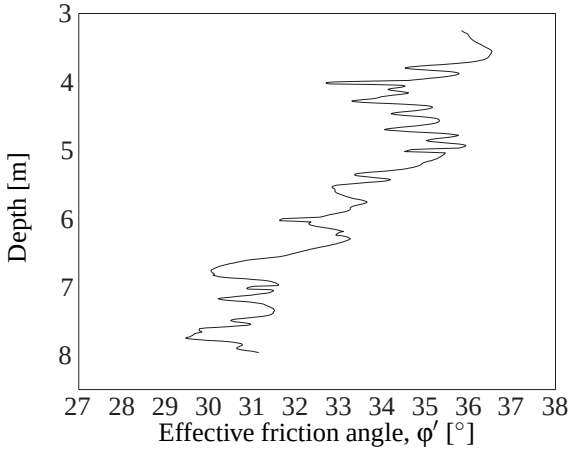

Figure G.14: *Appertaining effective friction angles.*

G.2 Semicovariance Functions for the Clay Site at Suderbovej

In the following all the results obtained for the spatial analysis of the CPTu tests at Suderbovej will be presented. The semicovariance functions are as follows.

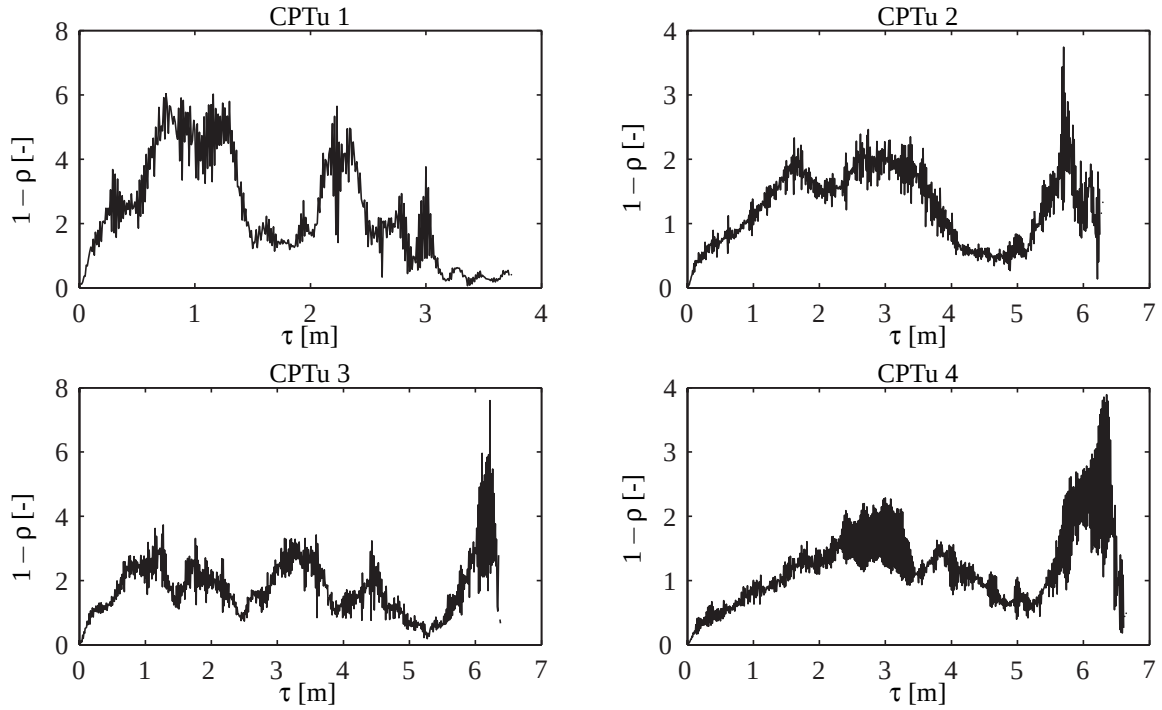

Figure G.15: *Semicovariance function for CPTu 1-4.*

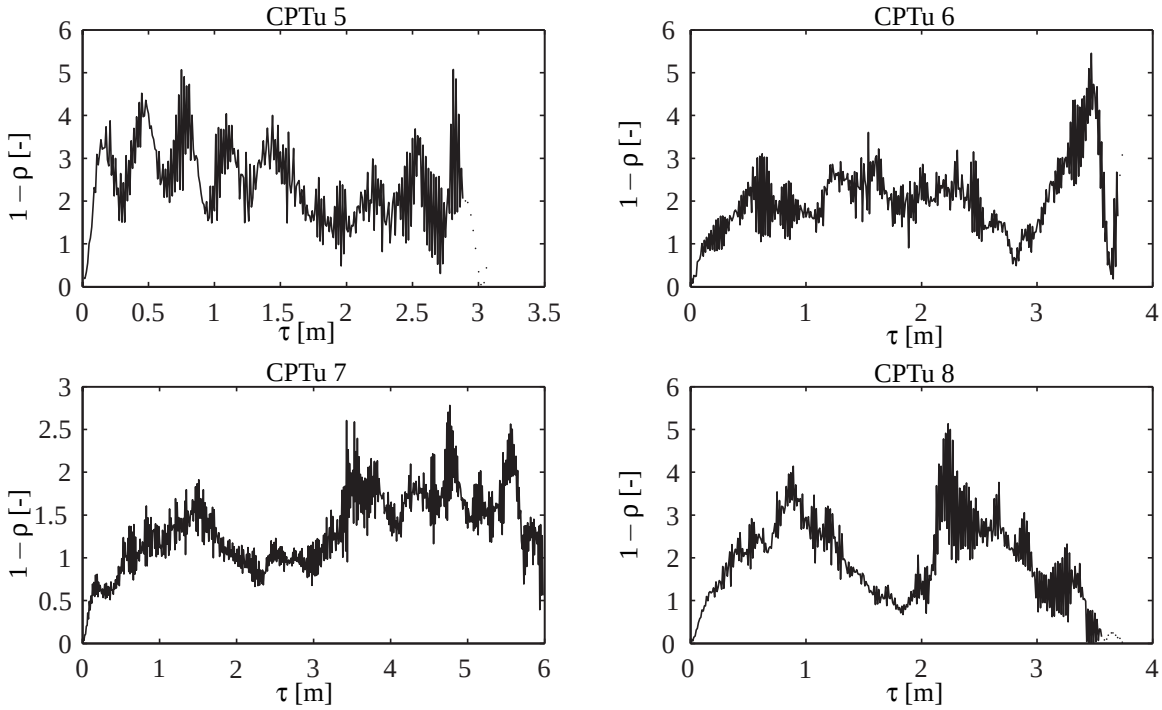

Figure G.16: *Semicovariance function for CPTu 5-8.*

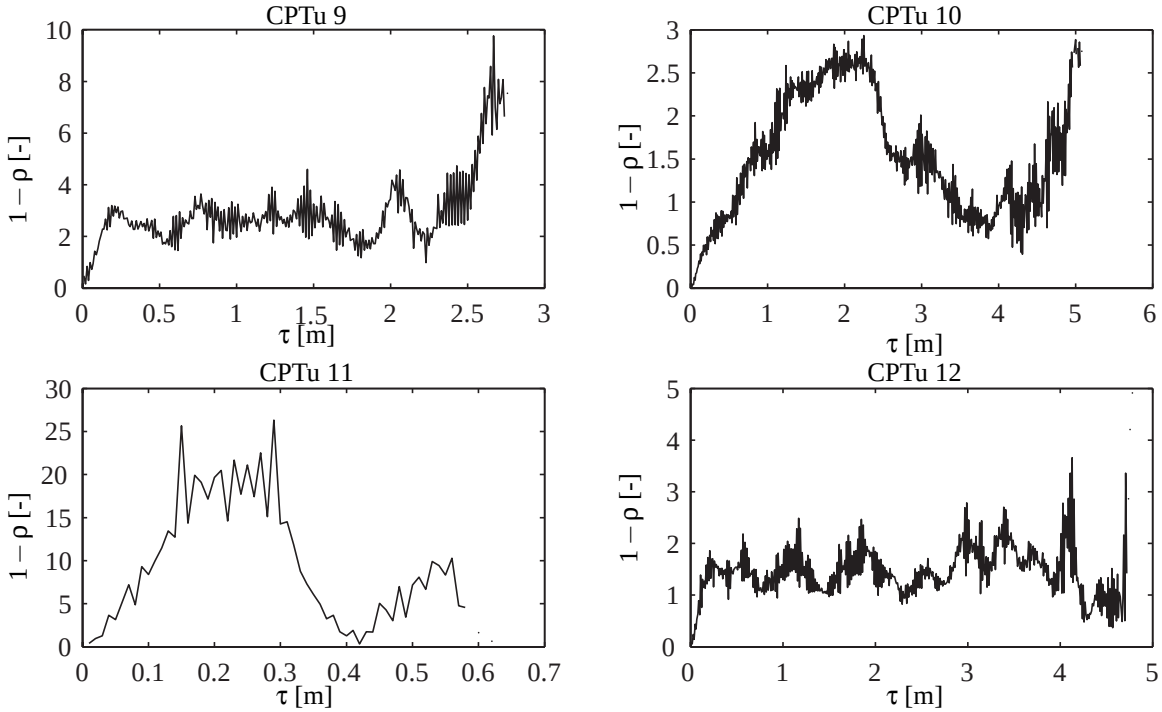

Figure G.17: *Semicovariance function for CPTu 9-12.*

Verification of LimitState:Geo

The FE programme LimitState:Geo will be used to calibrate the response function for gravity based surface foundation installed on sand. This appendix will be used to validate the use of the programme. The verification will be based on a simple footing exposed to pure vertical loading. The situation that will be tested is presented in Figure H.1.

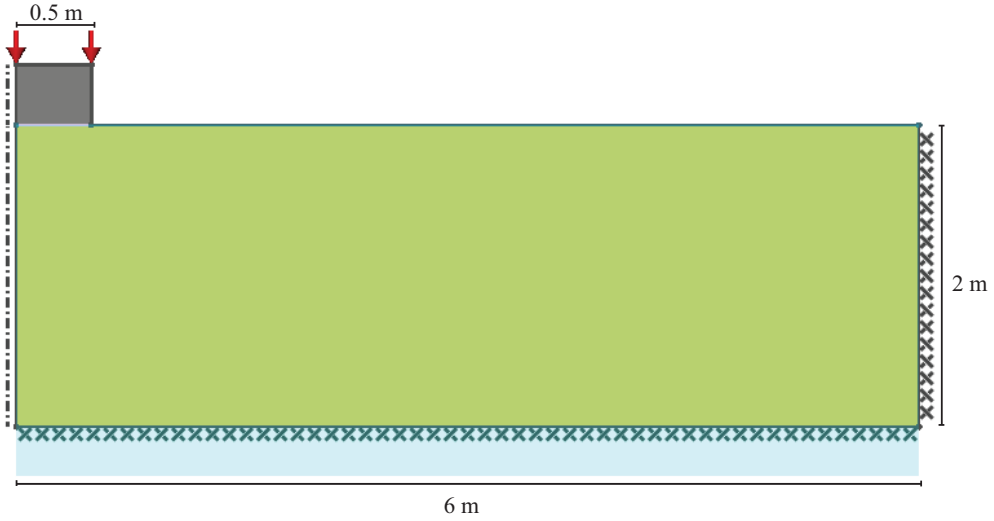

Figure H.1: *The figure shows the situation that will be tested.*

From Figure H.1 it can be seen that the footing is placed on top of a homogeneous soil layer. The soil chosen for the verification is a default sand, *medium dense sand*, with the properties presented in Table H.1.

Table H.1: *Material parameters.*

Parameter	Value	Unit
φ'	37.5	°
γ_{sat}	20	kN/m^3
γ_{dry}	16	kN/m^3
c'	0	kPa

Due to symmetry conditions only half of the failure domain is modelled. This is done in order to minimize the use of computer power. The dashed line on the left boundary indicates symmetry. Furthermore it is noted that a phreatic level is placed at foundation level.
Since it is the bearing capacity of the soil that is of interest, the footing material will be modelled as a rigid material. LimitState:Geo is a 2D programme and therefore considers plane strain. Therefore no 3D effects are included in the

output from LimitState:Geo, but these can be included by the use of shape factors.

The output from LimitState:Geo is an adequacy factor which gives the ratio between the applied load and the load that causes failure. The bearing capacity from LimitState:Geo will be compared to the bearing capacity determined from Equation (H.1).

$$R = \left(\frac{1}{2}\gamma' \, B' \, N_\gamma \, i_\gamma \, s_\gamma\right) B' \tag{H.1}$$

where

R	Vertical bearing capacity at the bottom of the foundation [kN/m]
γ'	Effective specific weight of the soil [kN/m^3]
B'	Effective width of the foundation [m]
N_γ	Bearing capacity factor [-]
i_γ	Inclination factor, 1 for pure vertical load [-]
s_γ	Shape factor, 1 for strip foundation [-]

LimitState:Geo which uses the Discontinuity Layout Optimisation procedure, automatically finds the most critical failure mechanism for the given situation. The critical failure mechanism for the considered case is shown in Figure H.2.

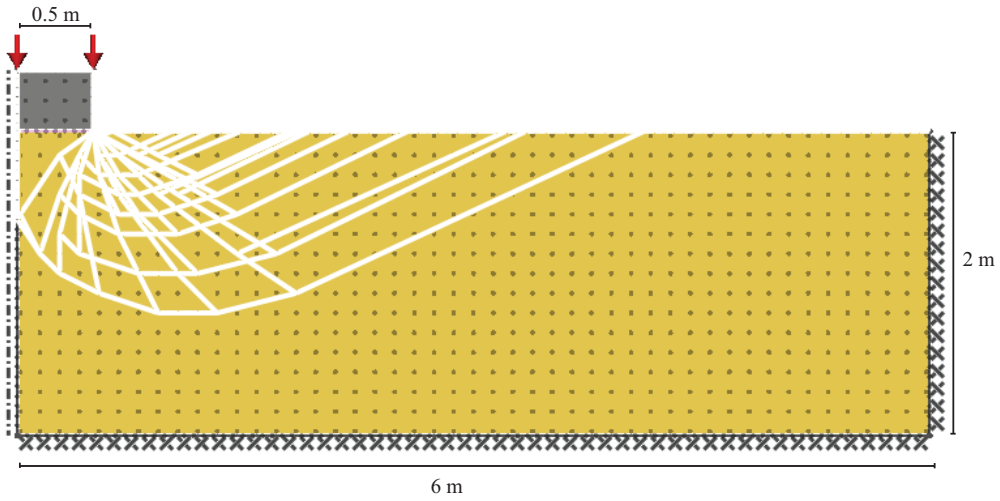

Figure H.2: *The critical failure mechanism.*

The critical failure mechanism illustrated in Figure H.2 consists of three zones. One zone with a shear fan with the shape of a logarithmic spiral in between zones with rigid sliding blocks.
The bearing capacity found through LimitState:Geo and Equation (H.1) respectively are presented in Table H.2.

Table H.2: *Comparison of the bearing capacity determined from the programme LimitState:Geo and from the analytical solution.*

	Bearing capacity	Unit
Limit State:Geo	344.7	kN/m
Analytical	343.8	kN/m

As seen from Table H.2 the deviation is of minor importance. This analysis is done for a wide range of foundation diameters in order to see if this minor deviation is general, cf. Table H.3.

Table H.3: *Comparison of the bearing capacity determined from the programme LimitState:Geo and from an analytical solution.*

Diameter [m]	LimitState:Geo [kN/m]	Analytical [kN/m]	Deviation [%]
0.5	87.1	86.0	-1.3
1	344.7	343.9	-0.25
2	1,394	1,375	-1.3
4	5,465	5,502	0.67
10	34,160	34,385	0.65
15	76,700	77,366	0.86
20	130,000	137,000	5.3
25	202,000	215,000	6.0
30	287,000	309,000	7.2
40	513,000	550,000	6.8

It is seen that the deviation increases with increasing width of the foundation which is also illustrated by Figure H.3.

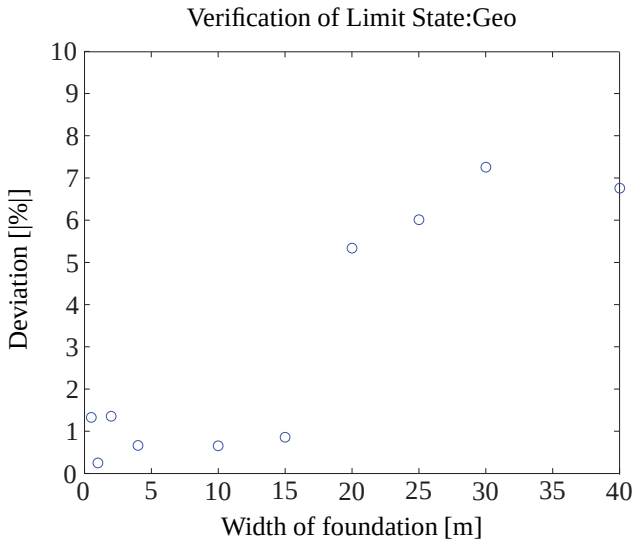

Figure H.3: *Deviation between LimitState:Geo and analytical solution.*

It shall be mentioned that in order to get a more accurate picture of the error for each model, a convergence analysis should have been performed for each LimitState:Geo model in order to confirm that a reliable result has been obtained. Such a convergence analysis will be performed for the model that will be used to calibrate the analytical expression used for the frictional soil.

Convergence Analysis for LimitState:Geo

In this appendix it will be investigated if the model used for determining the model uncertainty for the gravitational footing on frictional soils converges. Also the required meshing for obtaining acceptable results will be determined. The programme LimitState:Geo is verified in Appendix H.

The construction of the model is described in details in Section 10.1.1 why only results from the convergence analysis will be described here.

The model has been run and convergence has been analysed. The results from different meshing densities are shown in Table I.1 and in the figures I.1 and I.2. In the figures it is also noticed that an exponential fit has been applied for the results.

Table I.1: *Results from the convergence analysis.*

Nodal density [1/m^2]	Total number of nodes [-]	Adequacy factor [-]
0.25	397	173.1
0.50	1,207	172.0
0.75	2,527	170.1
1.00	4,207	167.6
1.25	6,457	166.5
1.50	9,013	165.8

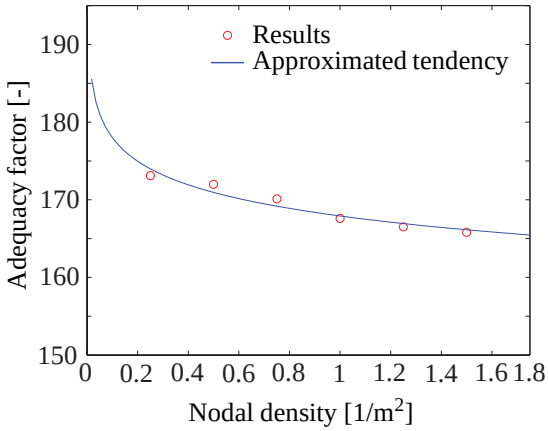

Figure I.1: *Convergence analysis plotted with nodal density.*

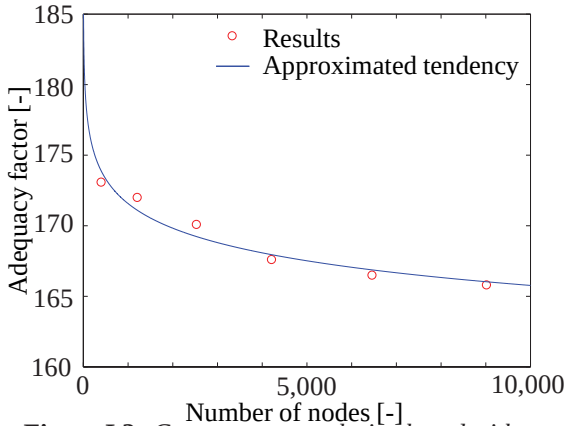

Figure I.2: *Convergence analysis plotted with number of nodes.*

From Figure I.1 it is hard to see if the model is converging, which is why also Figure I.2 is presented. From Figure I.2 it is observed that the model had a slow but fair convergence tendency. From the point with 4,207 nodes the gaining from refining the mesh any further is almost negligible and not worth the extra computation time. This corresponds to a nodal density of 1 node pr. m^2. Therefore it has been chosen to continue to use a nodal density of 1 node/m^2 for the simulations for the failure surface of the foundation.

Effects of Domain Size in LimitState:Geo

In the figures describing the failure domains, e.g. Figure 10.5, it is seen, that the failure domains are very close to the geometrical boundaries in the model. Therefore a small study has been performed to enlighten which influence this might have on the obtained results. For this purpose a model with a horizontal attack point 80 m above the surface of the soil has been used as an example. Different geometrical dimensions of the soil volume has been applied, which are clarified in Table J.1.

Table J.1: *Dimensions for the models.*

Parameter	Symbol	Used model	Larger model	Unit
Horizontal dimension	x_{min}	-50	-75	m
Horizontal dimension	x_{max}	75	100	m
Vertical dimension	y_{min}	0	-10	m
Vertical dimension	y_{max}	30	30	m

Simulations have been performed for each situation, which have resulted in the failure domains shown in Figure J.1 and J.2.

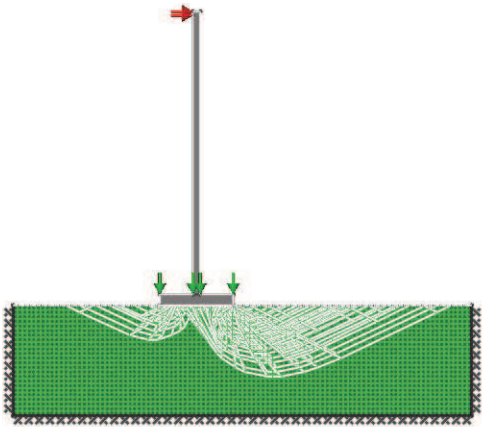

Figure J.1: *Failure domain for the footing with the used geometrical boundaries.*

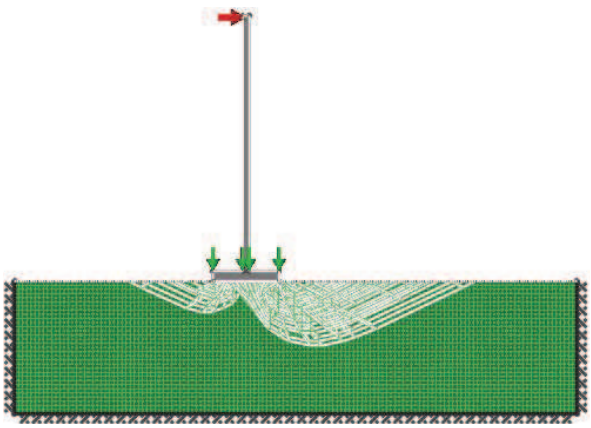

Figure J.2: *Failure domain for the footing with larger geometrical boundaries.*

From Figure J.1 and J.2 it is seen, that the failure domains are similar to one another, and therefore the results are expected to be similar. An adequacy factor has been appointed to the horizontal load and the result is presented in Table J.2 to enlighten the described similarity in the simulations.

Table J.2: *Results obtained for different domain sizes.*

Parameter	Used model	Larger model	Unit
Adequacy factor	8,164	8,164	-

The results presented in Table J.2 shows that nothing is gained from increasing the domain size, which also was expected as it is mainly a geometric problem for which the solution will remain the same as long as the nodal density and soil properties are not changed. It should be mentioned that the results will change significantly if the domain size is reduced to be lower than that of the failure domain, which is reasoned by the fact, that the failure domain is prevented from following its natural path.

Reliability Index and Sensitivity Parameters

The procedure for determining the reliability index, β, is presented in the following. Reference is made to [Sørensen, 2011]. The probability of failure can be calculated from Equation (K.1), when β is calculated.

$$P_f = \Phi(-\beta) \tag{K.1}$$

where

P_f	Probability of failure [-]
β	Reliability index [-]

Nonlinear, non-Gaussian distributed stochastic variables needs to be transformed to the normalised uncorrelated U-space in order to calculate β. The transformation is dependent on the distribution for the given variable. Lognormal and Gumbel distributed stochastic variables are described in the following in accordance with [Sørensen, 2011].
The Lognormal distribution is given by Equation (K.2).

$$F_X = \Phi\left(\frac{\ln x - \mu_L}{\sigma_L}\right) \tag{K.2}$$

where

$$\sigma_L = \ln\left(\frac{\sigma^2}{\mu^2} + 1\right)$$
$$\mu_L = \ln(\mu) - \frac{1}{2}\sigma_L^2$$

σ	Standard deviation [-]
μ	Expected value [-]
x	Realisation of X [-]
X	Stochastic variable [-]

Independent Lognormal distributed stochastic variables can be transformed to the normalised U-space in the following way.

$$x = \exp(\sigma_L\, u + \mu_L) \tag{K.3}$$

$$u = \Phi^{-1}(F_x(x)) \tag{K.4}$$

where

u	Realisation of U [-]
U	Stochastic variable [-]

The Gumbel distribution is shown in Equation (K.5)

$$F_X(x) = \exp\left(-\exp\left(-a\,(x-b)\right)\right) \tag{K.5}$$

where

$$a = \frac{\pi}{\sqrt{6\,\sigma}}$$
$$b = \mu - \frac{0.5772}{a}$$

Independent Gumbel distributed stochastic variables can be transformed to the normalised U-space as shown in Equation (K.6).

$$x = b - \frac{1}{a}\ln\left(-\ln\left(\Phi(u)\right)\right) \tag{K.6}$$

$$u = \Phi^{-1}\left(F_x(x)\right) \tag{K.7}$$

When the stochastic variables are transformed to the normalised U-space, the reliability index, β, can be found from the optimisation problem given in Equation (K.8).

$$\beta = \min_{g_u(u)=0} \sqrt{\sum_{i=1}^{n} u_i^2} \tag{K.8}$$

where

$g_u(u)$	Limit state function in the normalised U-space [-]
n	Number of stochastic variables [-]

This is an optimisation problem with a non-linear constraint and a quadratic objective function, which is solved by the NLPQL algorithm in the attached programme, see CD Appendix A.

K.1 Sensitivity Parameters

When the reliability index, β, is known, different sensitivity factors can be calculated. In the following the methods for calculating the omission sensitivity factor and the elasticity coefficient are presented.
The omission sensitivity factor, ζ, gives a measure of which relative influence each individual stochastic variable has on β if they were fixed. It is shown in Equation (K.9).

$$\zeta_i = \frac{\beta_i'}{\beta} = \frac{1-\alpha_i\,\frac{u_i^0}{\beta}}{\sqrt{1-\alpha_i^2}} \tag{K.9}$$

where

β	Reliability index [-]
β'_i	Reliability index when stochastic variable no. i is considered deterministic [-]
α_1	Unit normal vector for stochastic variable no. i [-]
u_i^0	Stochastic variable no. i at the β point [-]

By setting u_i^0 to the mean value of the i'th stochastic variable in the normalised U-space, $\mu = 0$, Equation (K.9) is reduced to Equation (K.10).

$$\zeta_i = \frac{1}{\sqrt{1-\alpha_i^2}} \tag{K.10}$$

The α-vector can be found from Equation (K.11).

$$\alpha = \frac{1}{\beta} u^* \tag{K.11}$$

where

u^*	β point [-]

Another sensitivity measure is the reliability elasticity coefficient, which is defined in Equation (K.12).

$$e_p = \frac{d\beta}{dp}\frac{p}{\beta} \tag{K.12}$$

where

e_p	Elasticity coefficient [-]
p	μ or σ [-]
β	Reliability coefficient [-]

The elasticity coefficient should be understood as the relative change of the reliabilty index if the parameter p is changed 1%. dβ/dp can be determined from Equation (K.13).

$$\frac{d\beta}{dp} = \frac{1}{|\nabla g|}\frac{\partial g}{\partial p} \tag{K.13}$$

where

∇g	$\sqrt{\sum a_i^2}$ [-]
a_i	$\frac{\partial g_u}{\partial u_i}$ [-]

Verification of Failure Domain

The following appendix will very briefly present the PLAXIS 3D model used to verify the failure domain found using LimitState:Geo. The model is build using the exact same assumptions and dimensions presented in Section 13.1. Only a few changes have been implemented, which will be commented upon in the following.

As the model needs to be defined in 3D an extra dimension is added. Also the domain for the model needs to be increased due to the FEM approach used for calculations in PLAXIS 3D. Therefore the dimensions of the domain have been implemented by the use of rules of thumb. The horizontal dimensions and the depth beneath the foundation are defined to be 4 times the foundation width.

In Figure L.1 a screenshot of the model build in PLAXIS 3D is presented. In the figure it is observed, that symmetry is used, and only half the model is build to save computation time. Therefore boundary conditions preventing the tower and soil to move across the plane of symmetry have been defined. Further it should be noted, that it is not possible to model rigid elements in PLAXIS, which is why the circular foundation and the tower has been defined as weightless material with strength parameters one million times greater compared to regular construction steel. This ensures rigid behaviour of the elements above the soil.

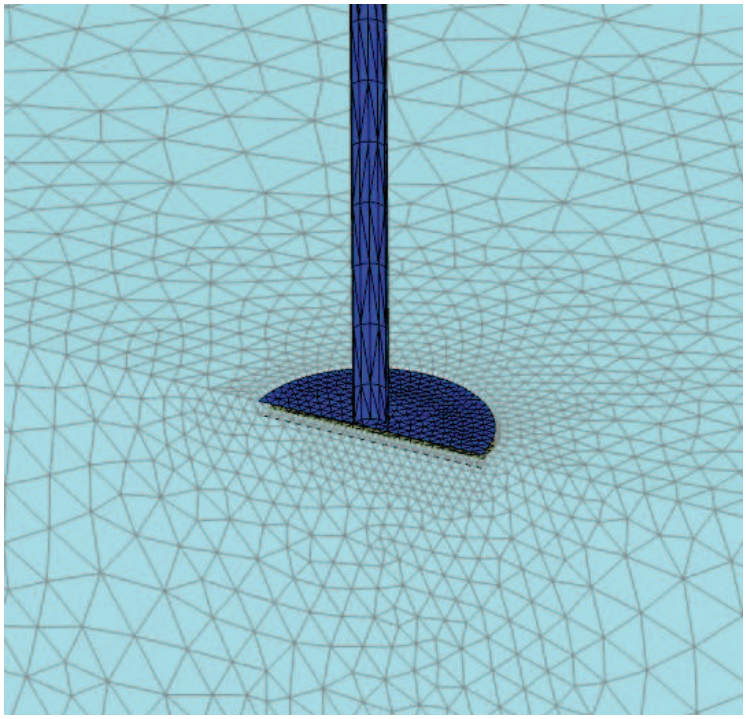

Figure L.1: *The meshed model constructed in PLAXIS 3D under the assumptions described in Section 13.1.*

For the calculations 3 different phases are defined for the model:

1. Initial Phase: Definition of the soil geometry and calculation of the initial stress conditions in the soil.
2. Element Phase: This defines the weightless and rigid foundation and tower.
3. Loading Phase: During this phase the loadings are applied. They are all defined simultaneous to ensure the development of the failure domain corresponding to the one in Section 13.1.

From this very brief description of the model and the assumptions, the results obtained will be commented upon shortly. PLAXIS 3D was set to perform the calculations and a plot revealing the total displacement of the soil volume has been subtracted from the available results. The plot is shown in Figure L.2.

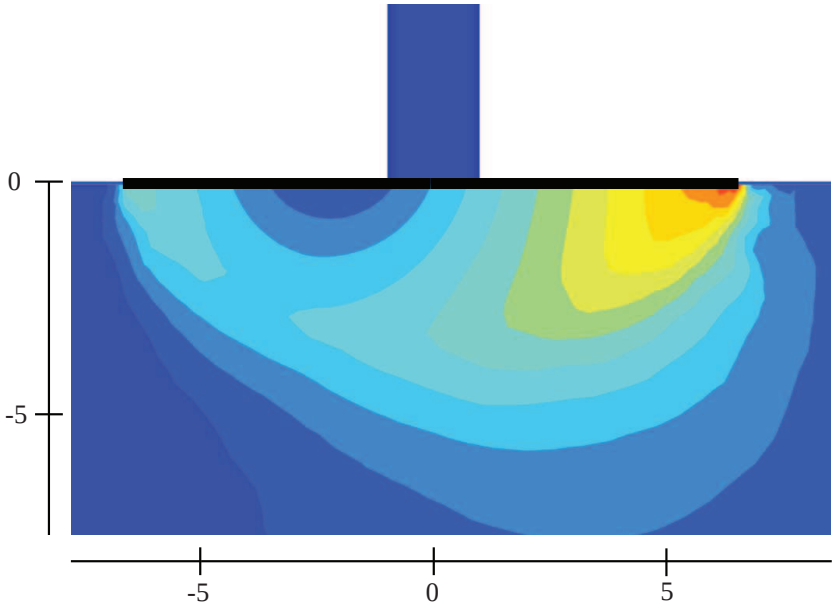

Figure L.2: *Failure domain found using PLAXIS 3D. The contours indicate the relative displacement of the soil volume. The warmer the colour the larger displacements. The unit of the axes is in meters.*

From Figure L.2 it is observed, that the failure domain observed in PLAXIS 3D is very similar to that from Limit-State:Geo. There is a very similar indication of the overall slip lines. Further the red zone indicated in Figure L.2 is located at the same place as the Prandtl zone in Figure 13.5. Therefore it has been concluded, that the tendencies and overall shape of the failure domain found in LimitState:Geo is applicable, and the geometry of the failure domain will be implemented in the stochastic field for further analysis.

Convergence Analysis for Asymptotic Sampling

In order to find a suitable number of simulations that should be used for the calculation of each support point, cf. Figure 13.11, a convergence analysis has been performed. The convergence analysis is performed for the limit state function for the undrained situation presented in Equation (13.6) and represented in Equation (M.1).

$$g = (c_u \, i_c \, s_c \, N_c) \, B' - V \tag{M.1}$$

where

c_u	Undrained shear strengh [kPa]
i_c	Inclination factor [-]
s_c	Shape factor [-]
N_c	Bearing capacity factor = π +2 for undrained condition [-]
B'	Effective width of the foundation [m]
V	Vertical load [kN/m]

The convergence analysis is calculated for the situation presented in Table M.1. The horizontal and moment load corresponds to the load situation with COV_{wind} = 5%. The mean value of the undrained shear strength, c_u, is the mean value of the 10,000 realisations obtained through the stochastic field described in Section 13.2. Furthermore the uncertainty parameters from Table 11.3 are connected to the horizontal and moment load.

Table M.1: *Load situation for convergence analysis.*

Paramter	Distribution Type	Mean value	Unit	COV
Vertical load	N	960,9	kN/m	5%
Horizontal load	G	24.8	kN/m	15%
Moment load	G	2,480	kNm/m	15%
Undrained shear strength	LN	184.7	kPa	15.6%
Width	D	13.82	m	-

An exact result is determined to β = 3.59, which is done through a Monte Carlo simulation with 10,000,000 samples. In Table M.2 the mean value and standard deviation from 20 runs can be seen for different numbers of simulations made for each support point. Each run corresponds to the procedure presented in Figure 13.10. The support points corresponds to the estimates of β, see Figure 13.11.

Table M.2: *Convergence analysis for asymptotic sampling.*

Sample points	μ_β	σ_β
128	3.4845	0.2385
256	3.5408	0.1910
512	3.5772	0.1587
1,024	3.5913	0.1081
2,048	3.5717	0.0700
4,096	3.5764	0.0638

In Table M.2 it can be seen that an acceptable result is obtained by the use of only 512 sample points. Though it is chosen to use 1,024 sample point due to the accurate result and the fact that the standard deviation is fairly low. The low standard deviation means that only few runs are required for each value of the undrained shear strength determined from the stochastic field. This is seen, as the procedure explained in Figure 13.10 is needed to be executed fewer times.

Foundation Installed on a Cohesive Soil

In Section 13.3.5 it was shown that the reliability index for a strong eccentric foundation is very sensitive. This is due to the fact that even a small fluctuation in the moment could result in a great percentile reduction of the effective area of the foundation. In this appendix the potential of probabilistic design will be evaluated for a foundation installed on a cohesive soil under normal load conditions. At first a deterministic design will be determined. This design will be used in the probabilistic design, where the reliability index will be used to evaluate the safety of the structure. The partial safety factor for the undrained shear strength will be calibrated before a sensitivity analysis will be performed.

N.1 Deterministic Design

The load situation for the foundation is shown in Table N.1.

Table N.1: *Design loads.*

Load	Value	Unit
V_d	2,000	kN/m
H_d	56.4	kN/m
M_d	5,642	kNm/m

In Table N.2 the characteristic undrained shear strength can be seen.

Table N.2: *Characteristic and design value of undrained shear strength. *The design value for the undrained shear strength is determined using a partial safety factor γ_{c_u} equal to 1.4.*

$c_{u,c}$ [kPa]	$c_{u,d}$ [kPa]
136.66	97.61*

The foundation is designed after the method suggested by [DNV/Risø, 2010], which is presented in Chapter 12. This leads to the foundation presented in Table N.3.

Table N.3: *Results obtained from the Rupture 1 design method.*

V_d [kN/m]	R_d [kN/m]	B [m]	e [m]	e_{crit} [m]	H_d [kN/m]	$B' c_{ud}$ [kN/m]
2,000	2,002	9.78	2.82	2.93	56.42	403.9

From Table N.3 it is seen that the eccentricity demand is respected.

N.2 Probabilistic Design

The design situation for the probabilistic approach can be seen in Table N.4.

Table N.4: *Mean value of the loads.*

Description	Abbreviation	Value	Unit	COV
Horizontal load	μ_{hb}	24.8	kN/m	5%
Moment	μ_{mb}	2,480	kNm/m	5%
Vertical load	μ_V	2,000	kNm/m	5%

The mean value and COV for the undrained shear strength is presented in Table N.5.

Table N.5: *Mean value and COV for the undrained shear strength used in the probabilistic approach.*

Description	Distribution type	μ	COV
Undrained shear strength	LN	10,000 values obtained through stochastic field	15.9%

The reliability index obtained through asymptotic sampling can be seen in Table N.6.

Table N.6: *Reliability index for different COV's.*

	Description	COV_{wind} = 5%
β	Reliability index	4.27
p_f	Annual probability of failure	$9.40 \cdot 10^{-6}$

The partial safety factor, γ_{c_u}, needed in order to obtain a target reliability index of 3.72 is presented in Table N.7.

Table N.7: *Calibrated* γ_{c_u}.

Situation	γ_{c_u}	β
COV = 5%	1.03	3.72

From this example it can be seen that the partial safety factor for the undrained shear strength can be reduced for an example where the loading is not strongly eccentric. This result should be seen in context with the assumptions made in order to obtain this result.

The omission sensitivity factor, ζ, and elasticity coefficient, e, for COV_{wind} = 5% can be seen in Table N.8 and Table N.9.

Table N.8: *Omission sensitivity factor for* COV_{wind} *= 5%.*

Variable	H_b	M_b	V	c_u	X_{exp}	X_{st}	X_{aero}	X_{dyn}	X_{sim}	X_{ext}
ζ	1.00	1.02	1.00	1.02	1.38	1.02	1.21	1.02	1.01	1.02

From Table N.8 it is seen that the uncertainty parameters regarding the terrain, X_{exp}, and aerodynamic effects, X_{aero}, are those variable connected with most uncertainty regarding the reliability index. It is furthermore seen that omission sensitivity factor regarding the undrained shear strength is 1.02.

Table N.9: *Elasticity coefficient e_μ and e_σ for COV_{wind} = 5%.*

Variable	H_b	M_b	V	c_u	X_{exp}	X_{st}	X_{aero}	X_{dyn}	X_{sim}	X_{ext}
e_μ	-0.01	-0.75	0.54	0.31	-0.36.	-0.77	-0.59	-0.77	-0.77	-0.77
e_σ	0.00	-0.08	-0.01	-0.04	-0.43	-0.03	-0.20	-0.03	-0.03	-0.03

In Table N.9 it is seen that the relative importance of the undrained shear strength is increased significantly compared to the results from the strong eccentric foundation, see Table 13.9. Hereby it has been emphasised that the eccentricity has a significant influence on the reliability analysis performed.